Spring 2009

# Development of an electronic governor system for a small spark ignition engine

Donald Ray Hibler



Department:

# DEVELOPMENT OF AN ELECTRONIC GOVERNOR SYSTEM FOR A SMALL SPARK IGNITION ENGINE

by

DONALD RAY HIBLER, III

A THESIS

Presented to the Faculty of the Graduate School of the

MISSOURI UNIVERSITY OF SCIENCE AND TECHNOLOGY

In Partial Fulfillment of the Requirements for the Degree

MASTER OF SCIENCE IN MECHANICAL ENGINEERING

2009

Approved by

Dr. J. Drallmeier, Advisor
Dr. J. Sarangapani
Dr. V. Flanigan

## ABSTRACT

The use of electronic controls on engines has been widespread and has now reached the small utility engine. The evolution from carburetion to electronic fuel injection has presented opportunity to implement additional controls with the intent to improve engine control and performance. In this study, an electronic governor system is developed for use on a small twin cylinder utility engine. This system is to replace an existing mechanical governor system, and it should have the potential as a production based solution that integrates with an existing fuel injection system. It must improve the speed droop characteristics over the current mechanical system and should not carry a large cost increase to the engine.

The methodology and approach of this study is that of a development engineer in industry. The tools and techniques developed for throttle and governor controllers are applied as necessary to characterize the system. A design utilizing a small throttle actuator is developed and various control strategies are applied to provide the control needed on such an application.

The engine dynamics were found to be very nonlinear in nature. The system provided adequate control at higher loads, and improved the speed droop to the targeted levels. However, at low load conditions and during transient operation, the system had instabilities that could not be overcome through software improvements alone. The controller development was not intended to provide adequate transient fuel compensation, and the resulting fuel delivery dynamics combined with system hardware limitations proved to be too great a challenge for the controller.

## ACKNOWLEDGMENTS

I would like to thank my advisor, Dr. James Drallmeier, for all the guidance and patience that has been needed for me to complete this work. Without his understanding and support, this would not be possible. I would also like to thank the Department of Mechanical Engineering, Kawasaki Motor Corporation, and Missouri University of Science and Technology (formerly University of Missouri – Rolla) for their financial support during this work. I would also like to thank the remaining members of my committee, Dr. Flannigan and Dr. Sarangapani, for their support and guidance in this project as well. Finally, I would like to thank my family for their continued support and encouragement. Without any of you, I would never have made it here.

# TABLE OF CONTENTS

## LIST OF ILLUSTRATIONS

Page

# LIST OF TABLES

Page

# NOMENCLATURE

# 1. INTRODUCTION

Small utility engines are defined as spark ignition engines below 25 hp (19 kW) that power off road equipment such as lawn mowers, generators, utility vehicles, and industrial equipment. To remain competitive in this market, the engine manufacturers are always striving to improve engine performance characteristics and durability while reducing costs. Until recently, these engines have not been subject to the strict emissions regulations that have been imposed on larger off road engines and on the on road markets and they have remained simple in design to keep costs low. However, in April 2007, the EPA proposed new regulations to reduce the amount of nitrous oxide and hydrocarbon emissions (NOx + HC) [1].

The current level of technology for fuel delivery is the use of carburetion. This system is inexpensive and robust; however fuel delivery inaccuracy makes it difficult to meet future emissions targets. The migration to more advanced engine control systems to deal with these new regulations presents significant challenges to the small engine development engineer. Previous work done at UMR addressed the issue of engine emissions with the development of an electronic fuel injection system that was cost efficient and reduced engine hydrocarbon emissions [2]. This system was designed around a basic speed density control and calibrated for steady state operation using available components. This simple approach allowed the costs to remain low, yet providing the air-fuel ratio control needed to reduce emissions.

With the introduction of a basic EFI system, next step is to have greater control over the engine speed through an improved governor mechanism. Currently, most small utility engines utilize a mechanical flywheel governor mechanism to regulate engine speed. This type of control uses only one input, engine speed, and it is exclusively a gain style controller. The relationship of the speed and torque is linear in nature, set by weights and springs. This relationship has the speed drop 10-15% from high idle to wide open throttle (WOT) conditions. This mechanism also has numerous parts whose tolerances and quality variances create a governor mechanism that is neither robust nor accurate.

With greater control over engine speed and fuel delivery, the engine can utilize the benefits of electronic controls and deliver improved performance. The purpose of this project is to develop and evaluate a new governor system for a small utility engine. The intent is to deliver improved governor performance characteristics over an existing mechanical system. This new system should be integrated to the new EFI system, and to utilize the benefits thereof. This new governor system should also reduce the component complexity for improved product robustness. Any cost impacts should be minimized, with the cost goal of meeting the cost of the current production mechanical system. The tools and methods to be used should be those available to any small engine development engineer, with this study to provide the background and direction for any such future development work.

# 2. REVIEW OF LITERATURE

## 2.1. GOVERNOR DESIGN AND PERFORMANCE

Kauckak [3] describes the basic parameters of a governor, notably that it is a device that controls the value of a specific parameter in a system through sensing and input devices. An engine speed governor regulates engine speed by modifying the fuel or airflow (depending if it is a Spark Ignition (SI) or Compression Ignition (CI) engine). His primary example is a CI engine, where fuel amount is regulated to meet a specific speed target.

The basic control setups for linkage type mechanical and fully electronic speed governor systems are presented. Mechanical systems behave in a similar manner to a proportional controller. This proportional relationship between engine speed and load creates a phenomenon called droop, which he describes as "the term applied to a governor characteristic that allows the steady state speed to change as load is applied". This is what one would characterize as a proportional relationship, and most mechanical governor mechanisms can be characterized this way. He also moves on to a PI and PID type setups and describes the speed to load relationship and accuracy involved.

On page 26, he describes droop as "the term applied to a governor characteristic that allows the steady state speed to change as load is applied". This is the definition of droop that will be continued throughout this paper. Specifically, droop will be classified as the following:

$$\%Droop = 100 * \frac{\text{High Idle Speed} - \text{Speed When Torque Curve is Reached}}{\text{High Idle Speed}} \quad (1)$$

The majority of work performed on utility engine speed controllers deals with CI engines. Due to their use of fuel as a control parameter, and the lack of an air throttle, one must limit fuel to maintain speeds/loads. With their widespread use and functionality, a good deal of work has been done in the development of CI governors and their performance characteristics. For many years, these utilized the basic mechanical proportional governors mentioned in Kauckak. In [4], Howes, et al. describe the use of retrofitting an electronic governor to a CI rotary pump. This application was to focus on two primary applications: agriculture tractors and AC electrical generators. In these

applications, the droop of the electronic governor was less than that of the mechanical system. This was beneficial to the overall performance, specifically with the generator and constant speed Power Take Off (PTO) applications. Further work was done in [5] to implement a practical governor to a production level product. This governor was evaluated on numerous applications, and it was found to be especially beneficial for agricultural work and generators. Taking from same the performance benefits, Yama et al. in [6] describe the development of an inexpensive yet reliable electronic governor for agricultural and industrial use in small CI engines. By this time, the electronic governor has been fully integrated into the CI engine platform.

However, the need and desire to develop an electronic speed controller for SI engines did not follow suit with the CI engines. With the use of a throttle to regulate airflow, the operator can directly impact the speed and/or torque output of the engine. Also, with the primary application of SI engines being on road transportation, there was little need for the engine to run in a similar manner as an industrial or agricultural CI engine.

The initial use of a speed controller on a SI engine was for idle speed control to enable accurate idle speed control over the life of the engine. Sans [7] presents the development of an idle controller, and the presentation of optimal control laws for implementation on other platforms. Optimal control was chosen over a PID type controller by Sans due to performance limitations, and a second order system was chosen as well.

Optimal control theory was also considered by Iwai et al. [8] for the development of an electronic governor for a generator application with a carbureted SI engine. They considered the Linear Quadratic (LQ) method for optimal theory in addition to the PID method. Unlike Sans, who was only considering idle speed control, they determined the PID method was the best solution due to its ease of implementation and simplicity. On engine tests, they found a properly tuned PID controller met the ISOA-1 requirements for generators.

A Linear Quadratic and Integral (LQI) observer was developed for idle speed control was developed in [9]. A linearized observer model is created by using engine response to step function inputs from a throttle bypass valve. This observer is setup to

have one input and one output, and thus is very straightforward to implement. The LQI is chosen to account for various possible disturbances to the engine system including air conditioning systems, clutch engagement, coasting, and short acceleration bursts. For idle speed control, the LQI method simplifies and provides adequate performance. However, an auxiliary air control valve is used in this study, and this controller is independent of the primary air throttle valve.

Nakamura et al. [10] applied the PID controller on a carbureted engine for a fork truck application with great success. They utilized a fuzzy logic algorithm for tuning the PID constants which resulted in satisfactory results. Bustamante et al. [11] applied the PID controller to a small 20 hp utility V-twin engine for hybrid power generation. This setup utilized a stepper motor and commercially available PID controller. This was also a carbureted engine, but was a small utility engine that is similar to the focus of this study.

In recent years, much work has been done on automotive “Drive-by-Wire” systems for throttle control. Increased complexity and flexibility in automotive drive trains both warrant and facilitate the ability of an electronic throttle controller to function. Yang [12] presents a model based analysis of electronic throttle controllers through numerical methods. Here, a PID system is derived, the governing equations are derived, and the system transfer function is realized. Previous generation controllers are analyzed using discrete methods, and their shortfalls are considered. Design considerations such as “limp-home”, throttle accuracy considerations (2° of throttle opening) are used in the analysis, and physical conditions such as dry-friction are considered to present a realistic analysis. Yang presents a consistent, yet accurate way to utilize computer based tools to design and develop a controller.

Emtage et al. in [13] develop an electronic throttle controller for use on an automotive chassis dynamometer. Here, the primary purpose of the throttle controller was to control engine torque output during testing, specifically for consistent transient testing and evaluation. In this control, maps are developed with engine speed and torque request as an input and a percent throttle as an output.

## 2.2. THROTTLE AIRFLOW

The airflow dynamics of a butterfly throttle are a primary control input to any spark ignition engine. Thus, there is a large body of work associated with the throttle valve, particularly the butterfly throttle valve. A common approach is to treat the butterfly valve as a nozzle with a variable area [14],[15],[16]. In doing this, the nozzle flow can be represented with the equation for mass flow:

$$\dot{m} = \rho A U \tag{2}$$

Velocity is defined by Mach number times the speed of sound:

$$U = Ma \tag{3}$$

With the Ideal Gas Law and the definitions for speed of sound in an ideal gas:

$$P = \rho R T \tag{4}$$

$$a = \sqrt{\gamma R T} \tag{5}$$

The pressure then becomes:

$$P = \frac{\dot{m}\sqrt{RT}}{MA\sqrt{\gamma}} \tag{6}$$

Assuming ideal, adiabatic flow, total temperature of a gas flow is:

$$T_0 = T + \frac{U^2}{2C_p} \tag{7}$$

Then substituting equation 3, $R = C_p - C_v$, and $\gamma = \frac{C_p}{C_v}$, the equation for total temperature then can be transformed to the following isentropic flow relationship:

$$\frac{T_0}{T} = 1 + M^2\left(\frac{\gamma - 1}{2}\right) \tag{8}$$

With isentropic flow, $PV^{\gamma}$ and $TV^{\gamma-1}$ are constant, therefore

$$\frac{T}{T_0} = \left(\frac{P}{P_0}\right)^{\frac{(\gamma-1)}{\gamma}} \tag{9}$$

And

$$\frac{P_0}{P} = \left(1 + M^2\left(\frac{\gamma - 1}{2}\right)\right)^{\frac{\gamma}{\gamma-1}} \tag{10}$$

Using equations 8 and 6,

$$P = \frac{\dot{m}\sqrt{T_0 R}}{MA\sqrt{\gamma}\left(1 + M^2\left(\frac{\gamma - 1}{2}\right)\right)^{\frac{1}{2}}} \tag{11}$$

From equation 10 and 11, the following expression can be written:

$$\frac{\dot{m}\sqrt{T_0 R}}{MA\sqrt{\gamma}\left(1 + M^2\left(\frac{\gamma - 1}{2}\right)\right)^{\frac{1}{2}}} = P_0\left(1 + M^2\left(\frac{\gamma - 1}{2}\right)\right)^{\frac{-\gamma}{\gamma-1}} \tag{12}$$

From this, mass flow through the nozzle can be found as a function of the flow area, mach number, total pressure, total temperature, specific heat ratio, and ideal gas constant:

$$\dot{m} = \frac{MAP_0\sqrt{\gamma}}{\sqrt{RT_0}}\left(1 + M^2\left(\frac{\gamma - 1}{2}\right)\right)^{\frac{-(\gamma+1)}{2(\gamma-1)}} \tag{13}$$

Solving for M from equation 10:

$$M = \left( \frac{2}{\gamma - 1} \left( \left( \frac{P_0}{P} \right)^{\frac{\gamma - 1}{\gamma}} - 1 \right) \right)^{\frac{1}{2}} \tag{14}$$

Substituting this into equation 13:

$$\dot{m} = AP_0 \sqrt{\frac{\gamma}{T_0 R}} \left( \frac{P_0}{P} \right)^{\frac{-(\gamma+1)}{2\gamma}} \left( \frac{2}{\gamma - 1} \left( \left( \frac{P_0}{P} \right)^{\frac{\gamma - 1}{\gamma}} - 1 \right) \right)^{\frac{1}{2}} \tag{15}$$

Simplifying equation 15:

$$\dot{m} = AP_0 \sqrt{\frac{\gamma}{RT_0}} \left( \frac{P}{P_o} \right)^{\frac{1}{\gamma}} \left( \frac{2}{\gamma - 1} \left( 1 - \frac{P}{P_0} \right)^{\frac{\gamma - 1}{\gamma}} \right)^{\frac{1}{2}} \tag{16}$$

This is ideal airflow through a converging/diverging nozzle for subsonic flow, and matches the results shown by Heywood [14]. For choked flow, the critical pressure ratio is:

$$\frac{P_{throat}}{P_0} = \left( \frac{2}{\gamma + 1} \right)^{\frac{\gamma}{\gamma - 1}} \tag{17}$$

At this critical pressure, mass flow cannot increase past a set value, but it becomes limited to a set value. By setting mach number to 1 in equation 10 and substituting into equation 16:

$$\dot{m} = AP_0\sqrt{\frac{\gamma}{RT_0}}\left(\frac{2}{\gamma+1}\right)^{\frac{(\gamma+1)}{2(\gamma-1)}} \tag{18}$$

Due to the assumptions made in the derivation, the actual mass flow through an orifice is lower than what is shown in equations 16 and 18. To fit these equations to actual data, a discharge coefficient is used, $C_d$. The basic definition for the $C_d$ is the actual mass flow over the ideal mass flow (so $C_d$ is always less then one). For a butterfly throttle, the Cd is usually found experimentally as a function of throttle angle [17], [14]. Some have formulated the value as a function of both pressure ratio and throttle area [15].

The throttle area can be found geometrically as a function of throttle angle, bore diameter, and throttle shaft diameter [14]:

$$\begin{aligned} A_{th} = {} & \frac{D^2\pi}{4}\left(\left(1-\frac{\cos\alpha}{\cos\alpha_0}\right)+\frac{2}{\pi}\left(\frac{d}{D\cos\alpha}\left(\cos^2\alpha-\frac{d^2\cos^2\alpha_0}{D^2}\right)^{\frac{1}{2}}\right)\right) \\ & -\frac{D^2\pi}{4}\left(\frac{2}{\pi}\left(\frac{\cos\alpha}{\cos\alpha_0}\right)\sin\left(\frac{d\cos\alpha_0}{D\cos\alpha}\right)-\frac{d}{D}\left(1-\frac{d^2}{D^2}\right)^{\frac{1}{2}}+\sin^{-1}\left(\frac{d}{D}\right)\right) \end{aligned} \tag{19}$$

Blair proposes a much simplified version of this which neglects the throttle shaft area [15] which is also used in other studies [18]:

$$A_{th} = \frac{\pi D^2}{4}\left(1-\frac{\cos\alpha}{\cos\alpha_0}\right) \tag{20}$$

These two area equations do match very closely along most of the throttle operating range; the value listed in equation 19 more closely matches the actual flow area.

From equation 16, when applied to the flow through a butterfly throttle, the final expression for throttle mass flow is as follows:

$$\dot{m}_{th} = C_d A_{th} P_{amb} \sqrt{\frac{\gamma}{RT_{amb}}} \left( \frac{P_{man}}{P_{amb}} \right)^{\frac{1}{\gamma}} \left( \frac{2}{\gamma - 1} \left( 1 - \frac{P_{man}}{P_{amb}} \right)^{\frac{\gamma - 1}{\gamma}} \right)^{\frac{1}{2}} \quad (21)$$

Note this expression uses the throttle area from equations 19 or 20, $C_d$ found experimentally or by other means. It also assumes an ideal gas with isentropic flow with no pressure recovery on the downstream side of the throttle.

### 2.3. ELECTRONIC FUEL INJECTION BEHAVIOR

Electronic fuel injection has been widely used on automotive applications for the last 20 years. As a result, a great deal of work has been done considering the performance aspects of the EFI induction system. One area of particular interest has been the performance characteristics during transient operation. Proper air to fuel (A/F) ratio control during transients is necessary for torque stability (also called “drivability”). The development of this control makes it necessary to properly describe the physical processes that govern transient operation.

One of the first papers written on the subject, Aquino [19] describes the nature of transient operation during a change in throttle angle on a 5 liter central fuel injected engine (CFI). In this testing, he finds there is a characteristic A/F ratio spike during one second throttle transients from a nominal closed throttle position to various final points. Manifold temperature and throttle body temperature were also considered as variables to determine the impact each has on transient operation.

There are two basic components driving A/F ratio changes during a change in throttle position (TP). First is the steady-state error in the fueling system itself. Second is the dynamics of the system at large. Ignoring the steady state errors, there are four factors driving the overall system dynamics during a throttle transient: fuel wall wetting causing a lag in fuel delivery; manifold air charging causing a delay in airflow to the cylinder; injector phasing impacting fuel delivery; sensor and calculation delays in the fuel injection system. To understand this phenomenon, he builds two basic models of describing the characteristics found: one for a fuel wall-wetting model, and one for a manifold air charging model.

For the fuel flow, an ambiguous model was built with the following equation:

$$\frac{dM_f}{dt} = \dot{M}_{in} - \dot{M}_{out} = X\dot{M}_{fm} - \frac{1}{\tau}M_f \tag{22}$$

X represents the mass fraction of the injected fuel that becomes entrained in the fuel pool, where tau represents the time constant for the fuel evaporation from the pool to the manifold. Note here that the X and tau values are based upon the fuel film mass.

To obtain values for the constants of X and tau, testing was carried out at various throttle openings and manifold temperatures. From this data, X was seen to be a linear function of throttle position, but independent of coolant temperature. Tau is solely a function of coolant temperature. Once the X and tau values are chosen, Aquino compares the predicted results to those seen experimentally. There is good correlation between the results of an uncompensated CFI engine and those predicted with the above models.

The manifold air charging model is based on a uniform flow model for the manifold. The continuity equation follows:

$$\frac{d\dot{m}_{air}}{dt} = \dot{m}_{th} - \dot{m}_{ap} \tag{23}$$

Aquino uses the following equation for throttle mass flow:

$$\dot{m}_{th} = \frac{C_d A_{th} P_{amb} 2\gamma}{R(\gamma - 1)\sqrt{T_{amb}}} \left[ \left( \frac{P_{man}}{P_{amb}} \right)^{\frac{2}{\gamma}} - \left( \frac{P_{man}}{P_{amb}} \right)^{\frac{\gamma}{\gamma+1}} \right]^{\frac{1}{2}} \tag{24}$$

The port flow is derived by the speed density equation and the ideal gas law. From these, one obtains the following relationship:

$$\dot{m}_{ap} = NV_d \eta_{vol} \rho_{man} \tag{25}$$

For this, volumetric efficiency is the item that must be modeled. If the $C_d$ is known through experimental work, the only variable that must be modeled is the volumetric efficiency.

While Aquino addresses each of these individually, but tests the data as a set. Throttle transients are run using two fuel delivery calculations: speed density and mass flow. Speed density is based on a basic intake manifold density calculation combined with a volumetric efficiency calculation to determine airflow. This is then used to calculate fuel flow to achieve a given A/F ratio. Mass flow uses a mass flow meter to calculate the actual mass flow and then determining the required fuel flow.

The difference between the two approaches is that the mass flow measurement (taken at the throttle body) will accommodate for the manifold air charging dynamic as it measures actual mass flow into the manifold. A speed density algorithm cannot as it is based purely upon manifold pressure. During manifold filling event, mass flow can increase while maintaining a constant pressure due to the time lags of the airflow dynamics and changes in intake manifold air density.

With this data, Aquino built two models: one for the manifold filling dynamics, and one for the fuel wall wetting. The sensor delays were addressed and the specific delays for the data analyzed (this does not have to be modeled as it is known). The injector pulse timing was investigated as well, but a mathematical model was not built. Instead, it was determined where the optimal timing was located, which was at top dead center (TDC) of the intake stroke.

Hires and Overington [20] take the approach a step further and apply a compensation algorithm to reduce the air to fuel ratio excursions seen during throttle transients. An airflow model is used to predict the intake manifold density in real time, and compensation is done by the addition of fuel to intake flow to overcome the air charging and fuel film dynamics.

Initially, the system is characterized through the use of different fuels (with differing vapor pressures) to confirm the existence of a fuel film. Then it is shown that superposition holds true for throttle transients. In this, the magnitude of the air to fuel ratio increase (or decrease) for a specific transient setting is equivalent to the sum of

smaller transients whose total equal the larger transient. This dynamic allows for a simple and basic compensation approach of fuel addition.

A basic compensator is used that differentiates the throttle position as the manifold pressure was intended to be used, but it had signal problems. Fuel is added to the nominal delivery pulse to compensate for the increase in airflow and fuel film. There is a delay portion of this algorithm (the tau value) that accounts for the fuel film decay and removes the fuel compensation at a certain rate. Results showed that compensation reduced the air to fuel ratio excursions up to 85%.

Aquino takes the study of these transients further in [21]. Here, he studies the impact cold temperatures have on the A/F ratio excursion in a PFI engine using a mass air flow (MAF) control setup. Here, he defines the value of tau as a traditional linear system time constant, i.e. it is 63% of the decay of the A/F ratio spike. In this testing, it is shown that temperature has a large impact on the A/F ratio spike. Also, injector timing and configuration were varied to obverse any impacts they may have on the A/F ratio spike. It is seen that timing can have a large impact, and this impact increases with lower manifold temperatures. From all of this, Aquino surmises that fuel dynamics, not manifold air charging, has the largest impact on A/F ratio spikes at cold temperatures.

Bossert, Shin, Cheng also study the impact of temperature and fuel distillation curves in [22]. Here, the distillation curve was modified by running various methanol indolene blends. Throttle opening tests were run at 40°C and 80°C to determine the X and tau constants from equation 2. Results show that for a warm engine (80°C coolant), there is little relationship between the constants X and tau and the fuel distillation points. However, at lower temperatures (40°C coolant), both constants were impacted by the fuel distillation points.

Shayler, Teo, and Scarisbrick see similar results to cold engine operation in [23]. Here, a PFI engine configuration was studied during cold warm up, and the impacts of cold manifold temperatures and engine speeds on X and tau values presented in the models from [22] and [20]. Initially, both throttle and fuel perturbations were to be used to determine the complete transient operating condition and present the impacts of each of these inputs on the X and tau values at cold temperatures. However, due to the complexness of the manifold system, particularly the nonlinearities associated with it's

mathematical descriptions, this was determined to be too complex and throttle perturbations were not used. Results show that as temperatures increase, the value of X decreases in a linear fashion and tau decreases to a value and remains constant at that point at all temperatures higher. As speed increases, X decreases at lower temperatures, though it is mostly independent of speed at higher temperatures. Tau decreases with increasing speeds as well.

In [24], Hendricks uses Aquino's work to derive a mean value engine model that utilizes the X-t model for a CFI engine. He places X as a function of throttle angle. He also includes a model for the manifold airflow, focusing solely on the throttle airflow model as it is most relevant to a CFI engine configuration. His model includes two independent functions that combine to describe the throttle flow. One is of a similar form to the manifold pressure terms in equation 16, and the other is similar in form to Blair's simplified throttle area function in equation 20.

He also uses these same functions in [18], though he takes this a step further and develops a compensator for the fuel film dynamics. This is done again for a CFI engine, but in a departure from Aquino, he assumes that the time constant of the fuel film is based solely on the mass flow rate, not the actual fuel film mass. This allows simplification, yet the final forms of the X terms are similar to those found by Aquino.

In [18], the speed density function used for the manifold pressure equation is shown. However, significant nonlinearities in this equation make it difficult to match and compensate for the system dynamics, particularly when steady state terms are used to calibrate the compensator.

In [25] Hendricks takes this study a step further and evaluates the errors of both speed density and Manifold airflow control strategies. In this study, both CFI and port fuel injected (PFI) systems are considered. The same fuel film models and manifold filling models presented above are used for evaluation, and it is noted that the use of the speed density system with a PFI induction system are suspect to the highest number of errors.

Practical system performance issues are seen in this study, including processor time limitations, physical response time, and system noise. One particular area of concern was the noise of the maifold air pressure (MAP) sensor. Since the MAP has a

large impact on both the mass air flow (MAF) and the speed density functions, it's accuracy and response time must be set to the highest level. But, given the dynamics of the sensor, the measurement techniques, and the pressure signal itself, the amount of noise makes the processing difficult. A processing filter is used on the signal to provide a more consistent MAP signal, however transient response may be slightly compromised as a result. This is also seen in [26] where MAP signal dynamics become complex for an observer/compensator setup for the basic performance models presented in [24].

In [27], the fuel film compensator derived in [18] is further developed, and it is applied to both a PFI and a CFI system. In this regard, the model for the PFI system is modified to have only one time constant (a "two pool model"). The results show that the X and tau terms needed to describe the model and correct fueling errors are found to be different, particularly when coolant temperature is changed. The PFI system has a smaller response characteristic than that of a CFI engine, and it is supposed by Hendricks et. al. that the port and valve temperature are less impacted by differing coolant temperatures than the intake manifold.

In [28], a PFI system is studied for the applicability of a two pool X tau model. Here, the port airflow is modeled with the speed density equation, and a two and single pool model are derived. During 50ms throttle ramps, it is seen that a single pool model fits the data set in this engine better. Also, it is seen that the manifold filling effects have a larger impact on A/F ratio excursions during positive throttle ramps, but that fuel film dynamics impact the negative A/F ratio excursion seen during negative throttle transients.

In [16], Hendricks derives a manifold air model that can apply to a broad range of engine configurations. The basic continuity equation shown in 23 is used, however the approaches for the throttle and port flows are modified. For the port flow, typically the volumetric efficiency is modeled [19] for the port airflow. Hendricks shifts the emphasis of the port flow function shown in from modeling the volumetric efficiency to the mass of the air charge. He also neglects the effects of the manifold temperature on the air charging. For the throttle flow, a new isentropic model is derived that uses a two zone model. With this approach, the subsonic region of the throttle flow is increased, allowing for more airflow.

In [29], Tseng and Cheng develop an adaptive controller during transients. This is also based on the X - tau method, but the model is simplified to a single parameter, fuel flow into the cylinder. To utilize this in an adaptive fashion, feed back was taken with a UEGO sensor. Sensor delays were taken into account, and it was found that time response of the sensor improves as load and speed are increased, as well as the transport delay became negligible at higher loads. With a feedback channel, the airflow is modeled using the manifold state equation shown in equation 25. Here, volumetric efficiency was also corrected using a predictor equation and the manifold pressure derivative. With the airflow and the A/F ratio feedback, the controller can adapt to provide the target A/F ratio during transients. Over most operating tests, the controller outperformed the production version based on calibrated X-tau values, with the exception of cold warm-up.

In [30], Simons et al. present a different model approach using a second order parallel path model for the fuel dynamics. The X tau model is still the basis, but residual gas fraction is taken into account by measuring the NO emissions of the exhaust gas during constant throttle fuel perturbations as tested on a PFI engine.

Not all experimental work saw the characteristic spike of a fuel film [31]. In this study, a FID was uses to measure A/F ratio spikes on a PFI engine during throttle ramps at warm (90°C) coolant temperatures. In this particular study, the fuel film was not detected, and had to be artificially created to observe the characteristics seen in other studies. However, there still is a A/F ratio spike, and it is shown that the manifold filling model explains these excursions. This agrees with Aquino's observation in [21] that injector and port configuration have an impact on the fuel film dynamics.

While there has been a great deal of work associated with the electronic fuel injection systems, and governors, there have been few publications on the implementation of electronic governors on small engines. Also, there is little shown for the integration of an electronic throttle controller with a fuel injection engine.

# 3. BACKGROUND

## 3.1. ENGINE TESTING PLATFORM

This study utilizes experimental facilities at the Engine Test Laboratory for development and testing. Both horizontal and vertical shaft engine configurations are used in this study, each utilizing a different test dynamometer. For both dynamometers, the EFI system utilized a high pressure fuel pump placed in a fuel can. This pump was run with the 12 volt battery used to run the engine and EFI controller. The system pressure was regulated to 43 psi (2.96Bar) using an adjustable automotive type fuel pressure regulator and pressure gauge. The carburetor engine setup used a separate fuel can which differed between engine configurations. The engine is designed to have a small amount of fuel pressure out of the fuel tank. On the horizontal shaft engine, this was not an issue, but on the vertical shaft engine, the fuel tank could not be placed such that there was sufficient pressure out of the fuel canister. To remedy this, a slight pressure of 2 psi set from a bottle of compressed nitrogen was placed onto the fuel tank to feel the fuel to the engine. The fuel used for all test is indolene test fuel. Appendix B has a summary of the fuel properties.

The air used for all tests is ambient test cell air. The air is taken into the engine through a production style air filter and housing. Ambient test cell temperature and pressure measurements are taken prior to each test, so all power and torque data shown is corrected to SAE J1999 unless otherwise stated. Humidity is not corrected; however engine exhaust emissions are not taken into consideration in this study, so it was not considered prudent information.

The exhaust systems differ for each engine. For the vertical shaft engine, the exhaust system is plumbed so that both engines on the stand can use the setup. It retains the stock exhaust manifold and silencer configuration, and the outlet connects to a pipe which contains a surge tank/resonance chamber to minimize dynamic flow effects of the exhaust.

The horizontal shaft engine connects to the same system, but it has a longer length of pipe before it reaches the surge tank. Two inch diameter flexible stainless steel pipe is used to connect the original exhaust silencer and manifold to the test cell exhaust system.

Since the engine configuration varies, the orientation and design of the manifolds are different between the engines. However, a significant performance difference is not seen between the two designs as the same intake manifold, port geometry, injector design, and injector placement is used between both engines.

**3.1.1. Vertical Shaft Dynamometer.** The vertical shaft engine is coupled to a Baldor Vector drive AC motor/absorber via a cog belt. This setup allows for constant speed operation of the engine, regardless of the load. This operation also includes the ability to motor the engine. All engine speed control is done via the vector drive controller, and the system has a maximum speed of 4000 RPM, maximum power absorption of 25 hp, and a maximum torque load of 60 ft-lbs.

The motor is mounted to the dynamometer chassis via a reaction torque transducer. This load cell is a Lebow 2404-5K with a rated capacity of 5,000 in-lbs. The transducer is operated by a Daytronic 3578 strain gauge conditioner with a digital readout. The dynamics of the belt drive and the v-twin engine are such that the instantaneous torque reading can vary greatly. As a result, the Daytronic 3578 outputs a signal to a National Instruments (NI) data acquisition card operating at 250 kS/sec. This card is mounted in a Dell 2.5 GHz PC computer, running NI LabView. The torque information is then read and averaged in the program, giving much more consistent results. The performance parameters of the transducer are listed in Table 3.1.

Table 3.1: Accuracy and Performance Characteristics of the Lebow 2404-5K Reaction Torque Transducer

**Lebow 2404-5K Reaction Torque Transducer**

| | | | | |
|---|---|---|---|---|
| Rated Capacity | 5000 | in-lbs | | |
| Nonlinearity | 0.02% | Full Scale | 1 | in-lbs |
| Hysteresis | 0.10% | Full Scale | 5 | in-lbs |
| Repeatability | 0.05% | Full Scale | 2.5 | in-lbs |
| Overload: | 50% | Full Scale | 2500 | in-lbs |

An NTK model TL-7111-W1 Universal Exhaust Oxygen (UEGO) sensor utilizing a TC-6000 controller is used to measure A/F ratio. The working range on the instrument is from 10 to 30 Air to Fuel Ratios, which corresponds to an output voltage of 1.875 and

3.75, respectively. This sensor is calibrated to a fuel with an H:C ratio of 1.85:1, with a stoichiometric A/F ratio of 14.57. This is applicable to indolene, the test fuel used throughout this study

Data was logged with a Tektronix TDS 2014 4 Channel Oscilloscope with data logging capability. It runs at 100 MHz with a 1 GS per second sampling speed, and has the ability to capture waveforms and save them onto a compact flash digital media. This data can then be read into a spreadsheet or code and converted, scaled, and reformatted for use in analysis and plotting programs.

Data was also taken with a 500 MHz desktop PC utilizing a NI data acquisition card. This card runs at 250 kS per second, and utilizes LabView based programs to log engine data. These programs were first developed for the EFI system in a previous project, and were carried into this project. These programs allowed the data logging of the MAP, intake temperature, Hall Effect signal, injector pulse width, and UEGO sensor readings.

With the mechanical governor mechanism in place, the throttle is actuated via a push-pull cable from the dyno control room to the engine room. For the setups not utilizing the mechanical governor mechanism or throttle control system, a stepper motor is used. This motor has 1.5° steps, and is connected via a four bar style linkage.

Thermocouples were used to monitor engine performance and operating condition. Table 3.2 below indicates the thermocouple placements and the type used.

Table 3.2: Thermocouple type and location

| Location | Type |
|---|---|
| Intake Air | Type K |
| Exhaust Port #1 | Type K |
| Exhaust Port #2 | Type K |
| Exhaust Muffler | Type K |
| Oil Temperature | Type K |

**3.1.2. Horizontal Shaft Dynamometer.** The horizontal shaft engine was tested on a water brake dynamometer system. The dynamometer system is produced by Land-and-Sea, Inc., and it incorporates a water brake, torque arm, load control valve, and a data acquisition computer. This was used to provide a test platform that allows the engine to independently control speed, an important aspect when attempting to test an engine governing system.

The water brake used is a torrid style brake which uses the viscous friction of water to create a load, with the energy being dissipated as heat to the water. The load is varied by changing the volume of water contained in the brake. With the energy dissipated as heat, inlet water temperature is very important, so the system was connected directly to the cooling tower of the MAE building to maintain a consistent inlet temperature.

Figure 3.1 shows a flow diagram of the water brake system. The water is sourced from the cooling tower, and is fed through the load valve. This valve regulates the mass flow into the brake, which develops a specific amount of load at a specific impeller speed. More info is shown in Appendix A. The water is then gravity drained into a holding tank where it is subsequently pumped back into the cooling tower water system

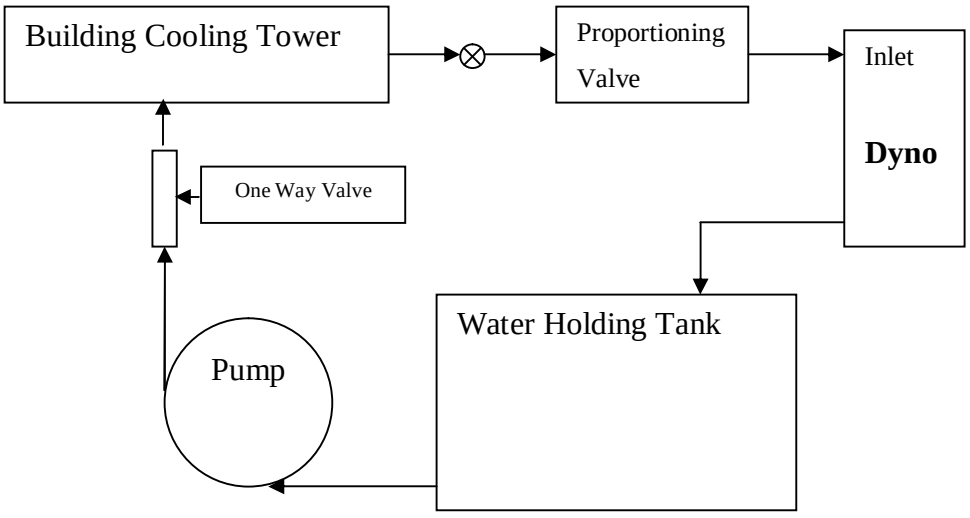


Figure 3.1: Water System Schematic for the horizontal engine system

The brake is mounted in bearings, and it is free to rotate. A torque arm is mounted to the brake and is pinned to the dyno stand, constraining the brake and providing a means for measuring engine torque via a strain gage bridge. This signal and a speed pickup on the brake are sent to the DAQ computer supplied by Land-and-Sea. In addition to these signals, the EFI system signals of MAP, intake temperature, the UEGO sensor output, and the throttle position sensor (TPS) are sent to the computer. The computer is then connected to a PC via a serial cable, and the data is converted to engineering units and logged on the PC for a specific period of time with a LabView code.

The load valve is rotational in nature and is manually actuated. For transient load tests, a consistent approach was needed to achieve repeatable tests. The solution was the use of a pneumatic rotary actuator, specifically a Bimba Pneu-Turn. This actuator rotates in both directions, and the rate of rotation can be varied by inlet needle valves. The actuator is operated by a four way valve connected to the building low pressure air system (which is set to 80 psi). A picture of the experimental setup is shown in figure 3.2

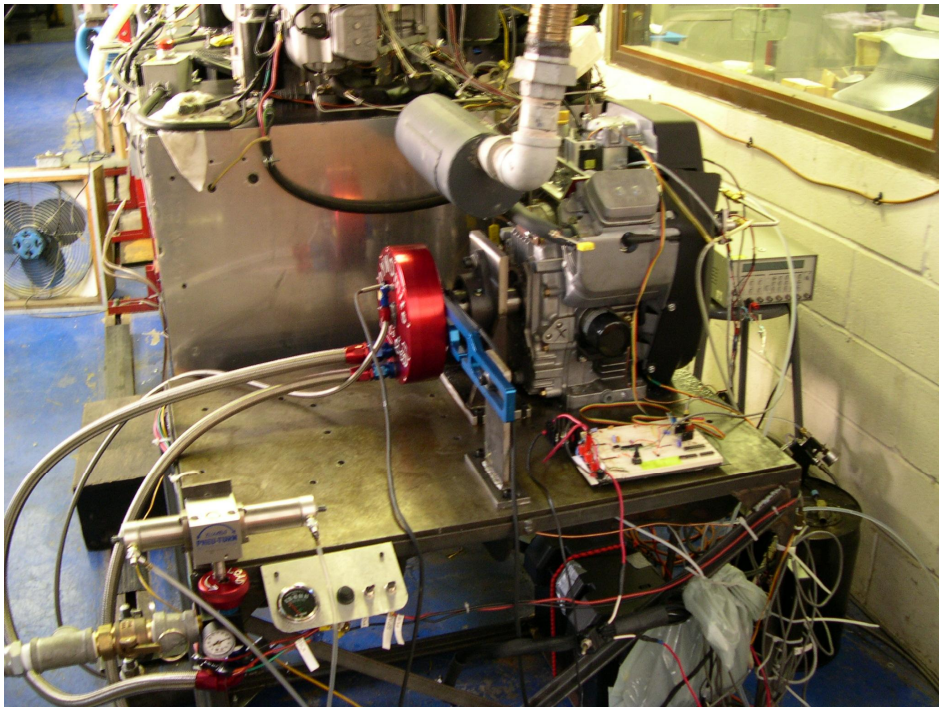

Figure 3.2: Water brake dynamometer test stand

The accuracy of the dynamometer's torque arm is ±1.5% of full scale torque. For this model, 200ft-lbs is full scale, so ±3 ft-lbs is the accuracy of the torque meter. The speed accuracy is ±5 RPM, and combined they give a power variance of ±0.00285 hp.

The engine data was logged with a LabView™ code written to interface with the DynoMite™ DAQ computer. Below is a screen shot of the program's user interface. The data was logged on a Dell 3.2 GHz Pentium processor computer via a serial cable connection.

## 3.2. PERFORMANCE EVALUATION PROCEDURE AND METRICS

This study is to replicate or improve performance of a mechanical system with an electronic controller, and as such no quantitative goals were set. Instead, comparison between the two systems will be made. The comparison will concentrate on two specific types of testing, steady state and transient performance.

**3.2.1. Steady State Performance.** Steady state performance is indicative of the ability of the engine control system to maintain a certain speed regardless of the load or throttle setting. As there is no industry standard for stability, it will be defined as the standard deviation of the speed over a specific period of time, and the maximum and minimums seen over that same period.

Idle stability testing was performed once the engine was warmed to an oil temperature of 150°F (65.5°C). For all governor systems considered in this study, the idle is set by a throttle stop screw on the throttle body/carburetor. This was set to 1550 RPM (the rated low idle) with the use of a spark inductance tachometer mounted to the engine. Low idle was tested by taking 30 seconds of high speed data on a warm engine.

For the high idle, the mechanical governor was set using the method outlined in the factory service manual. This was set to 3600 RPM as read on the inductance tachometer with no load on the engine. The high idle was to be controlled by the electronic governor, so no mechanical adjustments were made to the setup.

Two different high idle tests were performed. The first was similar to the low idle tests, with 30 seconds of high speed data taken during torque curve and governor curve testing. The second test was to determine if there were any larger time constant dynamics

taking place that were not captured on the 30 second test. This involved 5 minutes of data logged at a slower rate while the engine was running at the high idle point.

The governor and torque curve were taken at the same time with 30 second data points. This allowed for temperature and UEGO sensor stabilization and for post test processing and data filtering and averaging. The test procedure for the torque curve required the dyno to set the engine speed, either through the controller on the vertical shaft dyno, or by manual manipulation of the load valve on the horizontal shaft engine. Since the torque curve is run in WOT, by manipulating the load, one can set the engine speed. Unfortunately, this method was not complete as it would cause the engine to stall below peak torque on the horizontal shaft engine. However, the torque curve at this point is not in the normal operating range of the engine, so this data was unnecessary.

**3.2.2. Transient Performance.** Transient performance is another area where the actual performance metrics are not well defined. By considering the engine's use in various applications, the engine is set to run on the high speed governor for the majority of the time. With a low amount of droop (as is desired here), the engine operates in essentially a constant speed, variable load scenario. This operation was used as the basis for the transient tests used in this study.

Six primary tests were devised to study the ability of the governor to maintain speed during load changes. The first three were positive load changes, from high idle (no load) to a high load setting with varying load application rates. The next three were negative load changes, from a high load to high idle (no load), also with varying load changing rates. The load rates were varied with needle valves on the pneumatic actuator, so the number of turns from fully closed was used as the measurable setting during operation.

Six secondary tests were conducted on selected versions of the system. These tests were to observe the performance when load was changed from midrange to high at differing load application rates. While these tests are valid, it will be shown that they are not the worst case scenario. Table 3.3 below outlines these twelve tests in detail.

The performance metrics for these tests varied based upon the system tested. The primary metric is the engine speed, and tracking how it varies as load is applied at differing rates and in different directions. Specifically, the engine speed overshoot (or

undershoot), and the RPM settling time are calculated For these tests, data was logged using the dyno-mite DAQ computer and then reduced using a FORTRAN code.

Table 3.3: Transient tests used for controller performance evaluation

| Test | Direction | Low Load, ft-lbs | High Load, ft-lbs | Opening Rate | Actuated Valve Setting |
|---|---|---|---|---|---|
| 1 | Low to High | 0 | 25 | slow | 1.5 turns from fully closed |
| 2 | Low to High | 0 | 25 | quick | 3 turns from fully closed |
| 3 | Low to High | 0 | 25 | fast | 4.5 turns from fully closed |
| 4 | High to Low | 0 | 25 | slow | 1.5 turns from fully closed |
| 5 | High to Low | 0 | 25 | quick | 3 turns from fully closed |
| 6 | High to Low | 0 | 25 | fast | 4.5 turns from fully closed |
| 7 | Low to High | 5 | 25 | quick | 3 turns from fully closed |
| 8 | Low to High | 5 | 25 | fast | 4.5 turns from fully closed |
| 9 | Low to High | 10 | 25 | quick | 3 turns from fully closed |
| 10 | Low to High | 10 | 25 | fast | 4.5 turns from fully closed |
| 11 | Low to High | 15 | 25 | quick | 3 turns from fully closed |
| 12 | Low to High | 15 | 25 | fast | 4.5 turns from fully closed |

## 3.3. ENGINE SPECIFICATIONS

The engine used in this study is a four stroke twin cylinder engine in a 90° V configuration. It is an air cooled, carbureted engine that employs the use of two overhead valves per cylinder operated by push rods and a single camshaft. This engine is defined as a small utility engine by the SAE (all engines under 20 kW or 26.8 HP) since it has a power output of 23 HP. It has a basic flyweight based governor system that is driven by the speed of the engine. The specifications are listed in the table 3.4.

**3.3.1. Carburetor.** The production version of this engine uses a Mikuni two barrel carburetor with each barrel feeding one cylinder. The intake tracts are independent with a balance passage in a spacer plate. The carburetor has an idle adjustment screw, an

electric fuel shutoff, and a manual choke to aid cold starting. The throttle is connected directly to the governor mechanism via wire linkage.

Table 3.4. Engine Specifications

| | | |
|---|---|---|
| Type | 90° V-twin | |
| Bore | 75.2 | mm |
| Stroke | 76 | mm |
| Compression Ratio | 8.1:1 | |
| Displacement | 675 | cc |
| Clearance Volume | 42 | cc |
| Connecting Rod Length | 116 | mm |
| Spark Timing | 21.5 | °BTDC |
| Cylinder #1 Intake Valve Opening @ 0.41mm lift | 16 | °BTDC |
| Cylinder #1 Intake Valve Closing @ 0.41mm lift | 44 | °ABDC |
| Cylinder #1 Exhaust Valve Opening @ 0.41mm lift | 40 | °BBDC |
| Cylinder #1 Exhaust Valve Closing @ 0.41mm lift | 12 | °ATDC |

**3.3.2. Mechanical Governor.** The governor system on this engine utilizes a flyweight system. These weights are large steel spheres and are coupled to the camshaft thru a slot and plate. They are allowed to move freely in the radial direction, but are restrained in the axial direction and tangential direction by the plate and slot. Using the equation for centripetal force (Eq 26), it is obvious that the weights will move outwards in the radial direction if left unrestrained.

$$F = m_{weights}\varpi^2 r \tag{26}$$

Figure 3.3 shows a drawing of the mechanical governor and how it operates. The flyweights push against the plate at a tangential angle of 30°, creating both a radial and axial force on the plate. The plate is unrestrained in the axial direction, so it is free to

move relative to the camshaft. It then pushed against arm #1and causes a shaft to rotate. This shaft runs through a sealed joint to the exterior of the crankcase and is attached to arm #2. Arm #2 is tied to the crankcase via a spring, and also connects directly to the throttle. This spring holds the entire assembly in tension, keeping the flyweights directly in contact with the plate.

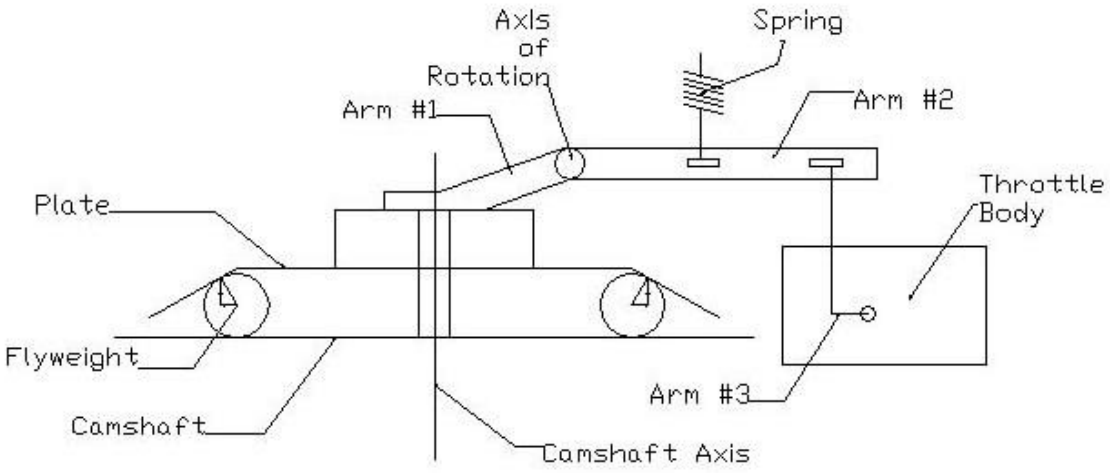


Figure 3.3. Drawing of the mechanical governor mechanism

As the engine speed increases, the flyweight pushes the plate upwards at a force equal to the square of the rotational velocity described in equation 27.

$$F = \sin(30°)\, m_{weights} \varpi^2 r \tag{27}$$

As this force increases, the force on the spring changes via arm #1, causing a displacement in arm #2. This in turn moves the throttle via arm #3. When the arm lengths and spring constant are designed properly, the system becomes a speed based throttle controller with a proportional gain response.

The engine is set such that the low speed idle is at 1550 RPM with a throttle stop screw. The high speed idle is set by changing the spring load to maintain the engine

speed to 3600 RPM with no load on the engine. This is done by moving a plate vertically.

The major drawback of this system is that the control of the throttle is based solely upon engine speed, not load. When a load is placed on the engine at high idle, the engine must slow to open the throttle further to compensate for the increased load. This causes the engine speed to decrease as load is increased.

Figure 3.4 shows the normalized governed and ungoverned maximum load curves of the engine. The torque output drops off significantly past 3000 RPM, and continues until it reaches zero at 3600 RPM. The ungoverned torque curve starts to decline at higher speeds, but it still maintains a high load even at 3600 RPM.

The target maximum engine speed for continued operation of the engine is 3200 RPM, and most operation takes place between 2400 and 3200 RPM. With the governor set to 3600 RPM, the engine is capable of applying some load at 3200 RPM, but not the peak output. For the production engine with the mechanical governor and carburetor, the droop was found to be approx. 15%.

**3.3.3. EFI System.** During previous work done by UMR [2], an electronic fuel injection system has been developed for this engine on the vertical shaft engine dynamometer. This system utilizes the speed-density type of approach to control air to fuel (A/F) ratio. This approach is based upon the following relationship:

$$\dot{m}_{air} = \frac{\eta_v V_d P_{man}}{R T_{man}} \tag{28}$$

By knowing the intake air mass for a given engine set point, the mass of the fuel can be found using the target A/F ratio of 12.5. For a fuel injection system, the width of the injection pulse is found by knowing the mass flow rate of the injector and the amount of fuel to be injected.

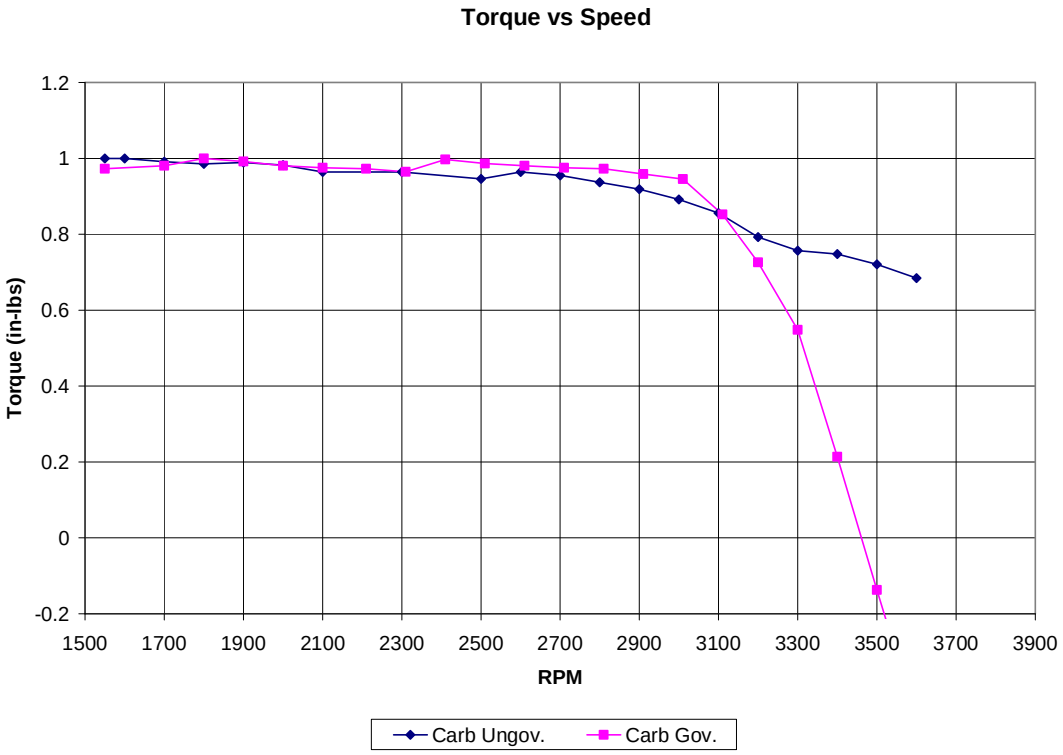


Figure 3.4. Normalized torque curves for governed and ungoverned load curves.

$$PulseWidth = \frac{\dot{m}_{air}}{\dot{m}_{fuel}\frac{A}{F}} \tag{29}$$

Thus, by knowing the intake air pressure, temperature, and volumetric efficiency at a given engine operating point, the constants of displacement, injector flow rate, target A/F ratio, and the gas constant can be use to determine the amount of fuel to be injected at a given set point. The intake air pressure is found by a sensor, as is the intake temperature. The only item left to determine is the volumetric efficiency, and this can be found in the laboratory using a standard flow measuring device such as a laminar flow element.

**3.3.3.1 Determination of Volumetric Efficiency.** The FH680V engine was tested in the laboratory to study the effects of MAP on volumetric efficiency. Figure 3.5 shows a plot of these results. There are two areas of operation, one on the low end of MAP for values below 83 kPa, and MAP pressures higher than 83 kPa.

The effect of engine speed was ignored to simplify the calculation of pulse width. This was done to reduce the number of inputs required to the EFI system, making it cheaper and easier to implement. This assumption was justified by the initial tests that showed volumetric efficiency has a small dependence on engine speed, as represented in figure 3.3.

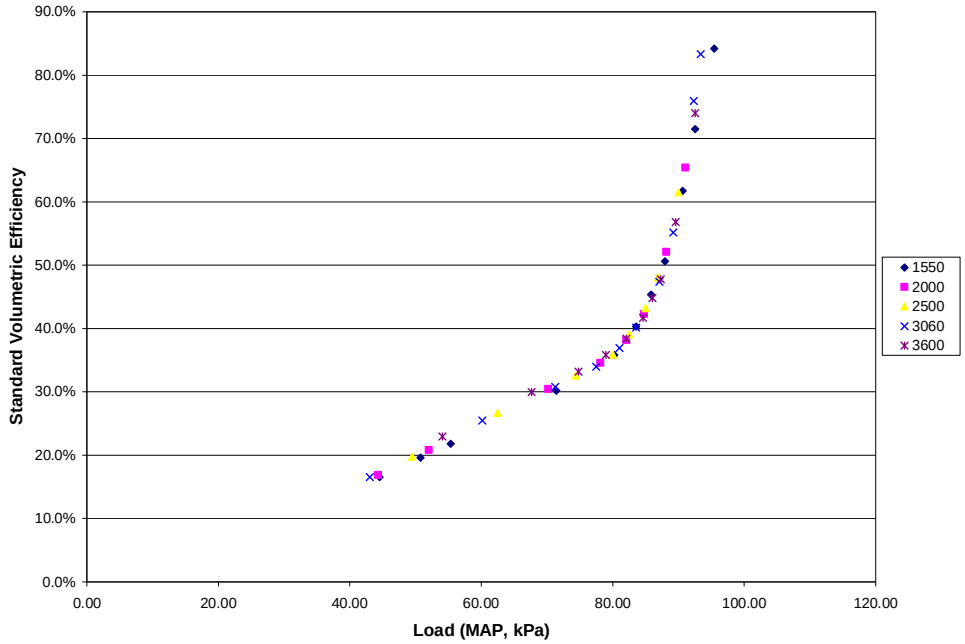


Figure 3.5. Volumetric Efficiency versus Manifold Air Pressure (MAP) [2].

**3.3.3.2 Hardware Implementation.** The basic system layout is a port injection type system. Here, the injectors inject the fuel spray directly on the intake valve. To trigger the injectors, a Hall Effect sensor is used, which in turn is triggered by the flywheel magnet used for spark inductance. This is permanently mounted to the engine, thus the injection timing is constant for every operating point. Figure 3.9 below shows the injection timing versus the valve timing.

A MAP sensor is placed directly behind the throttle plates in the throttle body. A thermistor is used to measure the intake air temperature. This is placed in the intake manifold, and is thermally isolated from the manifold with a polymer insert to reduce the amount of heat transfer received by the sensor. All of these sensors interface with the Engine Control Unit (ECU) which contains the appropriate control program outputs to drive the fuel injectors. Figure 3.6 is a schematic of the system.

**3.3.3.3 Manifold Pressure Sensor Signal Conditioning.** With the V-twin configuration using separate intake runners, the pressure signal in the intake manifold is very cyclic. This can cause issues with the ECU since the moving pressure signal implies a change in mass air flow of the engine. This will in turn cause the A/F ratio to cycle, making the engine unstable. A similar issue was seen by Hendricks et al.. in [25], where they utilized electronic signal conditioning as a solution to this problem.

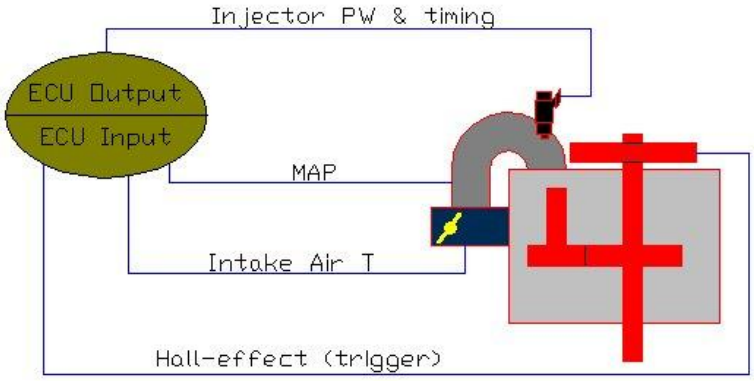


Figure 3.6. Schematic of electronic fuel injection system used in the study [2]

For a simple solution, a 150cc damping volume was introduced between the sensor and the intake manifold. Initially, this volume was made sufficiently large to dampen the signal. But, it was not designed for transient response, so the minimum volume needed to dampen the signal without drastically sacrificing the transient response of the MAP signal was not found on the first iteration.

From here, the task was to create a variable volume that can show the impact of different volumes on the MAP signal and thus the A/F ratio. Five volumes were used and the MAP and A/F ratio signals were logged for a short period of time. The signals are plotted below in Figures 3.7 and 3.8.

Figure 3.7 shows that the smaller the damping volume, the larger the amplitude of the MAP signal. But, even at 146cc, one cannot completely remove the cyclic nature of the signal. The most important aspect of this is the effect this signal has on engine operation, specifically the A/F ratio. The reason the A/F ratio is impacted the more signal damping the system receives is due to a couple of factors. One is the reaction time of the EFI system. With a large pressure change of almost 14 kPa for 18cc volume, the EFI system modulates the pulse width to suit these different signal levels. But, in reality, the actual airflow is between the two values, driving the errors into the system.

The other factor has to deal with the nature of the EFI system. The system reads MAP values at a rate of 20MHz, and it keeps a rolling average of these for use on the pulse width calculation. But, as the system is interrupted to deliver fuel every revolution, those values are dropped and new ones replace them. With the high speed of the signal sampling, a small portion of the overall signal is utilized. One tenth of 20 MHz is 5 x 10^-7 seconds, or about 0.5 milliseconds of data for the ten MAP values used. The largest signal period is on the order of 0.1 seconds, or 100 milliseconds, a thousand times larger. With such a small sample of the overall wave, the averaging is somewhat ineffective without additional sample signal conditioning.

Along with MAP, A/F ratio was logged for each volume, and it is shown in Figure 3.8. While not cyclic in nature, there is a noticeable difference between the nominal value produced by the smallest volume, 18cc, and the next largest volume of 44cc. From that point, there are small variations, but not on the order of the difference between 44cc and 18cc. By using a volume between 44cc and 145cc, we can eliminate much of the impact of MAP signal oscillations on engine operation. The impact of the signal damping must be minimized on transient response, so the smallest volume should be used, ideally 45-50cc.

For packaging purposes, an alternative to the volume is the use of an orifice to dampen the pressure waves. This gives a much smaller solution, but yields similar results to the damping volume. Three different orifices were tested to see which size gave similar results to the 50cc surge tank. The sizes were 0.004 inches, 0.008 inches, and 0.015 inches.

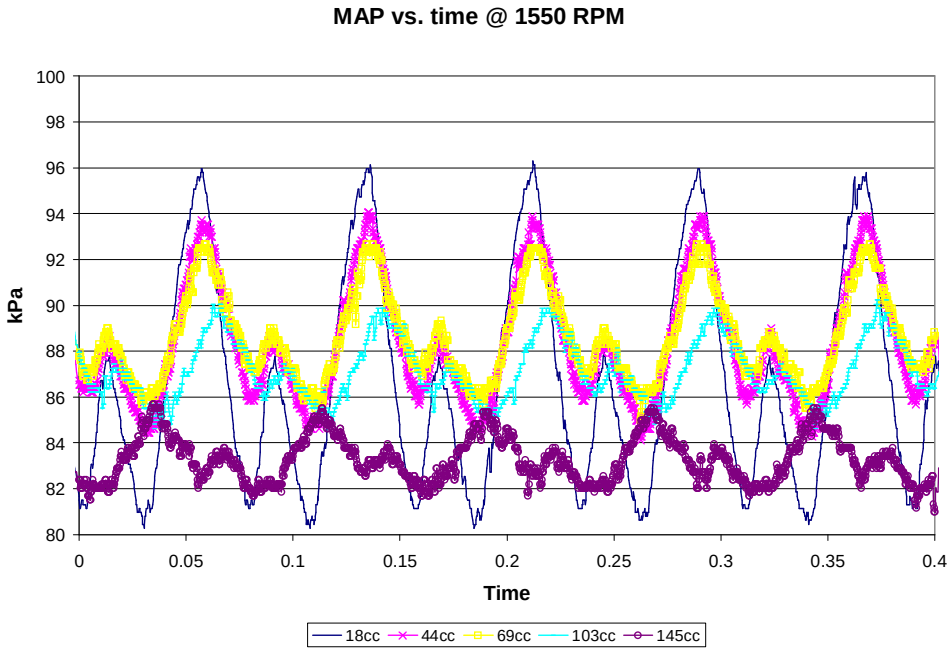


Figure 3.7. MAP versus time for varying pressure damper volumes at 1550 RPM, wide open throttle

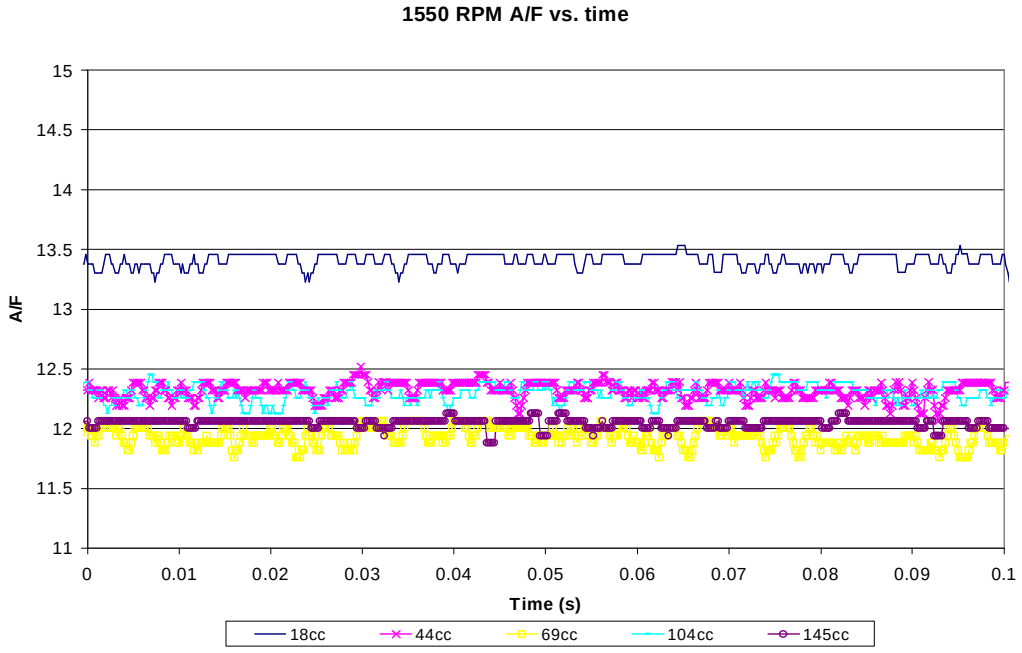


Figure 3.8. Steady State Air/Fuel (A/F) Ratio signal for the various pressure damping volumes

Figure 3.9 shows the steady state damping characteristics of the orifices. As one can see, the smaller the orifice, the more damping the signal receives. At 0.004 inches, the signal is very flat, much more than the 146cc damping volume. At 0.015 inches, the signal for the MAP is damped more than the 68cc volume, making the effective equal damping volumes between 68cc and 150cc.

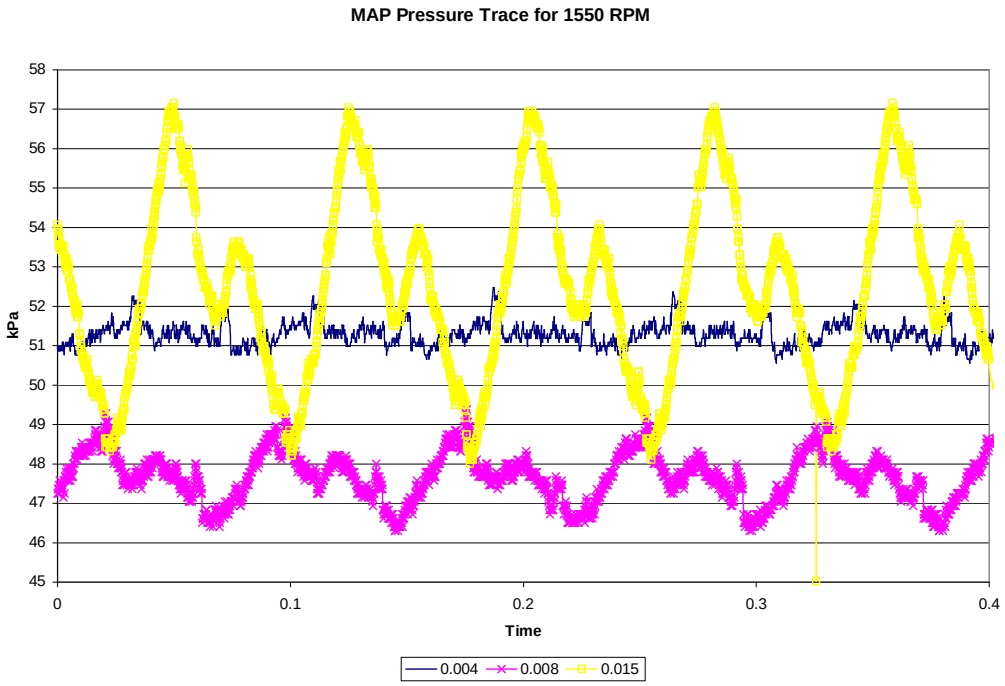


Figure 3.9. MAP trace for pressure damping orifices.

Figure 3.10 shows the A/F ratio plot for the orifices. Discounting the large negative spike in the 0.015 data (system noise), it seems the 0.004 and 0.008 inch orifices keep the A/F ratio at a richer level, and right on the target A/F ratio of 12.5. The 0.015 inch orifice keeps it an entire 0.5 higher.

For this system, a compromise between the two extremes was made. The 0.008 inch orifice was used for the MAP signal damping because it gave good steady state A/F ratio control, but it allows more flexibility for transient testing in the future.

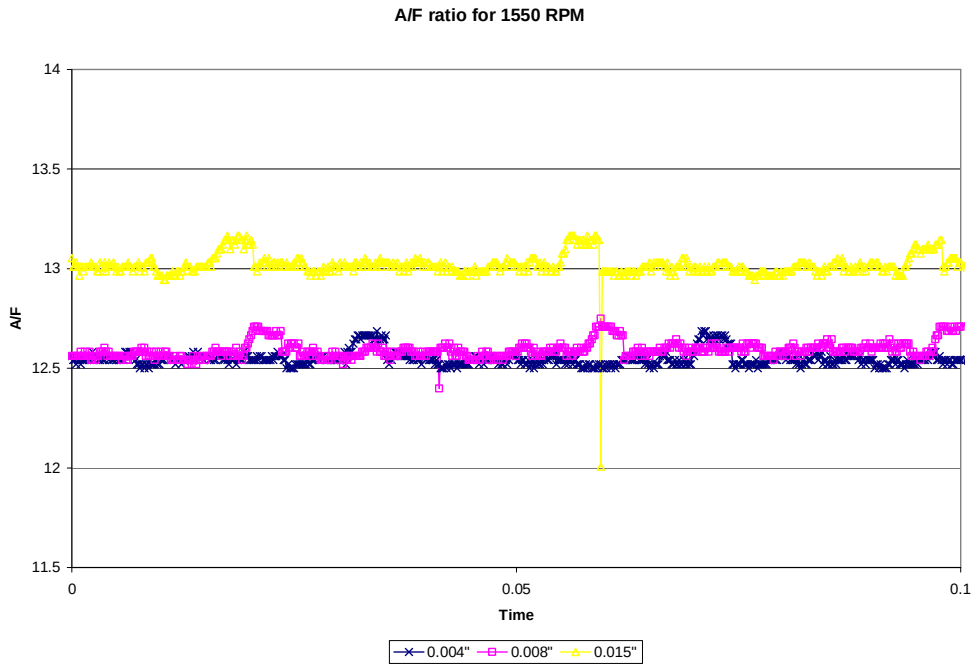


Figure 3.10. Steady State A/F ratio traces for the pressure damping orifices.

**3.3.3.4 Hall Effect Sensor.** The Hall Effect (HE) sensor is mounted next to the flywheel. When the flywheel magnet comes into the proximity of the sensor, the sensor triggers a voltage signal that is detected by the ECU. The sensor is mounted at 134° after TDC, and the magnet is 14 CAD wide. The HE sensor sends a negative square wave, and the triggering is set for a positive voltage rise. So, the actual injection timing is at 147° ATDC, at the end of the magnet.

The location of the HE sensor was selected to give the best timing strategy. The injection timing is triggered directly from the HE sensor signal, so there is only processor delay between the initial pass of the magnet to the sensor. The location of the sensor relative to TDC of the cylinders sets the injection timing of the system.

Figure 3.11 shows the injection timing compared to the intake valve opening events for an entire cycle. This system utilizes a simultaneous injection strategy where both injectors fire at once. Since the trigger is based upon the crank position, not the camshaft position, there are two HE signals, thus two injector pulses per cycle. Additionally, Figure 3.11 shows the timing of arrival of the fuel onto the intake valve surface for 1550 and 3600 RPM.

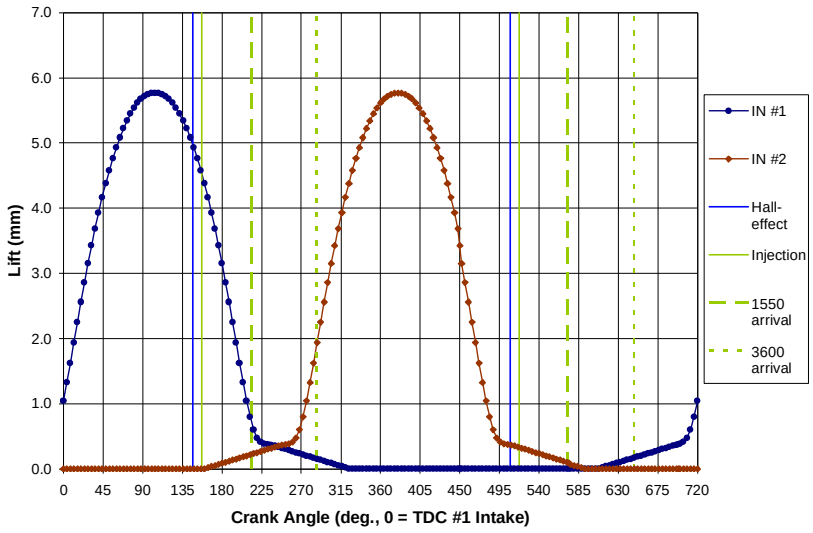


Figure 3.11. Injection Timing relative to intake valve timing and the Hall Effect Sensor [2]

**3.3.3.5 EFI Controller.** The controller consists of a microchip processor containing the EFI control software and appropriate interfaces to the sensors and injectors. The chip utilized in this system is a PIC16F876A-I/SS that is used to modulate the injectors based upon sensor inputs. The basic control algorithm and code will be covered to give a full understanding of how the system operates.

**3.3.3.5.1 EFI Algorithm** The basic control approach is outlined in Figure 3.12. The system operates in a continuous loop that is interrupted by the Hall Effect sensor. The system then goes through the interrupt routine and returns to the main control loop. The interrupt loop is what initializes the injectors and opens them for the appropriate amount of time. This is shown in Figure 3.13.

**3.3.3.5.2 EFI Fuel Map.** The fuel map is the preprogrammed injector pulse width for each respective temperature and MAP. This map acts as a two dimensional table, with the locations determined by the temperatures and MAP values. The temperatures are on a 10°C step from -30°C to 50°C. The MAP values are stepped every 0.426 kPa, which corresponds to one binary bit when the analog signal is converted to an 8 bit binary scale. The lookup is done to the closest value that is lower than the measured value. So, even at 39°, it uses the 30° value, not 40°.

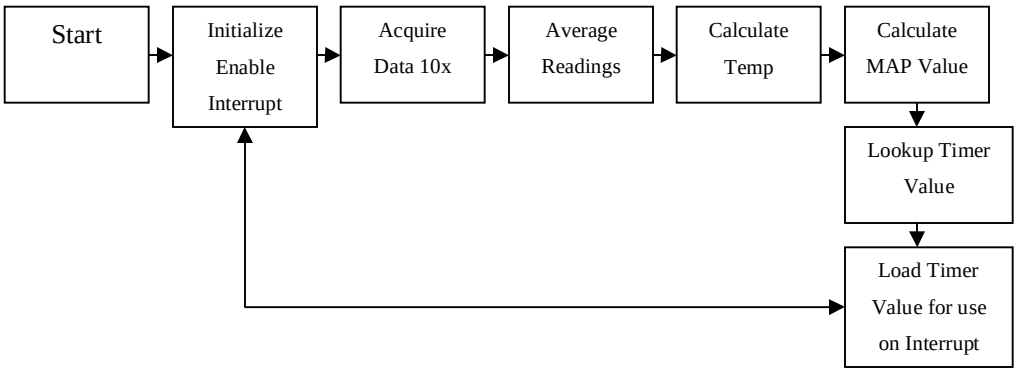


Figure 3.12. Main EFI program loop

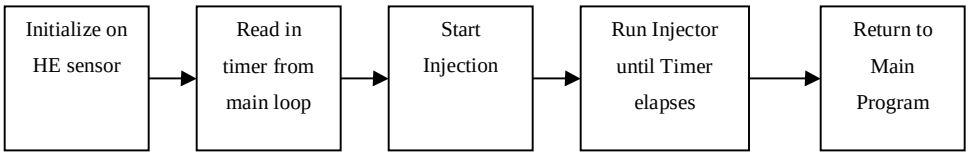


Figure 3.13. EFI Interrupt Loop

The map was developed base upon a data from a single ambient temperature and varying engine load at a specific speed. The pulse widths are scaled to 0°C based on a square root of the absolute temperature in K. A curve fit for the pulse width as a function of MAP is found for the zero scaled pulse widths, and the pulse width is found for each MAP value in the fuel map. This is the final fuel map that is then converted to the necessary syntax for the chip to use.

Below is an example of the fuel map. The top horizontal axis is the temperature in °C, and the far left vertical axis is the MAP in kPa. In this case, the external temperature is 15°C, and the engine is running at 45 kPa MAP. Follow the red line for the MAP value, and the yellow column for the intake temperature. Where these two meet at the orange box is the pulse width for this set point, which is 3.762 ms.

Table 3.5. Fuel Map Example for 15°C and 45 kPa

| MAP, kPa | Temperature, °C -30 | -20 | -10 | 0 | 10 | 20 |
|---|---|---|---|---|---|---|
| 42.46936 | 3.747905 | 3.673089 | 3.602582 | 3.535985 | 3.47295 | 3.41317 |
| 42.89488 | 3.802041 | 3.726145 | 3.654619 | 3.58706 | 3.523115 | 3.462471 |
| 43.3204 | 3.855312 | 3.778352 | 3.705824 | 3.637319 | 3.572477 | 3.510984 |
| 43.74592 | 3.90774 | 3.829733 | 3.756219 | 3.686782 | 3.621058 | 3.558729 |
| 44.17143 | 3.959344 | 3.880307 | 3.805822 | 3.735468 | 3.668877 | 3.605725 |
| 44.59695 | 4.010148 | 3.930097 | 3.854656 | 3.783399 | 3.715954 | 3.651991 |
| 45.02247 | 4.060172 | 3.979122 | 3.902741 | 3.830595 | 3.762308 | 3.697547 |
| 45.44798 | 4.109438 | 4.027405 | 3.950096 | 3.877075 | 3.807959 | 3.742413 |
| 45.8735 | 4.157967 | 4.074965 | 3.996743 | 3.92286 | 3.852928 | 3.786608 |

**3.3.3.5.3 Fuel Map Refinement.** Much of the latest work on the EFI system has been spent on refining this table to deliver the A/F ratio targets for the EFI system. The first version, version 1.2, and the final version, 1.72, of the fuel map are explained.

Initially, a fuel map was built based only upon a measure of the volumetric efficiency of the engine. Efficiency measurements were made at different engine speeds, and the results are plotted in figure 3.1. As mentioned earlier, the volumetric efficiency is mostly a function of MAP, and the engine speed was removed from the equation for simplification.

For further simplicity, the equation for PW was taken to the point where no calculations are needed in the program. Since the only two true variables are MAP and intake temperature, the pulse width map can be built based only upon those values. A basic lookup is then put together for use in the program code as described in table 3.1.

Version 1.2 builds the fuel map where the engine would operate. After a complete test, the A/F ratio is shown in Figure 3.14. Note that there are inconsistencies in A/F ratio between MAPs at similar engine speeds, with the A/F ratio decreasing with increasing engine speed. Also, there are inconsistencies between engine speeds, which are contradictory to the previous assumption that engine speed does not impact volumetric efficiency.

The results show volumetric efficiency is slightly impacted by engine speed. While not on the order of MAP, it impacts the mass flow of air enough to drive the A/F ratio lower as engine speed is increased (at MAPs over 50 kPa). While this can lead to a decreasing A/F ratio, the system can be tuned to minimize the impact by maintaining a steady A/F ratio for each speed over the MAP range.

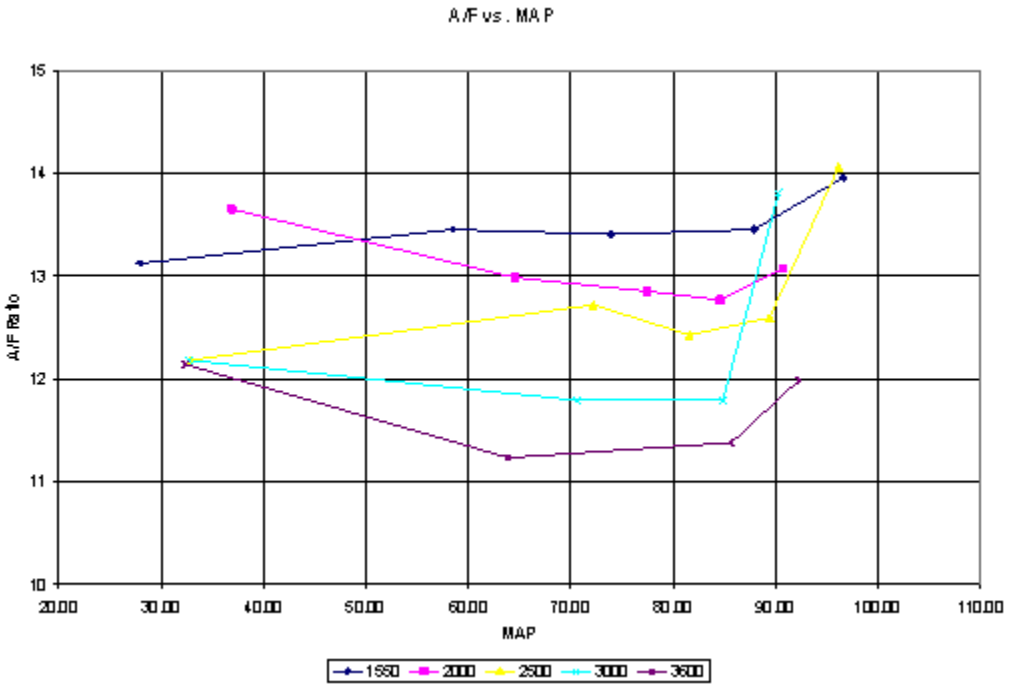


Figure 3.14. Steady State A/F Ratio response for EFI version 1.2 at various engine speeds and MAP settings.

From version 1.2, numerous changes were made. The final version was 1.72. This version was based upon a set of tests performed by a laboratory injector driver called DAVID. The pulse width was found that gave an A/F ratio of 12.5:1 over a range of MAP values. Since the control does not have any sort of compensation for engine speed, a speed of 2800 RPM was chosen for this testing. This was used since it is in the middle of the normal operating range of 2400 thru 3200 RPM, and the spread of the A/F ratio would put the normal operating range within the closest tolerance of the 12.5:1 target.

At low load settings, the lowest engine speed of 1550 was used as the baseline engine speed for tuning. This is the low speed idle set point and the engine must have a smooth idle without risk of overheating. From 20kPa to 45kPa, the fuel map was tuned for a target A/F ratio of 12.5:1 at this speed. The pulse widths were then adjusted to blend them to the 2800RPM data to give a smooth fuel map curve and remove discontinuities in the transition zones of the fuel map.

For these tests, a correlation between engine speeds and loads was determined that stated the typical loads at which the engine was run. For 5 different engine speeds, 1550, 2000, 2400, 2800, and 3200 RPM, the typical engine operating points are listed in table 3.2. Note that the engine is usually not run at the highest load settings for 1550 and 2000 RPM. Also, for loads less than 50 kPa, the engine will not maintain higher engine speeds. While these set points have been tested, they do not represent realistic operating conditions for this engine.

Table 3.6. Engine Speeds and Normal Load Conditions

| Speed | Low MAP Level | High MAP Level |
|---|---|---|
| 1550 | Fully Closed | 45 kPa |
| 2000 | Fully Closed | 75 kPa |
| 2400 | 40 kPa | WOT |
| 2800 | 55 kPa | WOT |
| 3200 | 55 kPa | WOT |

Figure 3.15 shows the final A/F ratio test. Considering the operating conditions listed in table 3.6, this chart is broken into a low load region of under 50 kPa MAP, and a high load region of more than 50 kPa MAP.

At the lower load conditions, 1550 and 2000 RPM are the most important values. 2400 RPM will be a transition speed as the engine goes from low speed idle to higher speed idle. Also, at low loads, the speed may drop to the low range during operation.

Therefore, it is important to see how the A/F ratio tracks for the lower speeds as well as the higher speeds.

Considering the low load region of Figure 3.15, there is quite a spread in A/F ratios. However, notice the 1550 case stays within 0.5 of 12.5 thru 55 kPa. This should give good low speed idle operation while ensuring that the engine operates within the target A/F ratio.

With exception of the lowest load point for 2000 RPM, both 2000 and 2400 RPM operate within 1.5 A/F ratios on the lean side, and 1 on the rich side. This should ensure that the transition from low speed idle to high speed idle is smooth and linear.

The high load case shown in Figure 3.15 has a little change over varying loads. But, it does reduce the A/F ratio as speed increases. This can be attributed to increased flow friction within the engine at higher engine speeds, which reduces airflow. The pulse width is based solely upon the MAP and intake temperature, not engine speed. The impact the increased flow friction has on volumetric efficiency is not taken into account, making the intake charge richer than at higher speeds. At this time, there is no provision in the EFI system to account for these losses.

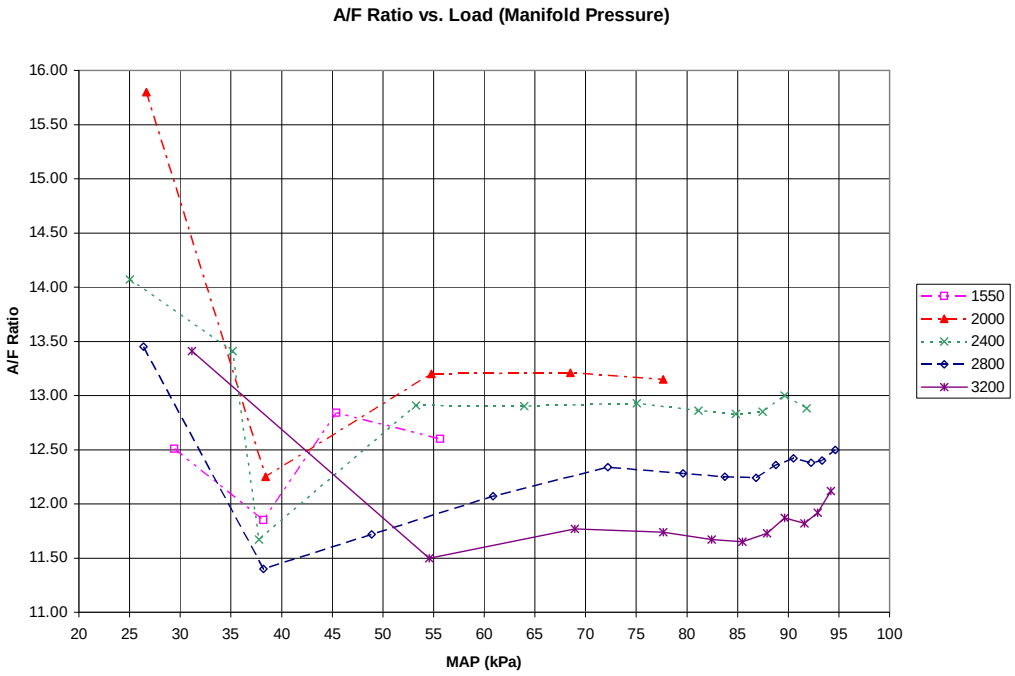


Figure 3.15. Steady State A/F ratio versus MAP for the final fuel map, version 1.72

**3.3.3.5.4 Cylinder Temperature Balance.** One issue with a twin cylinder engine is the balance between the cylinders. If one of the cylinders is producing less power than the other, the engine will run rough and unstable. So, to verify the cylinder balance, exhaust temperature was tracked for each cylinder. While this is not an exact approach (it would be better to measure A/F ratio for each cylinder individually), this does give a good indication of flow distribution and power variability. Figure 3.16 shows the difference in exhaust temperatures over the load and speed range.

Cylinder 1 is higher below 75 kPa, but not alarmingly so. With the exception of a few data points, the cylinders are within 100°F of each other. Above 75 kPa, cylinder 2 is warmer, but not by more than 50°F. With these being so close, especially considering the range of temperatures are between 1200 and 1400 °F, the cylinders seem to have very good balance over the normal operating ranges. This verifies the benefit of the port injection system to maintain a consistent fuel delivery to each cylinder.

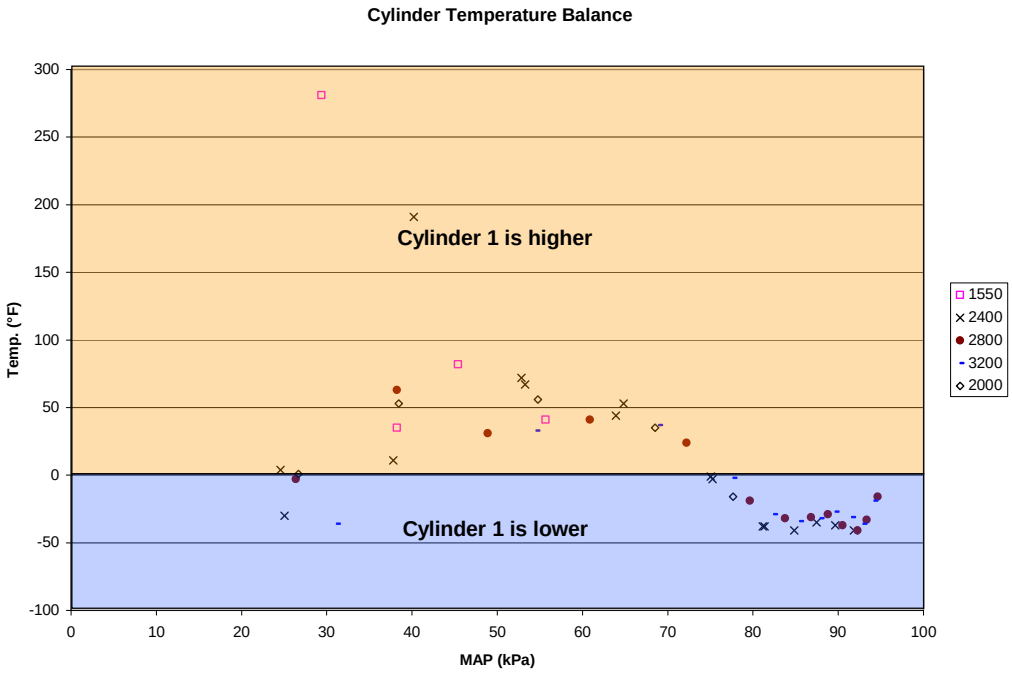


Figure 3.16. Temperature difference between cylinders 1 and 2. Positive temperatures indicate cylinder 1 has a higher temperature.

# 4. CURRENT SYSTEM CAPABILITY

## 4.1. MECHANICAL GOVERNOR WITH CARBURETION

The engine is originally configured with a mechanical governor with a carburetor. This original setup sets the baseline performance by which improvements will be judged.

**4.1.1. Steady State Performance.** For low idle, the most important operation is to be able to maintain smooth engine operation. During low idle operation, the engine was run at idle and the data was logged for 30 seconds. This allows for the calculation of the highest and lowest engine speed during idle, as well as the standard deviation of the idle operation. Table 4.1 below shows the results from the Mechanical Governor set with the Electronic Fuel Injection system installed. The load at which was determined to be the torque curve is listed in the table as well for reference. Note that the droop percentage increases as load is increased, following the slope of the governor curve. Also, the high idle was set to both 3600 and 3200 RPM for the testing.

Figure 4.1 below shows the plots of the mechanical governor tests using the carburetor. The exact point where the torque curve meets the droop curve, or the breakaway point, is not easily found. Instead, a load target is used for comparison, and this gives a consistent point to compare the respective droop curves for all operation. Both the curves exhibit similar slopes, as their droop values are 12.59% for the 3600 RPM high idle and 11.64% for the 3200 RPM high idle at 28 ft-lbs. For the majority of the curve, the slope is similar. Only at the top does it diverge, and this can be attributed to the torque curve meeting the droop curve.

The high idle standard deviation for the data sampled is 22 RPM, and the high load standard deviation is 14 RPM.

**4.1.2. Transient Performance.** The transient tests outlined in table 3.6 were performed on this engine with the high idle set to 3600 RPM. During the positive load transient tests 1 through 3, the engine speed remained stable and did not incorporate any detectable over or undershoot. However, the final speed at the end of the load step does correspond to a lower engine speed, as would be concluded from the droop curves shown above. With increasing load acceptance rate, the rate speed drops down the droop

Table 4.1: Mechanical Governor results for both the carburetor and EFI induction systems

| | **High Speed Idle** | **Speed at Load** | **Load Target** | **Speed Error** | **% Droop** |
|---|---|---|---|---|---|
| | *RPM* | *RPM* | *ft-lbs* | *RPM* | |
| Mech. EFI 3600 | 3590 | 3480 | 10.0 | 110 | 3.06% |
| Mech EFI 3200 | 3269 | 3127 | 10.0 | 142 | 4.36% |
| Mech Carb 3600 | 3570 | 3462 | 10.0 | 108 | 3.04% |
| Mech Carb 3200 | 3213 | 3081 | 10.0 | 131 | 4.09% |
| | | | | | |
| Mech. EFI 3600 | 3590 | 3437 | 15.0 | 153 | 4.27% |
| Mech EFI 3200 | 3269 | 3039 | 15.0 | 230 | 7.04% |
| Mech Carb 3600 | 3570 | 3417 | 15.0 | 153 | 4.27% |
| Mech Carb 3200 | 3213 | 3032 | 15.0 | 181 | 5.63% |
| | | | | | |
| Mech. EFI 3600 | 3590 | 3370 | 20.0 | 220 | 6.13% |
| Mech EFI 3200 | 3269 | 2981 | 20.0 | 288 | 8.82% |
| Mech Carb 3600 | 3570 | 3337 | 20.0 | 233 | 6.53% |
| Mech Carb 3200 | 3213 | 2977 | 20.0 | 235 | 7.32% |
| | | | | | |
| Mech. EFI 3600 | 3590 | 3285 | 25.0 | 305 | 8.48% |
| Mech EFI 3200 | 3269 | 2818 | 25.0 | 451 | 13.80% |
| Mech Carb 3600 | 3570 | 3233 | 25.0 | 337 | 9.43% |
| Mech Carb 3200 | 3213 | 2895 | 25.0 | 317 | 9.87% |
| | | | | | |
| Mech. EFI 3600 | 3590 | 3201 | 28.0 | 389 | 10.85% |
| Mech EFI 3200 | 3269 | 2804 | 28.0 | 465 | 14.22% |
| Mech Carb 3600 | 3570 | 3121 | 28.0 | 449 | 12.59% |
| Mech Carb 3200 | 3213 | 2839 | 28.0 | 374 | 11.64% |
| | | | | | |
| Mech. EFI 3600 | 3590 | 3068 | 30.0 | 522 | 14.54% |
| Mech EFI 3200 | 3269 | 2743 | 30.0 | 526 | 16.08% |
| Mech Carb 3600 | 3570 | 2857 | 30.0 | 713 | 19.98% |
| Mech Carb 3200 | 3213 | 2771 | 30.0 | 441 | 13.74% |

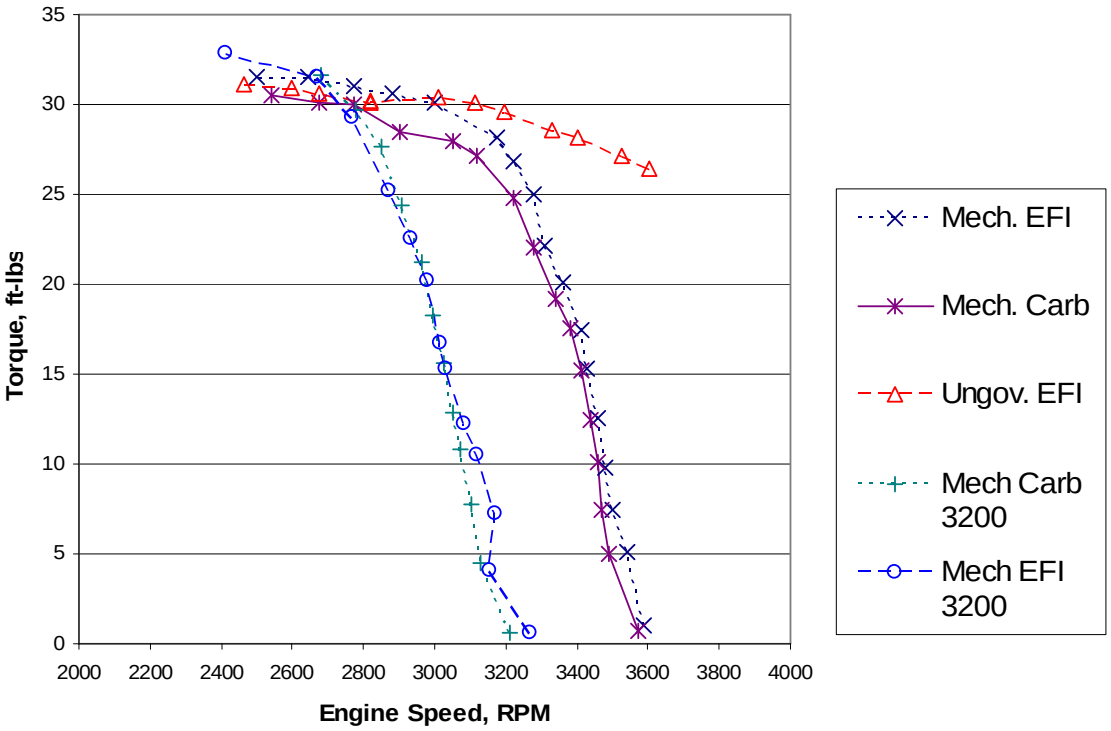


Figure 4.1: Mechanical governor droop curves for the carbureted and EFI versions of the engine. Note the ungoverned EFI curve is presented for reference.

curve changes, but the performance characteristics are very similar with differing load acceptance rates. The speed response for these load acceptance tests are shown in figure 4.2.

During negative throttle transients (load is removed from the engine), the tolerance stack up and mechanical slop can be seen in the speed response. During test 4, as load is removed, the speed increases. There is an over-under shoot characteristic for this as the load reduction promotes acceleration and the governor must "catch" it along the governor droop curve. This could be a characteristic of the mechanical linkage "slop" due to tolerances in such a mechanism. Figure 4.3 shows the speed response for this test and tests 5 and 6.

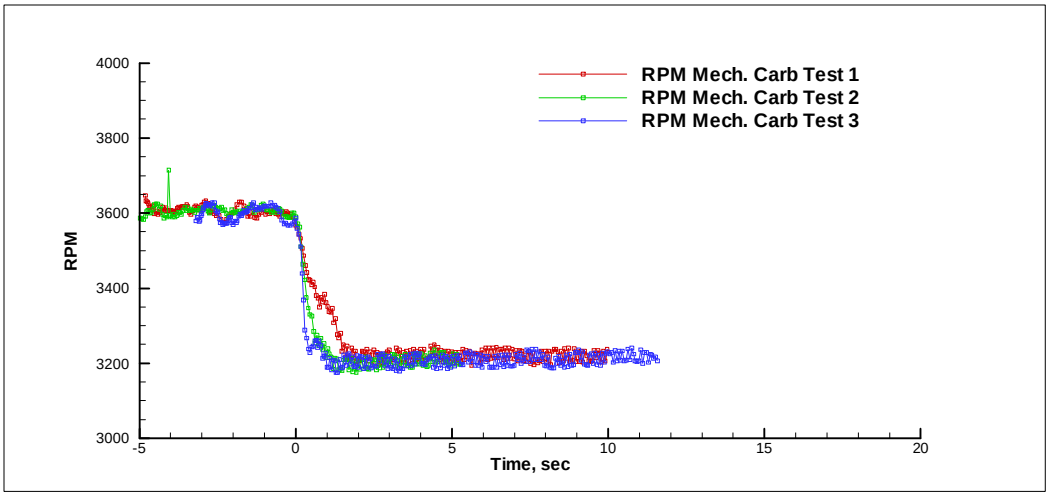


Figure 4.2: Speed trace during positive load acceptance test for the mechanical governor with a carbureted engine.

During negative throttle transients (load is removed from the engine), the tolerance stack up and mechanical slop can be seen in the speed response. During test 4, as load is removed, the speed increases. There is an over-under shoot characteristic for this as the load reduction promotes acceleration and the governor must "catch" it along the governor droop curve. This could be a characteristic of the mechanical linkage "slop" due to tolerances in such a mechanism. Figure 4.3 shows the speed response for this test and tests 5 and 6.

There is also an over shoot and slight instability seen in the two seconds of the test. As load rate is increased, this overshoot increases, however it stabilizes to the desired high idle speed in 2.5 seconds. The load trace for these tests is plotted in figure 4.4, and the differing load reduction rates can easily be seen. Note the load reduction is smooth with little to no overshoot.

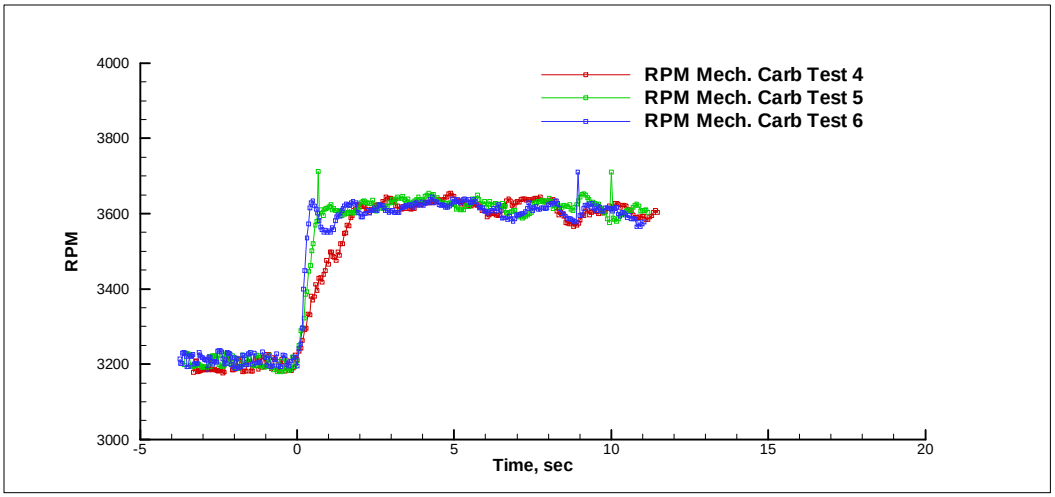


Figure 4.3: Speed response for the mechanical governor with a carburetor on negative load transients 4 through 6.

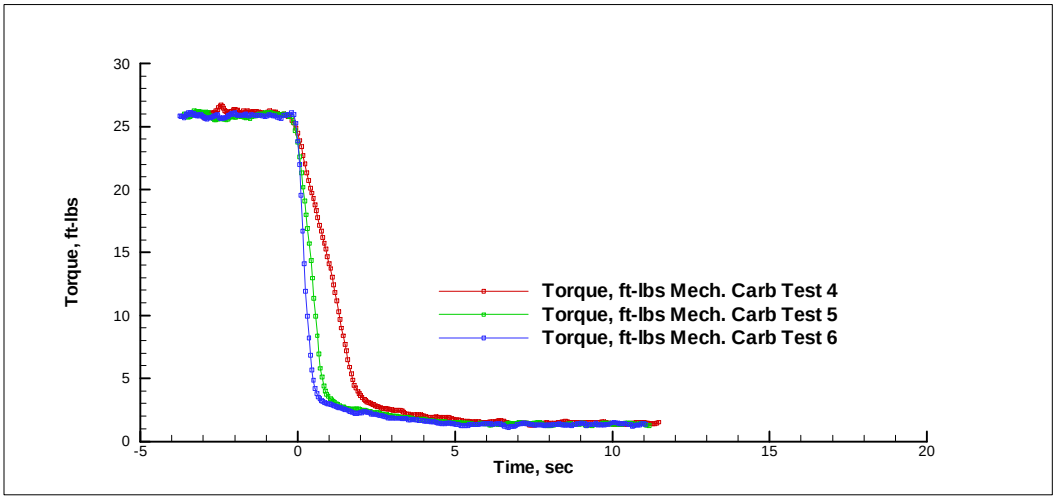


Figure 4.4: Load trace for negative load transient tests 4 through 6 with the mechanical governor and the carburetor

The impact of varying load starting points and load acceptance rates during positive load acceptance tests is seen from tests 7 through 12. These tests agree with the results of the first six tests. The varying load starting points does not improve or reduce the level of performance. On the contrary, it is nearly transparent as the engine starts at a

lower speed (as dictated by the droop curve), and has a shorter distance to travel before the torque curve is reached.

## 4.2. EVALUATION OF THE MECHANICAL GOVERNOR WITH THE EFI SYSTEM

The next step in the evaluation of the engine is to consider the performance of the engine with the EFI system installed with the mechanical governor. By comparing this to the mechanical governor with the carburetor, the impacts of the EFI system on performance can be seen.

**4.2.1. Steady State Performance.** The EFI system has little impact on the steady state operation of the engine when coupled to the mechanical governor. The steady state droop curves, for both the 3200 and 3600 high idle set points, follow the same slope as the carburetor. The governor curves are plotted in figure 4.1, along with the ungoverned torque curve using the EFI system. The droop at 28 ft-lbs is 10.8% for the 3600 RPM high idle and 14.2% for the 3200 RPM high idle points. The standard deviation of the high idle is 13 RPM and for the rated load (with the 3600 RPM governor setting) is 16 RPM, both of which are very close to the carbureted version.

**4.2.2. Transient Performance.** The EFI system has a significant impact on the transient performance of the engine when compared to the carbureted version. The poor performance from the EFI system during positive throttle transients causes the engine torque output to drop during the transient, reducing the engine speed to drop to satisfy the load requirements of the dyno with rotational inertia. The governor reacts by opening the throttle, and the speed then recovers.

Figure 4.5 shows the speed trace for transient tests 1 through 3. For the positive throttle transients, the larger the load application rate, the larger the speed undershoot. Figure 4.5 shows the A/F ratio traces for these tests as well, and the faster the load application rate, the larger the A/F ratio spike. This also corresponds with a faster MAP increase, and is shown in Figure 4.6. This follows from the manifold filling dynamic described earlier where the time for the manifold filling event is based on the throttle opening rate, so as the load rate is increased, the throttle is opened faster, and there is a larger A/F ratio spike. However, with the faster application of load, the engine has less

time to recover and meet the loading requirements of the dyno, causing speed to decrease further.

The impact load rate has on settling time is less apparent. At the slower load rate in test 1, the speed does not drop below its final stable value, but instead jumps higher. At this point, the manifold filling dynamic has less of an impact on the speed reduction due to the slow application of load, however the throttle is opened too far for the point on the droop curve, and the engine speed increases, so the governor pulls the throttle closed for a short period before it finally stabilizes at the wide open condition. However, once the load application rate is increased, the manifold filling dynamic takes precedent and the stabilization times are consistent. Without the speed oscillation seen in test 1, the settling time is shorter, and is not impacted by application rate.

The load starting point does have an impact, again due to the dependence of manifold filling has in the change in MAP (or torque). As load starting point is increased, the amount MAP changes decreases, and the total A/F ratio spike is decreased, and the speed undershoot is reduced. If the starting load is high enough, the speed undershoot is not seen, nor is the A/F ratio spike. This can be seen by comparing the traces for the A/F ratio and engine speed in Figure 4.7 below.

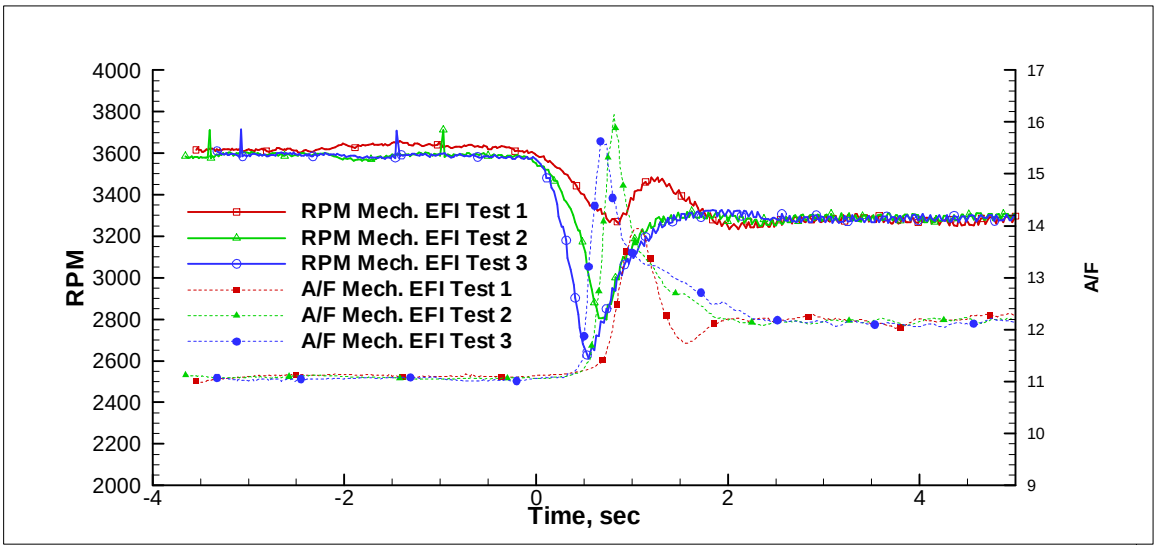


Figure 4.5: RPM and A/F ratio for transient tests 1 through 3 for the mechanical governor with the EFI system

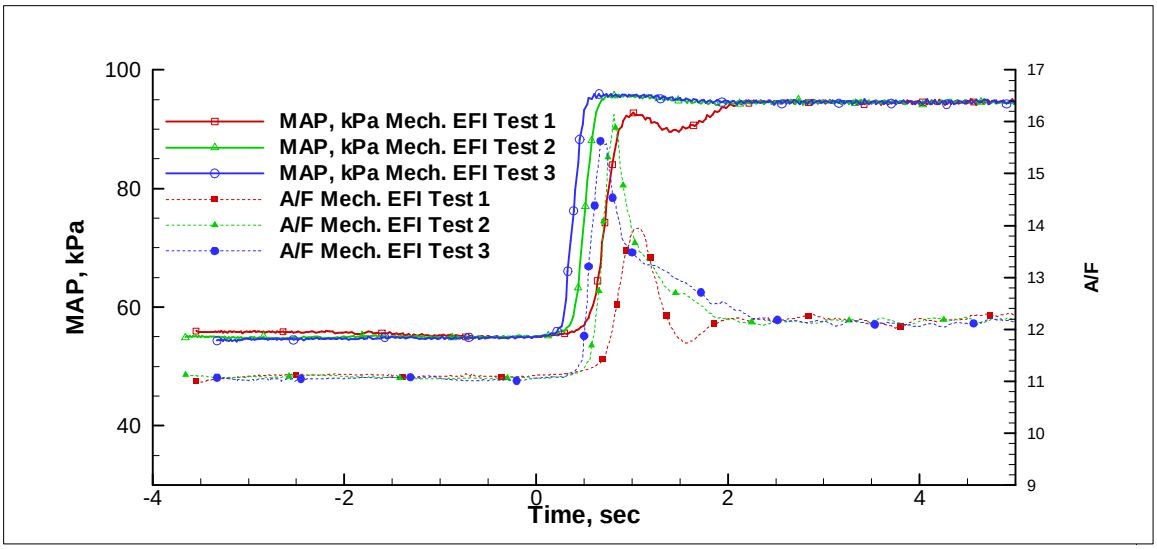


Figure 4.6: MAP and A/F ratio for transient tests 1 through 3 for the mechanical governor with the EFI system

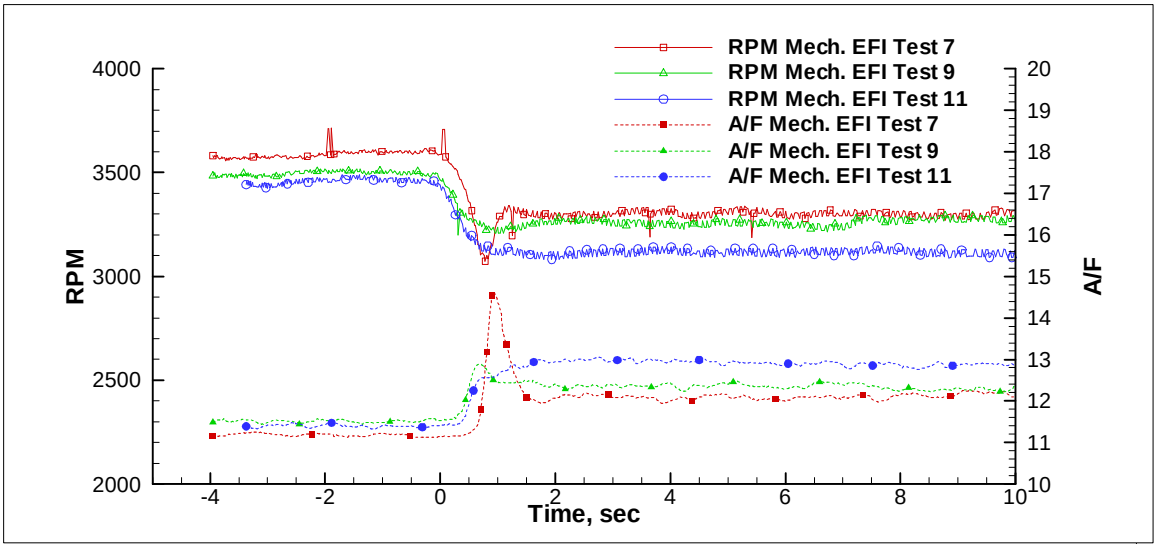


Figure 4.7: RPM and A/F ratio traces for transient tests 7, 9, and 11. All these tests have the same load application rate, but have differing initial torques.

Negative speed transients behave in a similar manner as the carbureted engine with the mechanical governor. The speed settles in 2.5 to 3 seconds, and there is some

overshoot, which is dependent on load reduction rate. The mechanical tolerances associated with the flyweight and linkages, as well as the inertial forces needed for the system to react to speed changes cause this overshoot, and there seem to be no significant impacts from the EFI system during these speed and load transients.

**4.2.2.1 EFI system transient dynamics.** In addition to the TCS system, the transient performance of the EFI system needs to be considered as it will have a large impact on the system response. As Hendricks described, the transient response of a port fuel injection system is very different from the production carburetor used by this engine. These responses must be kept in mind when considering the performance of the electronic throttle system, and how it is reacting to the system changes of both load and speed [24], [25].

To characterize the EFI system's impacts on the engine system, throttle perturbations were used at set rates. While many studies determined that fuel perturbations made the fuel film analysis more straightforward [24],[23],[30], the use of a production ECU did not allow for this type of test. Instead, throttle perturbations were done at differing rates, endpoints, and directions.

With the limited amount of data taken, the complexities of the fuel injection system are not always separable. Manifold dynamics and fuel film dynamics were considered in conjunction, and this does complicate the analysis. However, correction or compensation techniques described above [20] are not utilized, so the net impact of both subsystems is the critical issue. The A/F ratio data includes both fuel and air dynamics, as well as transport and sensor delays. The manifold air pressure is tied to the signal damping orifice and the ECU and DAQ computer processing delays, and the air dynamics of the engine, throttle, and manifold. Volumetric efficiency data previously taken on the vertical shaft engine is used in conjunction with equation 28.

**4.2.2.1.1 <u>EFI Transient Performance Impacts.</u>** With the system utilizing a previously designed EFI system, improvements or changes to the overall system were out of the scope of this project. As a result, the impacts the current EFI system has on the engine during transient operation needs to be understood. Figure 4.8 shows the A/F transient track over time for a positive throttle transient, and it includes engine speed and the carburetor speed trace for reference. The A/F transient to the positive end develops

after the load input begins. The load is applied, the speed drops, and the throttle opens. There is a small delay until the pressure changes, and the signal is sent to the EFI computer. The A/F ratio increases dramatically, causing the speed to drop even further. The governor mechanism then responds by opening the throttle, thus increasing engine speed. The engine speed settles at the portion of the droop curve set for this load, in this case ~3300 RPM.

Figure 4.8 also shows the speed trace for the same test with the carburetor induction system with the same mechanical governor. Note that the speed does not drop, but rather it settles quickly to the droop curve setting. From this it is apparent that the EFI system involves transient dynamics not present in the original induction system, and these dynamics.

An important aspect of this relationship is the effect on A/F ratio has throttle position and manifold pressure change. During a positive load increase, the high A/F ratio excursion can cause lean conditions in the cylinder for a short period of time. This can cause the engine to reduce the torque output for a brief period, causing the throttle position to overshoot the position it would hold on a normal steady state basis. For this type of disturbance, the engine responds to throttle position changes on a longer time scale. This is evidenced in Figure 4.9 [25].

As shown, the performance of the governor will be impacted by the use of the EFI system. With the use of the models presented earlier, a more detailed picture of the system dynamics can be shown.

**4.2.2.1.2 <u>Throttle Airflow.</u>** The airflow past the throttle is derived from the manifold pressure data signal, the throttle position, and the throttle flow calculation derived by Heywood and presented earlier [14]. Assuming a specific heat ratio of 1.4 for ambient air, the pressure ratio of 0.528 marks the transition from choked flow (ratios higher than 0.528) and unchoked flow. The value used for the discharge coefficient, $C_d$, is calculated as a function of throttle position by using the area ratio between the area and the maximum area using equation 19 [17].

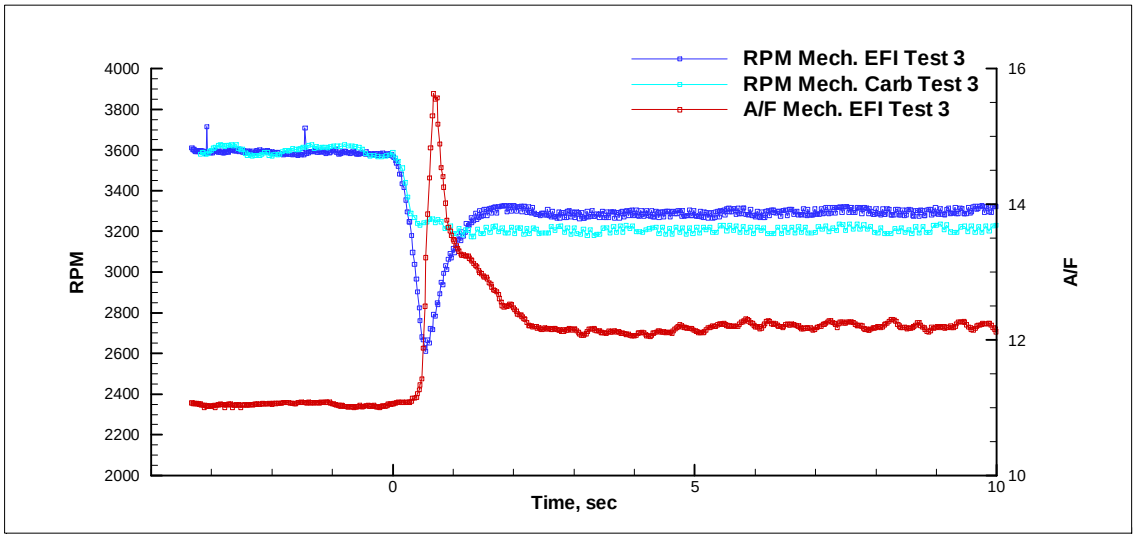


Figure 4.8: Typical plot of A/F ratio and speed for a port injected EFI system during a positive load transient. The speed trace of the same test with a carbureted system in included for reference.

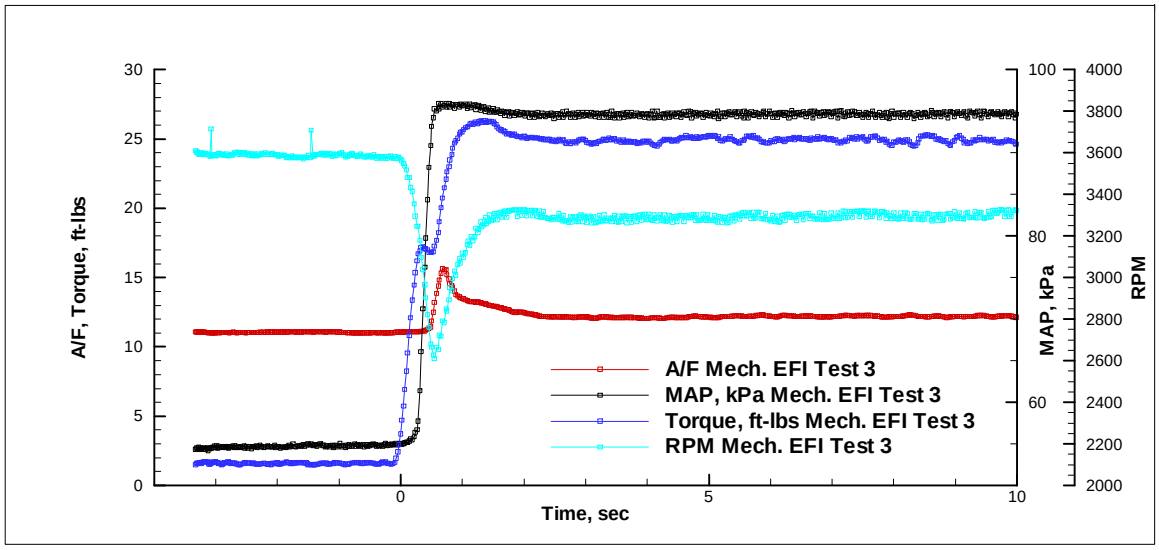


Figure 4.9: Plots of RPM, Torque, MAP, and A/F ratio for a positive load transient in a port injected EFI engine

$$C_d = \frac{A(\alpha)}{A_{\max}} \tag{30}$$

While this is not exact, airflow data was not available to determine this experimentally. Also, this value is independent of manifold pressure, which is contradictory to work done by Blair [15]. However, assuming adiabatic flow through the throttle, this gives a close estimation for the throttle $C_d$ calculation and suits the needs of this analysis.

With a discharge coefficient, air temperature, and the pressure ratio known, equation (2) can be used to calculate throttle airflow for each cylinder (assuming independent manifolds and throttles).

**4.2.2.1.3 Port Airflow.** Port flow is based solely upon equation (25), which utilizes volumetric efficiency, engine speed, displacement volume, and inlet air density. The port airflow measurement becomes a function of volumetric efficiency when the engine constants and intake conditions are measured (and the ideal gas equation is applied). The volumetric efficiency data used is from the EFI system development work done earlier.

**4.2.2.1.4 Airflow Comparison.** At steady state conditions, the port airflow should match the throttle airflow via continuity. If the fuel flow is calculated through the PW tables and the injector flow factor, airflow can be found with the use of the UEGO signal. When this is compared to the throttle and port airflow calculations, the results indicate shortcomings and strengths of the approach taken for each airflow model.

Comparing the port airflow to the fuel flow based airflow, at low throttle openings the fuel flow based numbers are approximately 20% higher than the volumetric efficiency based numbers. The throttle airflow calculations were another 18% higher than the fuel flow based numbers, giving close to 40% higher airflow numbers between throttle airflow and port airflow values at low throttle openings.

The reason for this discrepancy is likely a combination of numerous factors. The volumetric efficiency numbers are likely not accurate at these low throttle positions. The throttle $C_d$ calculation is not complete at these levels as well, driving errors at the lower throttle openings. Also, the throttle leak area is not taken into account for this study, a factor that could be significant at lower throttle openings [17].

As the throttle area increases, the airflow numbers begin to converge. This indicates that at a larger throttle area, the $C_d$ calculation is more accurate, as is the

volumetric efficiency numbers used in the port airflow calculation. There is less than 2% error between the volumetric efficiency and A/F ratio measurements, and less than 4% error between the A/F ratio measurements and the throttle airflow calculation at high loads. The airflow based on fuel flow is not without errors since the fuel flow is calculated from a pulse width and not directly measured, however the close correlation between the three different methods indicate the models used are predictive of behavior in this region of operation.

With the port and throttle plate airflows, the manifold air charging can be seen during positive throttle ramps. The airflow through the port is driven by the manifold and cylinder conditions when the intake valve is open. The mass flow into the manifold is based upon the conditions in the manifold and at the throttle. When the throttle opens, the manifold charges with air as the conditions at the throttle allow for higher airflow then those at the intake port. This can be seen in the plot in Figure 4.10 where the throttle airflow increases dramatically faster than the port airflow and stays above the port flow number for close to a second after the throttle is opened.

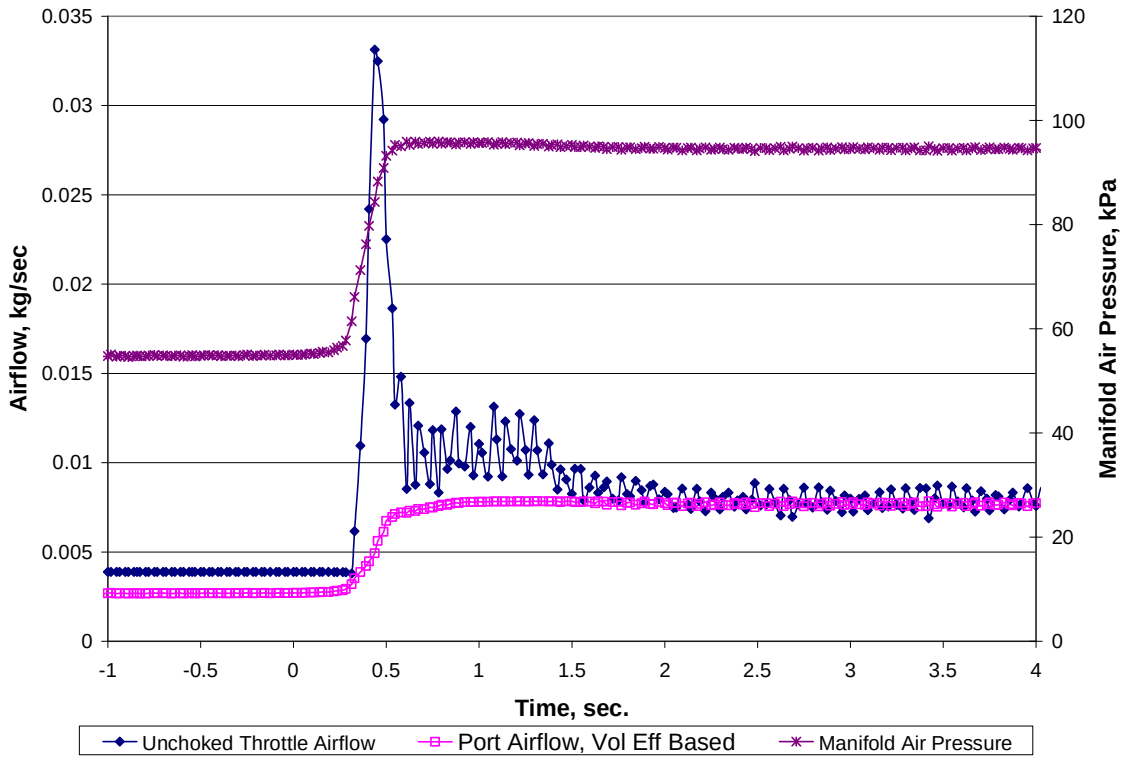


Figure 4.10: Port and throttle airflow with manifold pressure during a positive throttle transient.

The impact the airflow spike has on engine operation can be seen in figures 3.19 and 3.20. Figure 4.11 shows the airflow spike with A/F ratio trace. The duration of the spike in A/F ratio coincides with the duration of the airflow spike, stabilizing within 0.5 A/F ratio in about 1.5 seconds. The peak of the spike is offset the airflow spike by 240 ms, which is close to the expected transport and sensor delays combined [18],[30]. The impact this has on engine operation is shown in Figure 4.11. The EFI system's speed response has a large speed undershoot when compared to the carbureted system, and this happens when the A/F ratio spikes. Given that both systems use the same governor mechanism and settings, this dynamic is exclusively from the EFI system and the manifold filling dynamic associated with it.

**4.2.2.1.5 Fuel Film.** The presence of a fuel film in the intake manifold cannot cannot be directly determined with the testing done in his study. As described by [23], independent fuel perturbations are the most logical manner to determine fuel film presence and characteristics. However, since a production style ECU was used in this study, fuel was not controlled independent of airflow. The manifold charging event can describe the majority of the positive throttle transient A/F ratio spike, so the fuel film dynamics do not have a large impact over these events.

During negative throttle transients, the presence of a film is not a significant contributor to the A/F ratio accuracy. With the combination of changing fuel and airflows during a transient, a film is not easily detected. To truly determine the presence of a film, one must completely remove the airflow dynamics from the data. When that is attempted, the resulting A/F ratio excursion is shown to nearly disappear. Given the geometry of the injector and port design, there is a possibility that no film exists in a fully warm engine. This was also seen by [31] with a similar port and injector design.

However, during engine start and cool running conditions, a significant amount of enrichment (done via the use of air choke plates on the engine) is needed to allow for consistent operation. Once the engine is warm (manifold temperatures above 30°C), these methods are no longer necessary. Given the cold operation characteristics seen in [22], [21], and [23], the presence of a film at these conditions is not only possible, but likely.

As shown , the EFI system, particularly a speed density based port injection system, is nonlinear and difficult to predict. Breaking down the EFI system's impacts on the engine operation, the primary loss during a positive load transient is the speed reduction which is driven by the manifold filling dynamic. This speed reduction, and subsequent loss of power, is currently not compensated, and will be present in any further governor system.

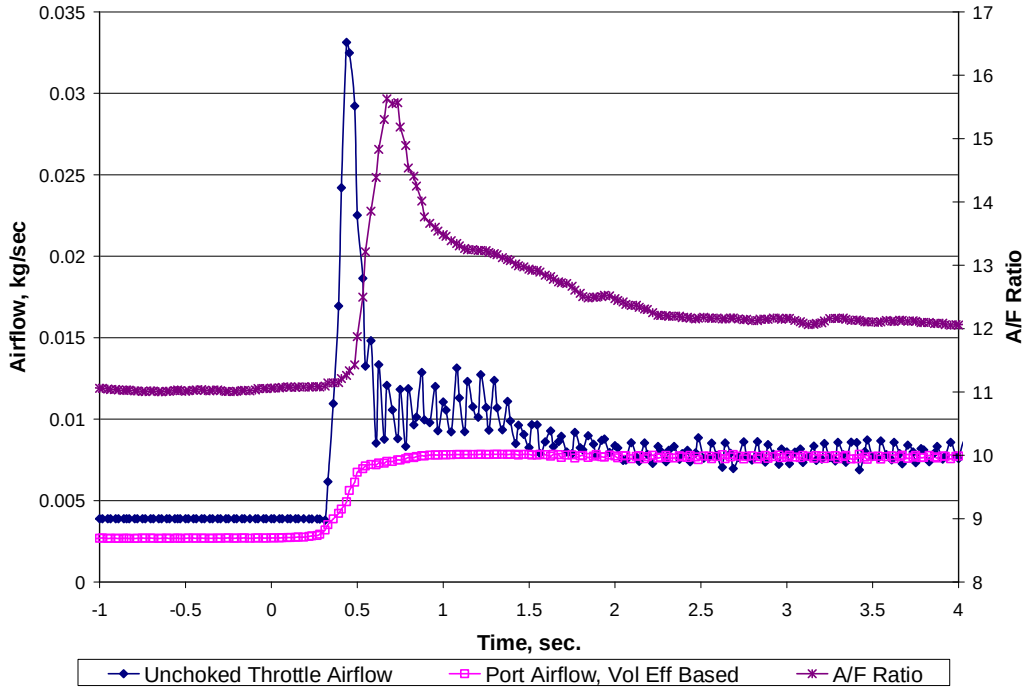


Figure 4.11: A/F Ratio plot and airflows for positive throttle transient

# 5. DESIGN OF NEW GOVERNOR SYSTEM

## 5.1. SYSTEM PERFORMANCE REQUIREMENTS

The purpose of this study is to develop a production oriented electronic governor. This is to enable the engine speed to be controlled to a specific target, while reducing the speed droop from 10-15% to 1-2% of full load rated speed. This governor system should also integrate with the EFI system as previously developed by UMR, while maintaining little to no cost impact over the mechanical governor system it replaces.

## 5.2. DESIGN

In order to meet the performance targets, a number of different governor designs were considered. To grade these designs against each other, seven performance criteria were determined based upon the system requirements listed above. Each design was given a score of 1, 3, or 5 in each category. The criteria were weighted based upon most importance. The criterion and their respective weights are listed in table 5.1

Table 5.1: Design Performance Criteria and their weighting

| Performance Criteria | Weight |
|---|---|
| Cost | 25% |
| Interface | 10% |
| Droop/Governor Performance | 25% |
| Transient Response | 5% |
| Stability | 10% |
| Complexity | 15% |
| Modifications Required to Engine | 10% |

### 5.2.1. DESIGN OPTIONS

**5.2.1.1 Electro hydraulic Actuator driven via fuel injector.** This system is to utilize a fuel injector driven from the same hardware as the EFI system. The system would incorporate a pressure chamber in which fuel or engine oil would be injected at

varying rates to move a spring backed piston. This piston would then be attached to the throttle via a linkage mechanism. A leakage orifice would be used to manage the flow of fluid through the chamber. The chamber pressure, thus the piston location, would then be controlled by regulating the pulse width of the injector.

The working fluid would be either engine oil or fuel. As the new EFI system would already require a high pressure fuel delivery system, this would be a logical choice. However, engine oil could also be used, and the risk of a fuel leak would then be reduced.

**5.2.1.2 Stepper Motor Actuator.** This system would incorporate a stepper motor to control the throttle position via a four bar type linkage that is similar to that currently used in the mechanical governor. This motor would need to have 1-2° steps to ensure that a high amount of precision is available, though a gear reduction system could broaden this requirement of the motor itself. A throttle position sensor would be needed to determine the throttle angle and position feedback. A stepper motor would also require a dedicated controller which may be relatively expensive, depending on the motor type and design.

**5.2.1.3 DC Motor Actuator.** This system would incorporate a DC motor to control the throttle position via a four bar type linkage that is similar to the stepper motor. A gear reduction would be needed to provide adequate precision and torque output from a small, inexpensive motor unit. The control of such a motor could incorporate the PWM output of the ECU, and would require little to no modifications.

**5.2.1.4 Linear Actuator.** This system would incorporate a linear actuator motor to control the throttle position. This linear actuator may be driven via a DC motor or other electronic device to move an actuator directly coupled to the throttle. The actuator would be driven in a similar manner as the DC motor.

**5.2.2. Design Analysis.** The four designs listed are evaluated against the parameters listed in table 5.1. They were scored in each category with a 1, 3, or 5, with the highest rating being a 1. Each of these numbers was multiplied by the weightings listed in table 5.1, and the scores were then summed. The strengths and weaknesses of each design will be discussed, with the final scoring listed in table 5.2.

Evaluating the electro hydraulic actuator, a major weakness of the design is the complexity of the hydraulic system. This will require a new fuel or oil delivery system, including hoses and fittings. With one direction of pressure control, the chamber will need to have a passive filling or evacuation control, and this will further increase complexity and possibly compromise performance. The strengths of this design will be possibly reduced cost, a very simple interface to the ECU, and possibility of high stability due to the nature of the hydraulics.

The stepper motor design should have very good stability and transient control with the position accuracy of the stepper motor. The governor performance should be very good as well, and the simplicity of incorporating a motor driven throttle reduces the modifications required and the hardware complexity. However, stepper motors are expensive, and their control is often takes a dedicated system. As such, interface and cost are the design's main weaknesses.

The DC motor's strengths are similar to the stepper motor. The reduced complexity of the setup and implementation are key strengths to this design. Unlike the stepper motor, the DC motor is very cheap, and the interface with the ECU is more straightforward with the ability to utilize PWM control input. However, a weakness is the lack of precise position control and subsequent compromise in stability.

The linear actuator's strengths align closely to those of the DC motor. The simplicity of the design, combined with the ability to directly couple it to the throttle, reduce the amount of changes needed to the engine platform. The actuator should have good transient response due to the direct couple to the throttle, however the stability of the system may be compromised if the actuator does not have enough precision in the position control, especially at low throttle openings. Interfacing with the ECU is unknown, and this carries some risk. Also, cost is unknown at this time.

The overall scores are posted in table 5.2 below. Based on this analysis, the DC motor solution scores the lowest at a 1.9, and this provides the best compromise between performance and cost while keeping the system simple and providing a high likelihood of interfacing with the current ECU.

Table 5.2: Design Option Scoring Matrix

| Performance Criteria | Electro-Hydraulic | Stepper Motor | DC Motor | Linear Actuator |
|---|---|---|---|---|
| Cost | 3 | 5 | 1 | 3 |
| Interface | 1 | 5 | 3 | 3 |
| Droop/Governor Performance | 5 | 1 | 3 | 3 |
| Transient Response | 5 | 1 | 1 | 1 |
| Stability | 1 | 1 | 3 | 3 |
| Complexity | 5 | 3 | 1 | 1 |
| Modifications Required to Engine | 5 | 1 | 1 | 1 |
| **Total Score** | 3.7 | 2.7 | 1.9 | 2.4 |

## 5.3. ELECTRONINC GOVERNOR DESIGN AND IMPLEMENTATION

**5.3.1. Controller System Design.** In order to effectively control engine speed, the system had to operate in a closed loop manner, utilizing engine speed feedback. It also had to directly input a change in throttle position, making the system a closed loop speed controller.

To reduce the complexity of the system, it was determined to make the Throttle Control System (TCS) independent from the EFI system. The EFI chipset does not have the memory to accommodate more program structure, and to keep the TCS design flexible, this was the most logical approach for a prototype. If it is needed, the system can later be integrated with the EFI system where appropriate.

As shown in Figure 5.1, the controllers will operate as separate subsystems of the total engine operational system. The TCS will receive a user requested speed input and a current engine speed. Using these two signals, it will determine if the engine speed needs

to be increased or decreased. It will then actuate the throttle to match the speed to the requested value. When the throttle is opened, the EFI system will operate the same way as described earlier. The ECU will receive the new MAP signal, and the intake temperature signal and find the appropriate injector pulse width from the look up table. As a new hall-effect signal is detected, this triggers the injectors. The increased air and fuel increase the engine speed, thus meeting the new speed requested by the operator.

The engine speed will be monitored by the TCS with the Hall Effect Sensor from the current EFI system. The throttle position will be monitored via a high precision, single turn potentiometer mounted directly to the throttle plate shaft on the throttle body. These will be the only two sensors utilized by the TCS system.

Figure 5.2 below represents the setup the controller will have. The actuator will be driven by its respective controller, and through a linkage, it will move the throttle as directed. The throttle will have a TPS as a position feedback. The speed signal will be utilized from the current EFI ECU, and this will also feed into the actuator controller.

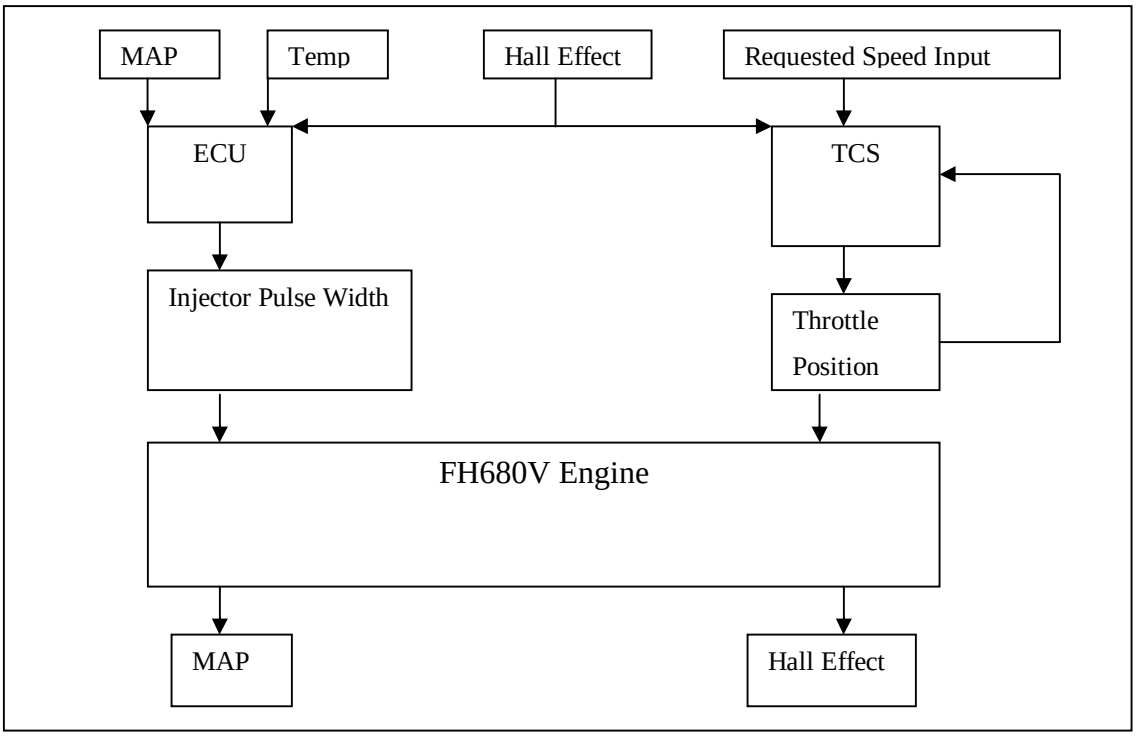


Figure 5.1: Schematic of the engine and controller systems

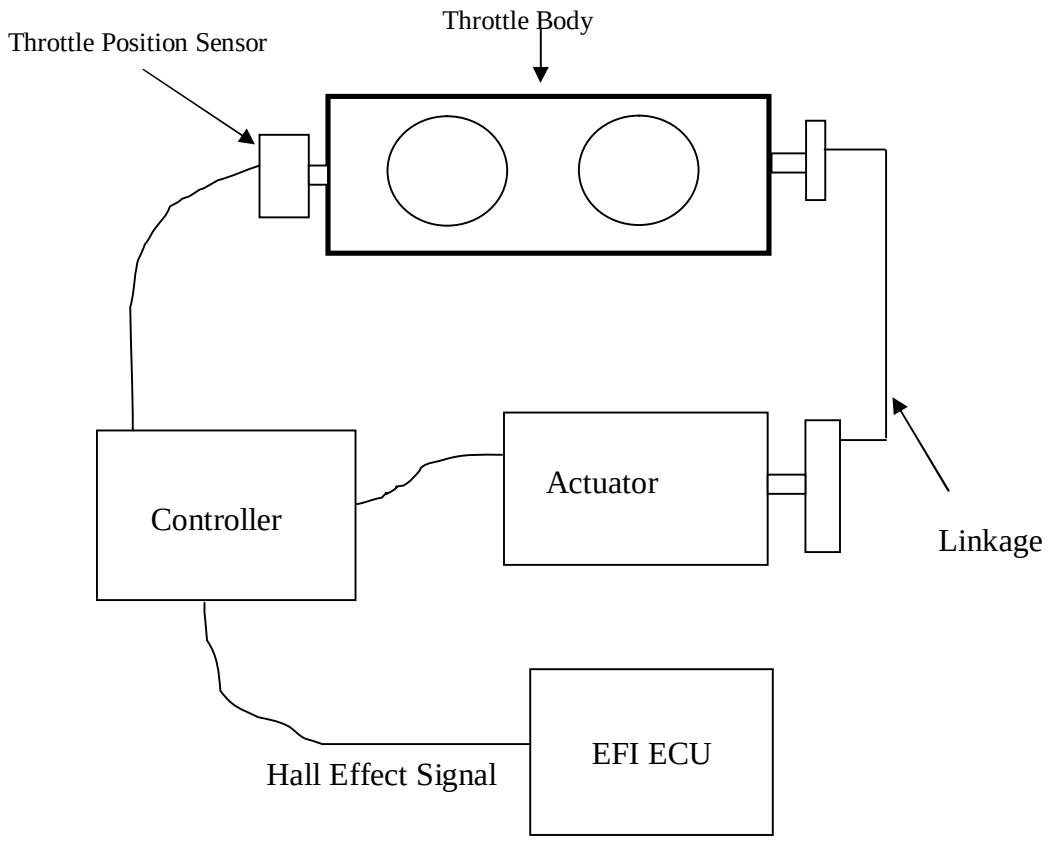


Figure 5.2: Schematic of the throttle controller.

As described earlier, the new TCS system must integrate with the new EFI system. The utilization of the existing Hall Effect sensor, and the integration of the current throttle body are consistent with this approach. The chipset used on the EFI system will also be used for the TCS, creating the possibility of integration further along in development.

However, by making this choice, there are some compromises that are made to the system's capabilities. The chipset, while inexpensive, cannot do complex mathematics or derivations. This reduces the possibility of doing a software based PID or optimal control approach. Instead, more simplified software approaches will be made that attempt to bypass the EFI system's transient shortcomings, while providing adequate control.

To determine the sensitivity of airflow to throttle position, Figure 5.3 below shows a plot of the airflow characteristics through the throttle body at various MAP and throttle positions. Notice at constant MAP, the airflow has a nonlinear response to throttle position (as shown earlier), however also notice that the sensitivity as MAP decreases with increasing throttle position, and the sensitivity to throttle position also decreases with increasing MAP. With increasing throttle position, MAP increases, so the combination dives to a decreased sensitivity to the single control input, throttle position, as the engine load is increased.

To provide adequate precision of the throttle position measurement, and subsequent control, a Vishay Model 357 single turn potentiometer was used. This was ran with a 0-5V signal, and input into the PIC chip as a 8 bit word. This provided 255 "steps" of throttle position control to the ECU, with each bit covering roughly 0.2° of throttle opening.

**5.3.2. Controller Hardware.** The DC motor drives a gear train with a final drive ratio of 400:1. The motor and gear train are housed in a plastic casing, which is then mounted to an aluminum bracket. This bracket is then mounted to the engine in the same location as the original throttle cable and governor bracket. The output shaft is connected to the throttle through a bent wire linkage, and this linkage is held in place with the original clips and a tension spring to remove slop in the mechanism. Figure 5.4 shows a picture of this setup.

The throttle position potentiometer is connected to the throttle plate shaft via a collar. It provides a 1:1 feedback of the throttle position, with 0.5V indicating fully closed throttle. This provides a 0.5-5V input to the controller, which converts this signal to 8 or 10 bit digital format. Figure 5.5 shows the location of the TPS sensor on the throttle body.

The controller receives speed feedback from the EFI ECU which processes the Hall Effect sensor signal into a single voltage spike. This signal is read along with the throttle position feedback from a potentiometer mounted to the throttle body. The controller then calculates and averages the engine speed (10 revolution rolling average), compares this to a requested speed given by an input potentiometer. If the speed is not calculated to be within the specified range, the PIC (PIC16F876A) chip outputs two

signals. First, the output is a PWM signal which is varied per each program. The second is a directional signal, output on either pin 14 or pin 15 from the PIC chip, depending on direction. To pass the PWM signal to the motor, an AND gate (DM74LS08) is used for the directional voltage output. This output is then passed onto an H-bridge style motor controller, which provides the necessary voltage and current to the motor.

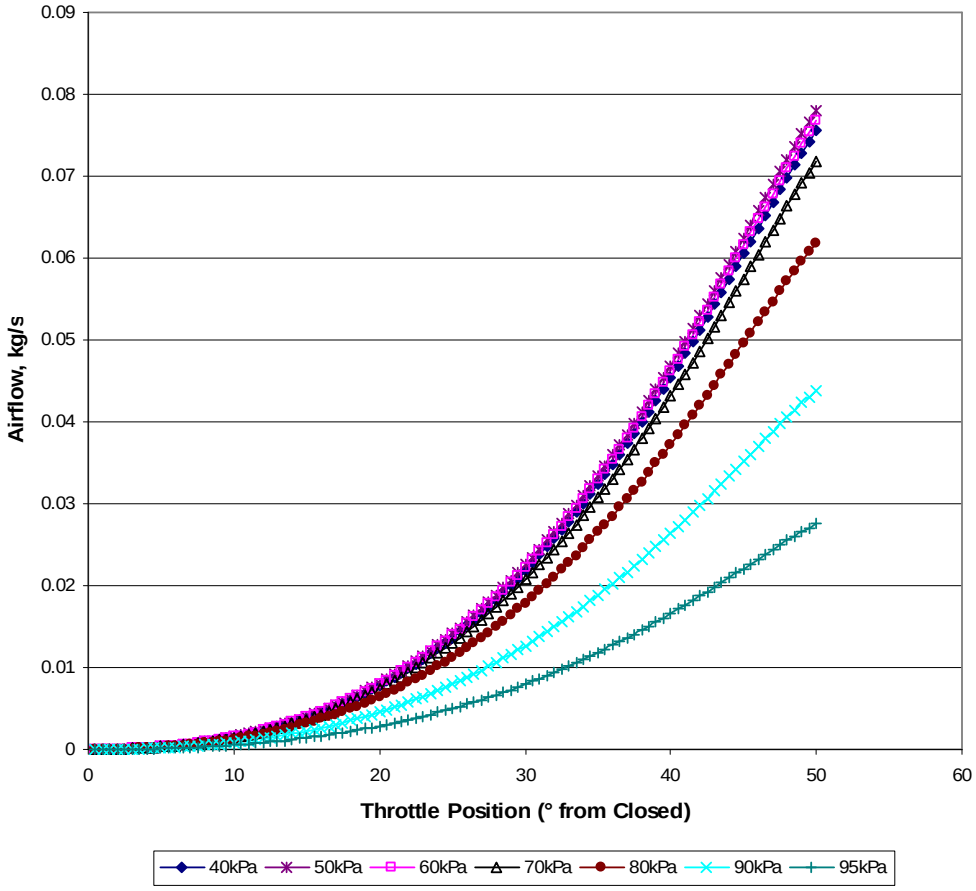


Figure 5.3: Airflow versus throttle position for various constant MAP settings.

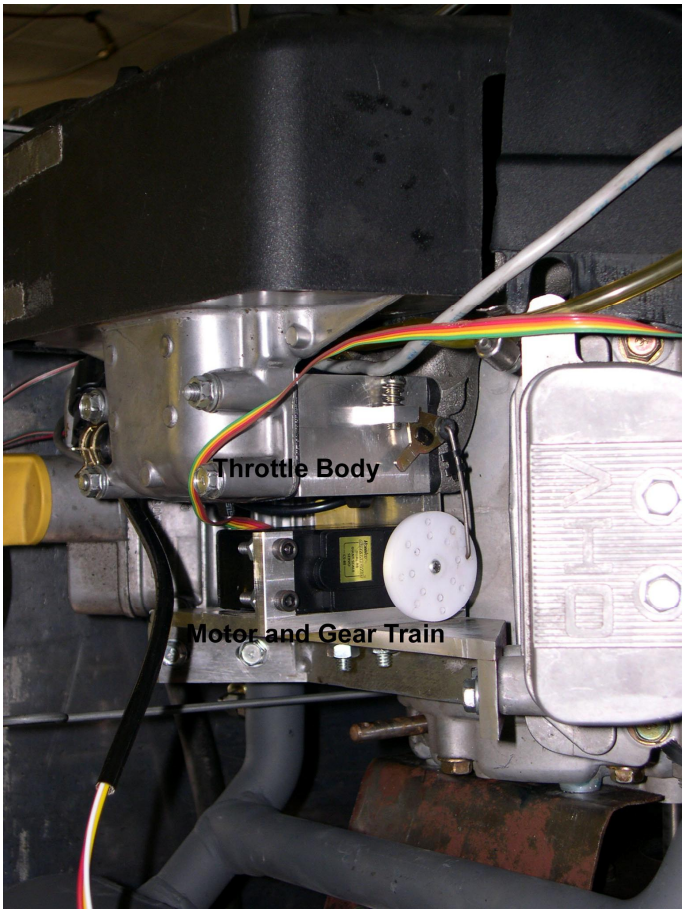


Figure 5.4: Throttle Controller as installed on the engine.

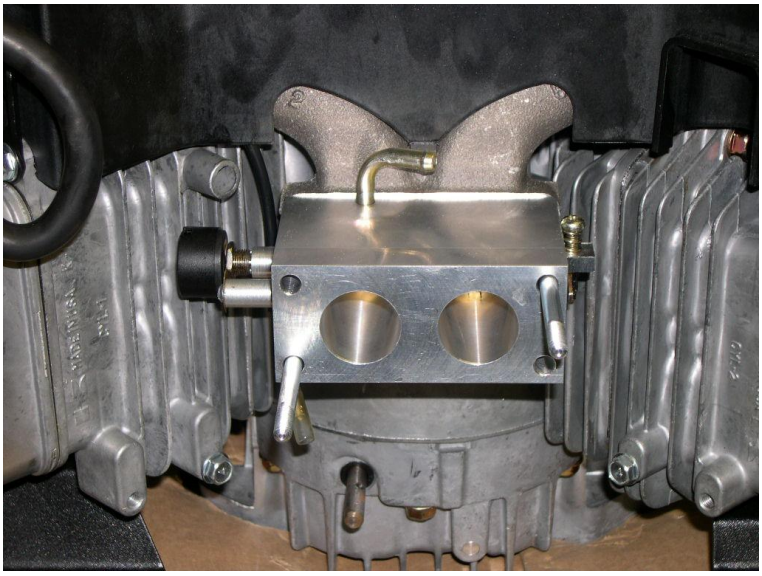

Figure 5.5: Throttle Body and Throttle Position Sensor as installed on the engine

The controller has a +5V voltage regulator that is connected to a 12V power supply. This is the same voltage input used by the EFI system, and should be available in most applications for this engine. A switch is placed inline to the positive power signal to enable the controller and provide a reset switch. The electronic control board is described in more detail in Appendix C.

**5.3.3. Controller Software.** The PIC chip is programmed using MPLAB Integrated Development Environment, PICBASIC Pro programmer, and a chip interface tool. The code is written in BASIC, and PICBASIC interfaces with MPLAB to convert it to assembly language and program onto the chosen PIC chip, 16F876A. The controller software reads all inputs in binary format, including the TPS signal and the PWM output. Appendix D includes the BASIC code for all programs used in this study.

**5.3.4. Electronic Governor Version 1.0.** Version 1.0 was the first attempt to develop the TCS. This version had very basic programming, with user voltage inputs to modify the rate and determine target speed. The basic algorithm reads the engine speed using the interrupt function on the PIC chip. By utilizing one of the internal timers, the engine speed can be calculated to a binary number. The program then compares this binary number to another based upon the speed request input voltage and determines the direction the throttle must respond to make them match.

The rate command is utilized as a delay in the calculation process. The binary number generated from the input voltage is reduced by one bit during each program loop. Once this value is equal to zero, the program is allowed to output the direction to the servo motor controller, which in turn drives the servo motor and actuates the throttle.

During the first prototype tests, the system response was tested on the vertical shaft dyno. The basic functionality of the system was proved, but an oscillation in the throttle response was found. Figure 5.6 below shows the throttle position for a throttle opening test for this version. This test was performed with the engine being run at a constant speed as the throttle was opened.

This issue was found to be caused from the external servo drive reaching a current limit. The controller had to be redesigned, and a new program had to be written as well.

**5.3.5. Version 2.0.** In addition to replacing the external servo controller with an H-Bridge configuration, the new system moved the external Analog to Digital converter to the PIC chip. Additionally, the external rate input was moved to the program as well.

With the exception of the hardware changes, the control algorithm was the same as the previous version. This system had drastic overshoot, driving the engine to very large speed oscillations. As a result, the system had to be reassessed and a new program was written.

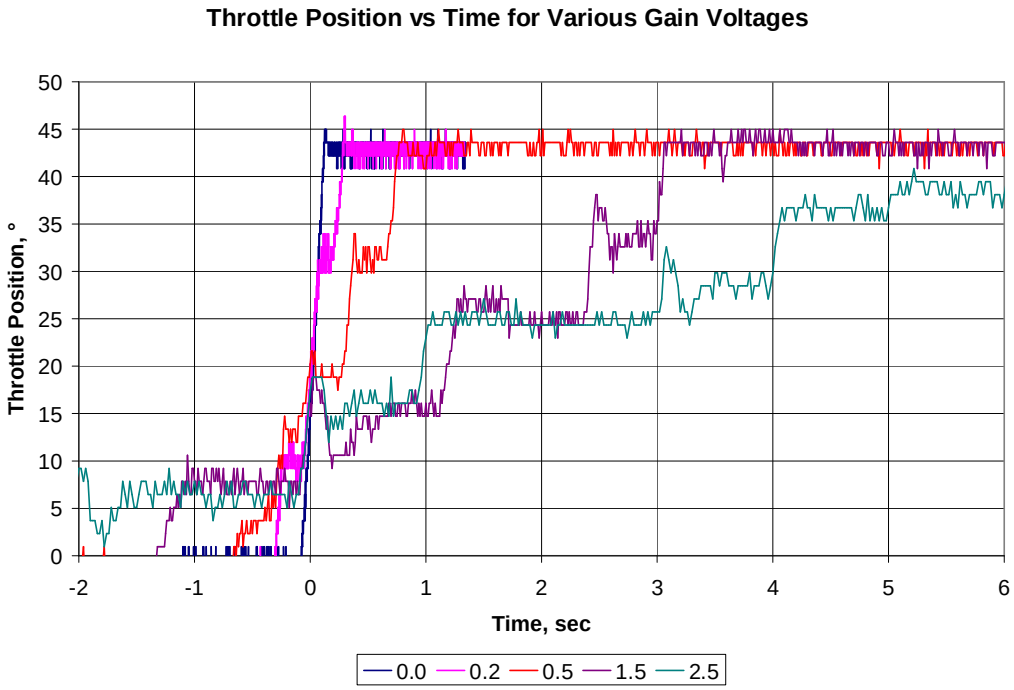


Figure 5.6: Throttle opening test for version 1.0

**5.3.6. Version 3.0.** The hardware of this system was similar to the previous design, but the servo speed was reduced to essentially reduce the gain on the throttle opening rate. This system moved the user input speed request to the program code. The input was then a switch, requesting either the low speed or the high speed idle for the system.

This was the first system to be tested on the horizontal shaft configuration, so little was known as to how the system would respond with the TCS controlling speed. Both load transient and steady state tests were performed on this setup.

The resulting performance was not far from what was seen on version 2.0. While the servo speed was reduced, it was still too fast for the EFI system's response time, and as a result, the methodology for the servo motor control was changed for version 4.0.

**5.3.7. Version 4.0-4.5.** From the previous version, it was obvious the throttle response time was too fast during positive load transients. The throttle opening rate had to be slowed, but the rate also had to be flexible to accommodate large load transients. As a result, pulse width modulation was used to control the servo motor opening rate.

This version of the program runs in a similar manner as the previous versions with respect to the speed control algorithm. It utilizes a 5 bit speed error band, giving a speed hysteresis zone of 225 RPM, with a target speed of 3150 RPM. This is also the first version to utilize a pulse width modulation (PWM) output signal to the servo motor. This PWM signal has a pulse width dictated by a duty cycle value set in the program code. This value can be constant or varied based upon other logic conditions set in the program code.

The duty cycle is set with a 10 bit binary number, which can range from 0 to 1024 bits. Bench tests of the servo motor show it will respond to a duty cycle from 700 to 1023. The max is set to 1020 to keep from the maximum value in the binary calculations.

The throttle position feedback is a voltage converted through the internal A/D converter in the PIC chip to an 8 bit number. The limits are 111 to 146 bits, which responds to fully closed and fully open, respectfully. This position feedback is used to adjust the duty cycle to reduce the impacts on the throttle opening rates at the smaller throttle angles discussed earlier.

Initially, the duty cycle was set to a constant to investigate the impact of a small and a large duty cycle on the operation of the system. The duty cycle was set to 750 bits and 900 bits and a steady state governor curve was found for both of these settings. The engine operation was again oscillatory in nature, but the differences in the throttle opening rate impacted the amplitude of the oscillations.

The lower the duty cycle, the more stable the engine performed. The maximum standard deviation of the speed oscillation is smaller at 750 bits than for 900 bits, as is the amplitude of the oscillations. While the speed is not stable, the reduced opening rate does reduce the oscillation, giving direction for the next iteration. Figure 5.7 below

shows the plot of the standard deviation for each setup for different loads. The smaller the duty cycle, the more stable the engine speed.

In versions 4.4 and 4.5, a variable pulse width was attempted, and a speed hysteresis band was utilized to attempt to bring the speed oscillations to a stop. The variable PW was based upon throttle position, with it driving slower at initial throttle opening and driving faster at more open throttle positions. This incorporated with the hysteresis band would sometimes work, but it was not a robust or consistent approach. The steady state speed error was set with a hysteresis of 2 bits, which is 180 RPM. With the target speed of 3150 RPM, this placed the high and low limit at 3330 and 2970, respectively. Version 4.4 was setup to mimic closely what the small duty cycle operation, but with a larger duty cycle implemented when the throttle position moved more open. Version 4.5 utilized a duty cycle based both upon the throttle position and the speed error at that time. This mimicked closely what the maximum duty cycle setting. The results of these setups are also included in the Figure 5.7.

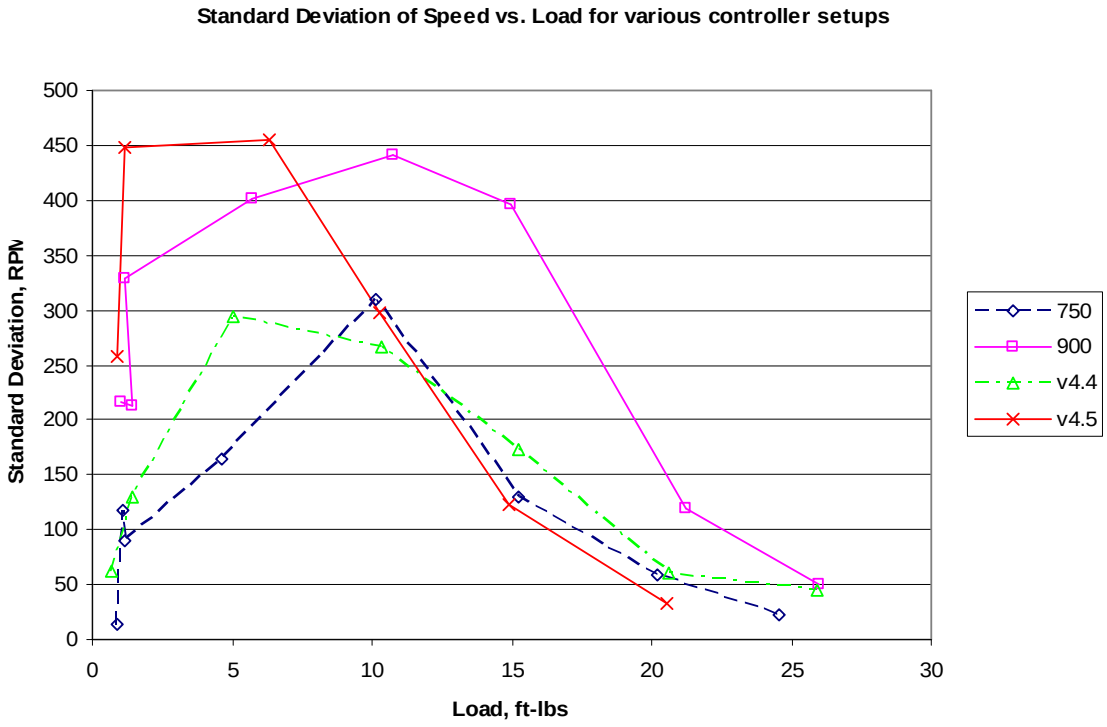


Figure 5.7: Standard Deviation vs. Load for various controller setups

The time averaged values for engine speed and torque were taken for the entire governor curve and the data is plotted in Figure 5.8. The maximum and minimum values are also shown, as are the maximum and minimums reached during each load step. The averaged speed fell within the error band for the majority of the curve, but the maximum and minimum were well outside the error below 15 ft-lbs. This translates to a MAP of approx. 80 kPa and a TP of approx. 12° from fully closed. High load 3200 RPM standard deviation was 131 RPM, high idle standard deviation was 104 RPM.

Under steady state operation, this version of the controller exhibited the best control for the constant duty cycle applications. With the constant duty cycle, the slower the motor was set to move, the more stable the high idle and constant operation throughout the governor curves. With the implementation of the variable pulse width in versions 4.4 and 4.5, the rate the motor moved was based on the throttle position. Version 4.4 had a steady state control that was close to the slowest constant PWM duty cycle setting, however, high idle and loads less than 15 ft-lbs were still a problem area. The motor used in this study was not accurate in the lower throttle opening ranges, and the sensitivities to the throttle position in terms of power output and engine operation were too high for the precision of the motor.

Transient response of this system was characterized along with the steady state response. For this setup, the same transient tests that were run on the mechanical governor were repeated here for version 4.4. This version was chosen since it performed close to the minimum duty cycle setting of 700, but with the variable PW, it was expected to produce better transient results.

Figure 5.9 and Figure 5.10 show the results for tests #1-#3. The initial settings were at high speed with no load, so the speed would oscillate. But, once the load was applied, the speed would settle after an initial drop. This speed drop corresponds with a temporary increase in the A/F ratio of the engine, much like the mechanical system. The recovery time is greater than the mechanical system, but the speed reduction from the droop curve is eliminated. The A/F ratio spike is lower than the test #3 results from the mechanical system (14.13 vs. 15.62), but the duration is longer.

The results from the negative load tests are shown in Figures 5.11 and 5.12. The speed traces shown in figure 34.7 indicate the speed overshoot seen on the mechanical

EFI system is present here. The slow response rate needed by the TCS for the positive load transients causes the speed to drastically overshoot to well above the high idle speed of 3600 RPM. Test #5 settles to the correct speed after about 10 seconds but tests #4 and #6 continue to oscillate from approx. 2800 to approx 3600 RPM on a 5 second period.

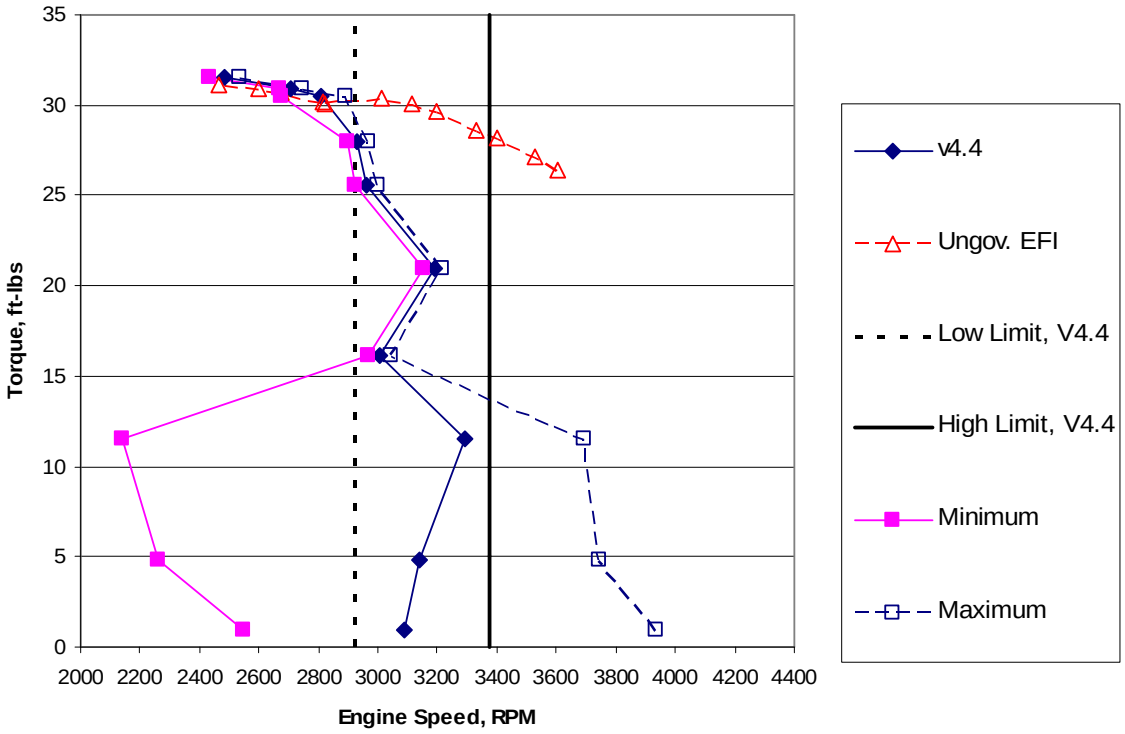


Figure 5.8: Governor curves for version 4.4 and the ungoverned EFI system

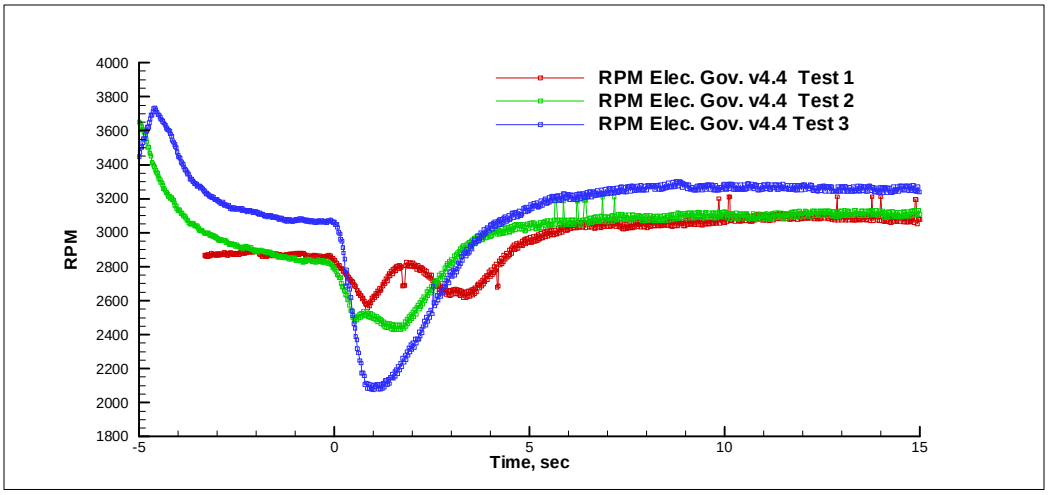


Figure 5.9: Speed traces for version 4.4 for transient tests 1 through 3

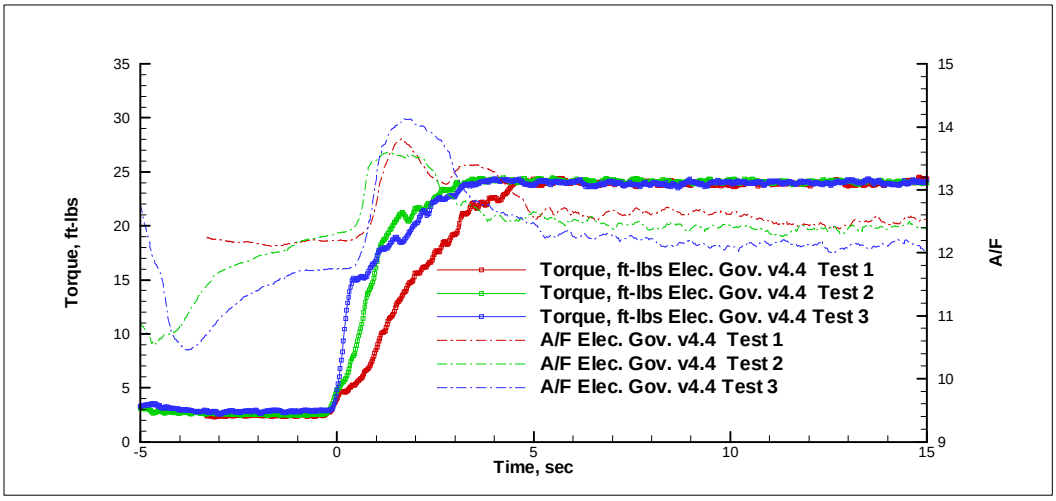


Figure 5.10: Torque and A/F ratio traces for version 4.4 transient tests 1 through 3

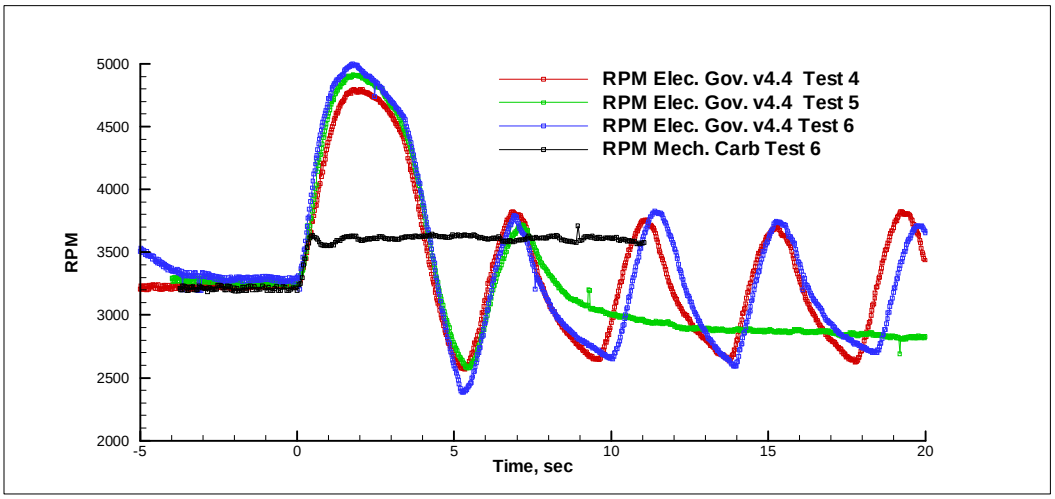


Figure 5.11: Speed trace for transient tests 4-6 with the electronic governor version 4.4. The speed trace for the mechanical carburetor test 6 is included for reference

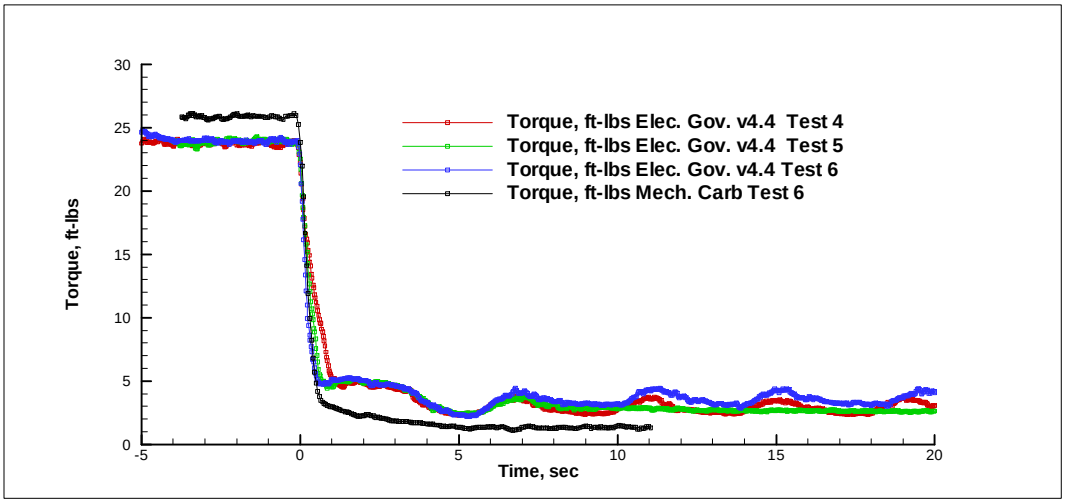


Figure 5.12: Load traces for transient tests 4-6 for electronic governor version 4.4. The load trace for the mechanical carburetor test 6 is included for reference

Figure 5.13 below shows the MAP and A/F ratio traces for the same tests. The A/F ratio has a similar response as the mechanical system relative to the MAP trace. The A/F ratio is reduced as the EFI system's transient fueling error is seen. But, unlike the mechanical governor system, this system attempts to compensate for the reduced speed by opening the throttle. This opening causes the positive throttle opening transient error

of lean operation, and this cycle is repeated once the engine speed responds to the open throttle and overshoots.

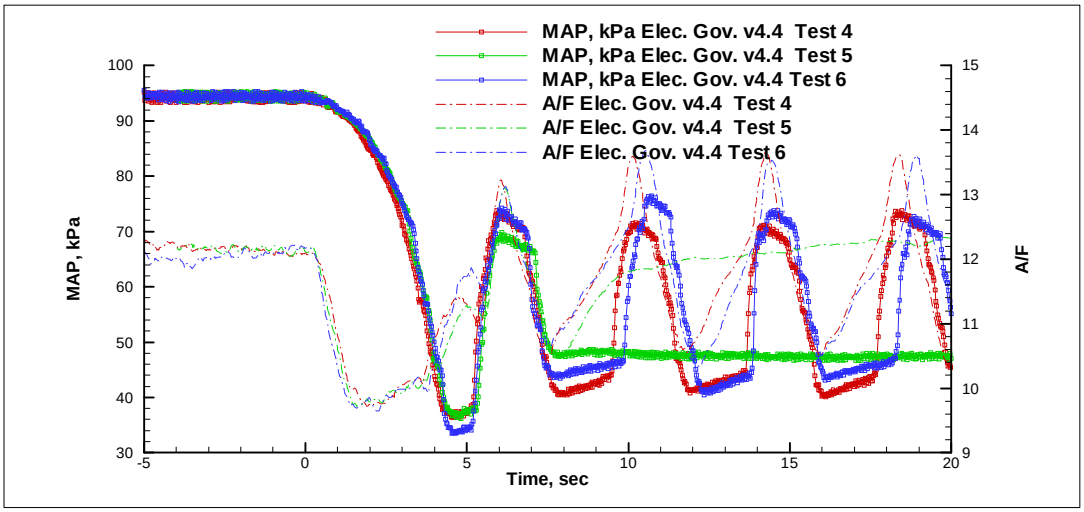


Figure 5.13: MAP and A/F ratio traces for transient tests 4-6 for the electronic governor version 4.4

With the slower throttle opening rate, transient tests show a decreased A/F ratio spike, thus a decrease in the manifold filling dynamic. Figure 5.14 below shows the A/F ratio and throttle position for version 4.4 with the mechanical governor during transient test 3. The slower throttle response is easily seen, as is the lower A/F ratio spike. However, the slow throttle response causes the engine to slow even further than the mechanical governor, as is seen in figure 5.15. With this slower throttle response, negative load transients become an issue when the load is quickly removed from the engine. Figure 5.16 below shows the speed trace for the mechanical governor and controller versions 4.4 and 5.9. Once the load is removed, the speed drastically increases as the throttle closes and reaches a level that may cause serious damage.

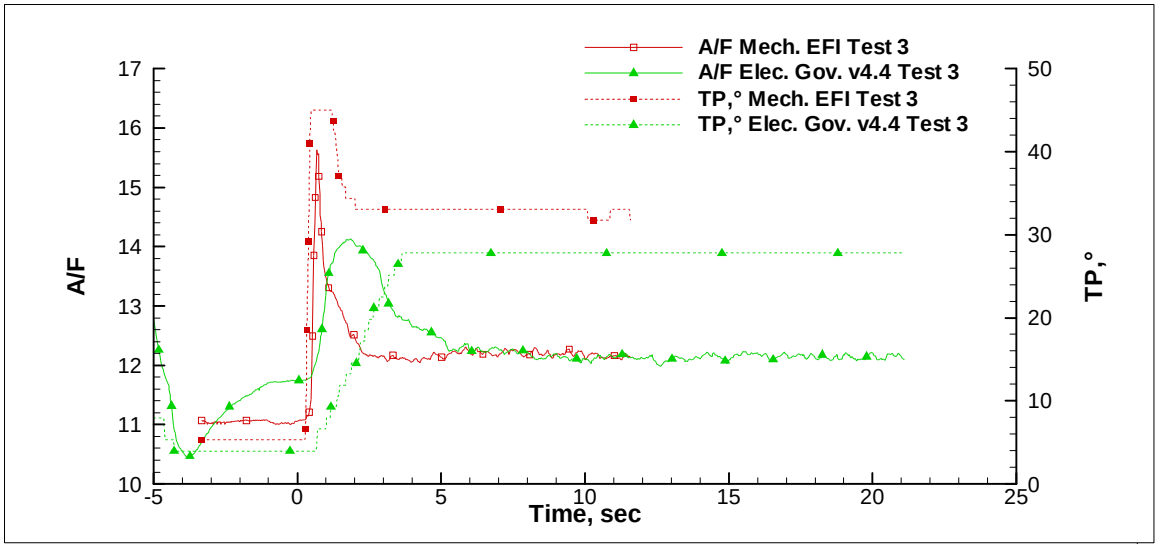


Figure 5.14: A/F and throttle position for transient test 3 with TCS version 4.4 and the mechanical governor with the EFI system

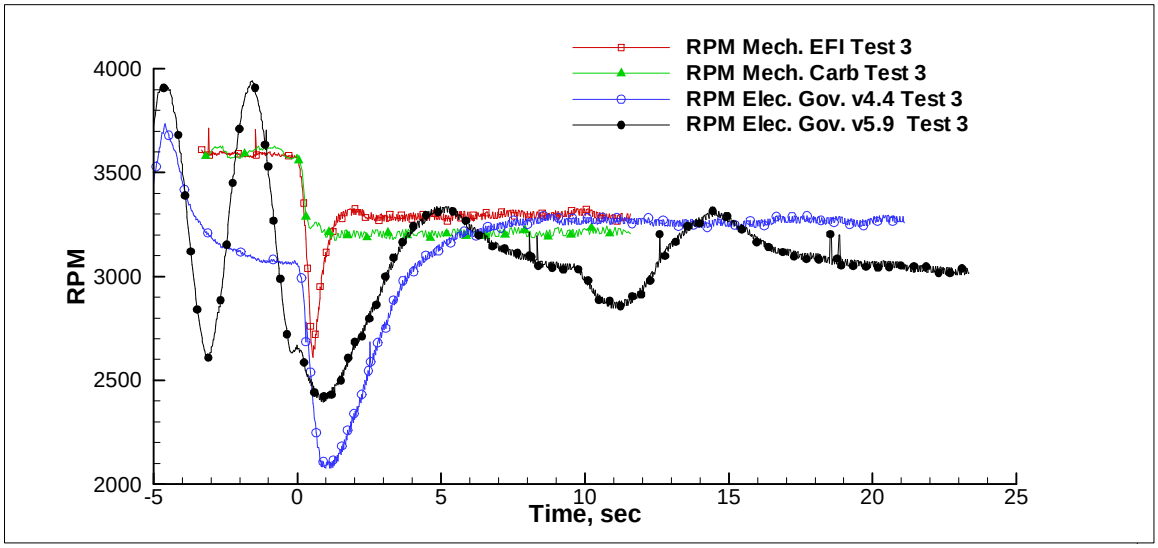


Figure 5.15: Speed traces for all governors for test 3

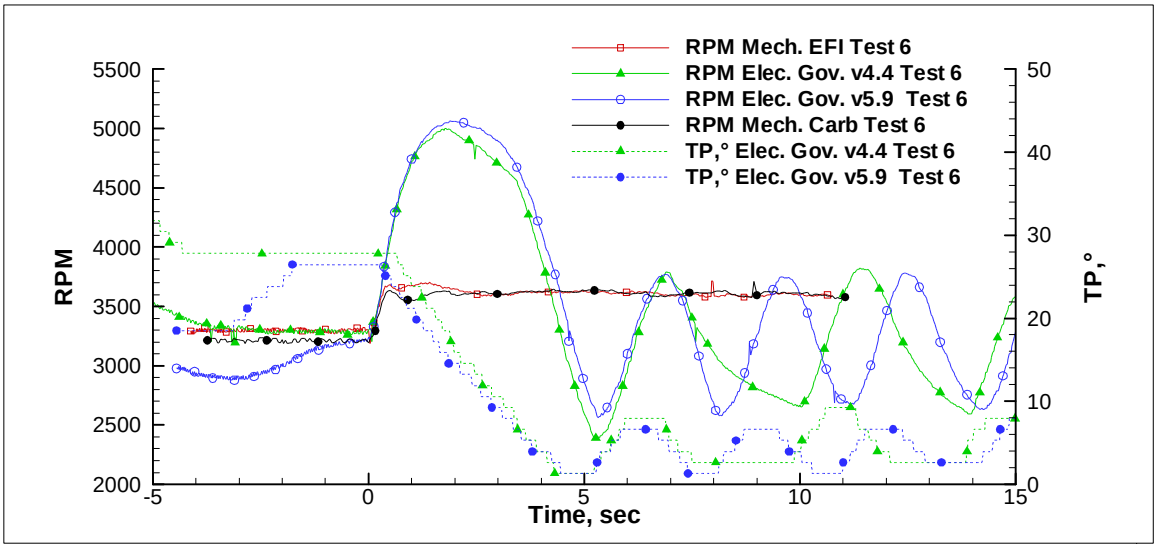


Figure 5.16: Speed traces for transient test 6. Also shown are the throttle position traces for the electronic versions 4.4 and 5.9.

During the development of this setup, several system limitations were seen that impacted the overall performance of the engine. While attempting to diagnose the high idle instability, the MAP damping orifice (described in section 3.3.3.3) used was found to have a direct impact on the amount of speed oscillation. In figure 5.17 below, TCS version 4.4 is tested using the 900 bit PWM setting with various damping orifices. By decreasing the amount of signal damping, and also decreasing the delay of the signal to the ECU, the speed oscillations are reduced. With the 0.004 inch orifice, the speed oscillates from 5000 RPM to 2200 RPM. With the 0.008 inch orifice (the one found to give the best compromise for consistent A/F ratio control), the oscillations are from 2800 RPM to 4000 RPM. With the 0.015 inch orifice, the oscillations drop to 3000 RPM to 3300 RPM. The speed oscillations have a direct correlation to the time constant of the overall fuel delivery system. The faster the fuel delivery system responds to changes in airflow, the less impact it has on the speed control system.

This is a significant divergence from what was found during the EFI system development (see section 3.3.3.3). The use of a volume or orifice to condition the signal has a contradictory effect on the engine performance targets. A simple compromise is not available that provides the adequate steady state averaging needed for consistent MAP measurements and one that provides adequate response times for the transient and

speed response. A program based signal filter is a possible, however programming limitations and processing capability of the software is limited. In the interest of idle stability, the largest orifice will be used for the next versions of the controller.

Hardware limitations were found in the motor, giving it limited response to the pulse modulation. Only a small range of rate variation was achieved, and even the lowest rate did not remove the oscillations at low loads and high speeds due to the limited amount of variability available with this mode of operation. During positive load transients, the throttle responds too quickly and allows a large increase in A/F ratio, which in turn causes a drop in speed until the manifold filling and wall wetting dynamics settle and the engine speed increases. During negative load transients, the throttle does not respond fast enough, causing a large overshoot in speed. The next version will attempt to address these shortcomings while taking into account system limitations.

**5.3.8. Version 5.9.** The final control program attempted to retain the strengths of the previous version, notably the higher load stability, while improving the high idle and low load stability. With the limitations of the servo motor, a new system was implemented that utilizes a position based speed control which has the motor driving to a throttle position determined by the program. The throttle position is determined by the speed error and is calculated by the program. This allows flexibility on the overall response time of the throttle controller while accommodating the speed response limitations of the motor. The TPS output was changed from an 8 bit to a 10 bit number with a position hysteresis of 5 bits. With the results from the previous version, the speed hysteresis was reduced to 1 bit, or 100 RPM, to make the system more accurate.

The system control loop uses the speed input voltage as a high-low setting based on the input voltage from the speed request potentiometer. This voltage level is a binary number, with a low voltage level corresponding to 525 bits or less setting a low idle speed target of 1625 RPM (93 bits). When the input is higher than 525, the speed target is 3125 RPM (45 bits).

The timer to calculate engine speed is run with an interrupt routine triggered by the Hall Effect sensor. The routine starts the timer and stops it for each interrupt trigger. The timer value is averaged over the last 10 timer cycles before it is passed to the program.

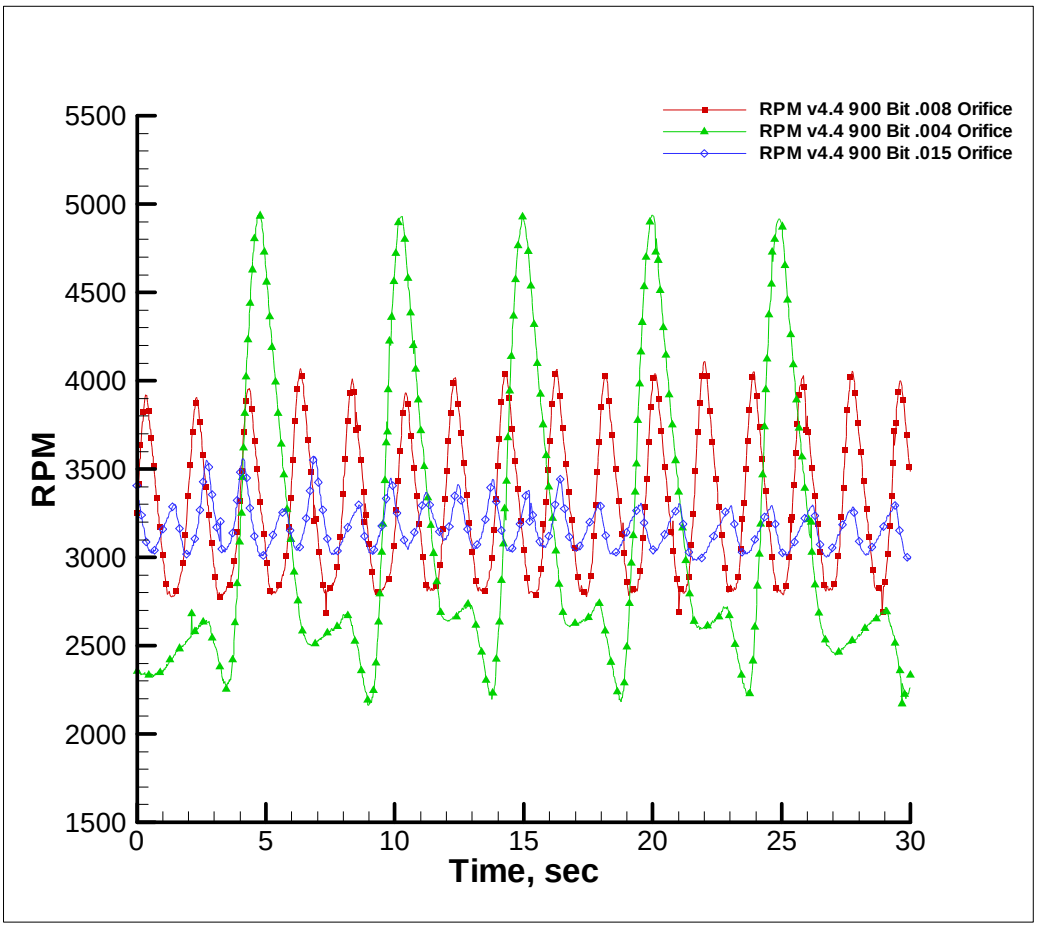


Figure 5.17: Speed trace at high idle for various MAP signal conditioning orifices. The TCS version 4.4 was used with a 900 bit duty cycle.

The program then takes this timer value and compares it to the speed target. If the difference between the two is less than the speed hysteresis value of 1 bit, the program does nothing. If the error is higher, the program then determines which direction to turn the throttle. If the speed is less, it opens the throttle, if the speed is greater than the target, it closes the throttle.

To reduce the overshoot, the throttle is not controlled directly proportional to engine speed. It is actually driven to a position that is calculated by the program. This position calculation is what interfaces the throttle control to the speed control, and this is

where the bulk of the corrections were implemented to account for the shortcomings of the previous systems.

The position is first determined by a default setting. Then, after the speed is compared, the position target is moved in the appropriate direction by one bit. This is continually done while the program is not in the interrupt sequence. Over the course of operation, if the speed is not on target, the position will continually move in the proper direction. The position does not move, however, until there is a total of 5 bits difference between the position target and the position feedback signal. Once this is done, a position driver subroutine is called to bring the throttle position to the prescribed location.

Once the position is found, the speed will change, and the process repeats. However, the program still runs very quickly. As a result, a delay was built into the program. Here, the program pauses during each loop of the program, the duration being set based on the calculated speed error. If the speed request is the high speed, but if the throttle position is less than 525 bits, then the delay is 15 milliseconds. This is to slow the controller response at high speeds light loading, and to try to reduce the sensitivity to the EFI system dynamics. Otherwise, it is 10 milliseconds at all other operating conditions.

The PWM approach was adapted to this program as well. The PWM duty cycle is based upon throttle position and speed error. The pulse width duty cycle is outlined in the table below.

Table 5.3: PWM correction for electronic governor version 5.9

| **TP Limit (min of 400, max of 660)** | **Duty Correction from TP** | **Duty addition from Speed Error** |
|---|---|---|
| TP less than 520 bits | 1000 (Max 1020) | None |
| TP between 520 and 600 | 900 | None |
| TP greater than 600 | None | 3 times the position error (with max of 1000) |

At first the throttle was attempted to be run very slowly during the first 550 bits of throttle position (the first 58% of throttle opening), but the throttle was difficult to open at these low manifold pressures (25-45 kPa), and the servo motor could not reliably operate. This is why the duty cycle is very high at early throttle openings. After the throttle started opening, it had to be slowed, thus the limit from 525 to 600 bits. Past this point, the rate was based on speed error, to allow at least some proportional compensation to speed the response time, specifically during negative load transients.

The PWM setup combined with the delay produced a more stable steady state operation. With the speed hysteresis of 1 bit, the speed dead band is 3050 and 3250 RPM. Even with the tighter speed control, the governor performed very well at loads higher than 15 ft-lbs. Under 15 ft-lbs, the speed average still falls within the dead band limits, but the oscillations show themselves again below 15 ft-lbs. Figure 5.18 below shows the torque curve and the speed control limits imposed during this version. Notice the maximum and minimum traces are very close to the average above 15 ft-lbs. Below this, however, there is a similar response as the previous version. The speed still oscillates ±200 to 400 RPM at lower loads with the high speeds.

The low idle speed standard deviation of 14 RPM is consistent with the previous versions. The max and minimum for the low speed idle of 1662 and 1572 respectively show good low speed and low load control characteristics. However, high idle is not good, with the standard deviation reaching 414 RPM with a maximum of 3916 and minimum of 2490. This is not as good as the previous version (296 RPM standard deviation).

The purpose of position based control was to decouple the throttle position subroutine from the position calculation portion of the program. This would have an impact with a decreased response time; particularly with the manner the position request is determined from the speed error. Additionally, this step allowed for a variable time delay to the program, essentially allowing for a variable control reaction based on any number of input variables. This did slow response time, however, the rate at which the throttle would physically move was still too fast, and as a result did not remove the speed oscillation. Figure 5.19 below shows the results from the high idle test for one of the speed oscillation periods. By tracing the engine speed, when it drops below the 3050

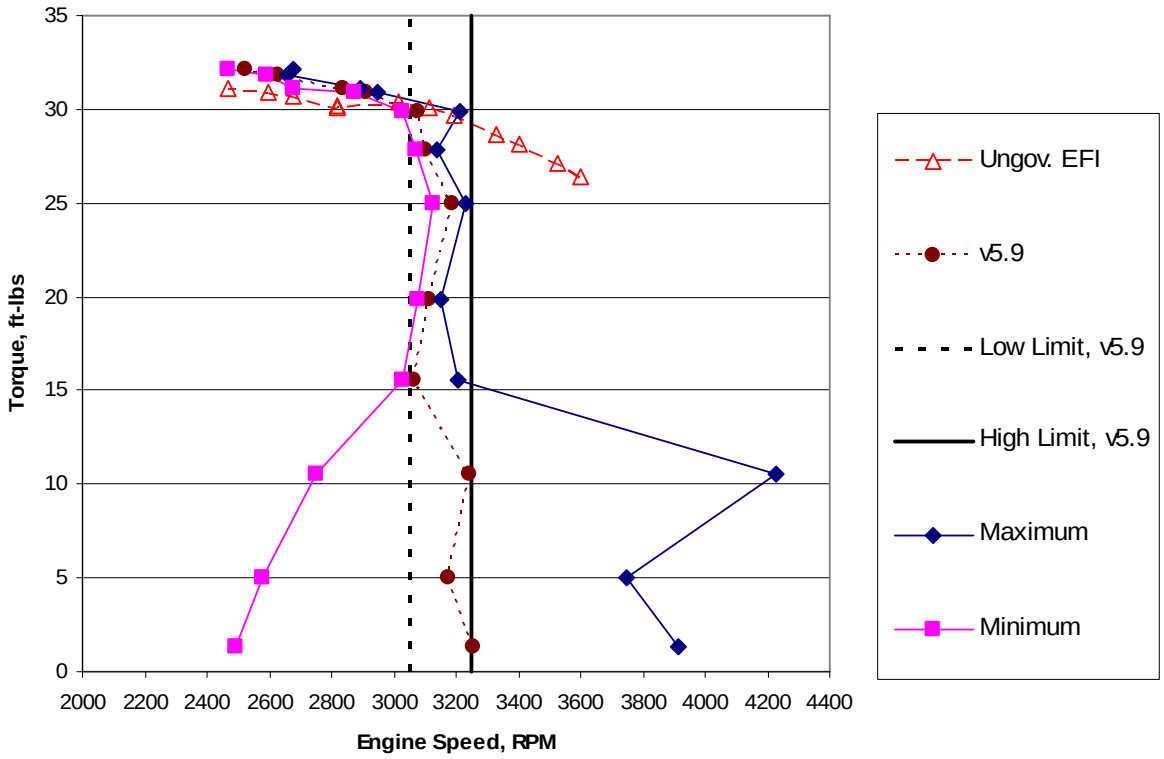


Figure 5.18: Governor torque curve for electronic governor version 5.9. The ungoverned EFI torque curve is included for reference

RPM low limit, the throttle controller responds by opening the throttle. However, the engine has inertia and EFI system limitations to overcome, and does not immediately respond to the throttle opening. As a result, the controller continues to open the throttle until the speed reaches the 3050 low limit. By this point in time, the throttle has opened considerably farther than needed, and the speed continues to increase and overshoot. The throttle then responds once the high limit of 3250 RPM is reached by closing the throttle. By this time, the engine has too much rotational inertia and does not immediately respond to the decreased air and fuel flow, causing the throttle to undershoot once more.

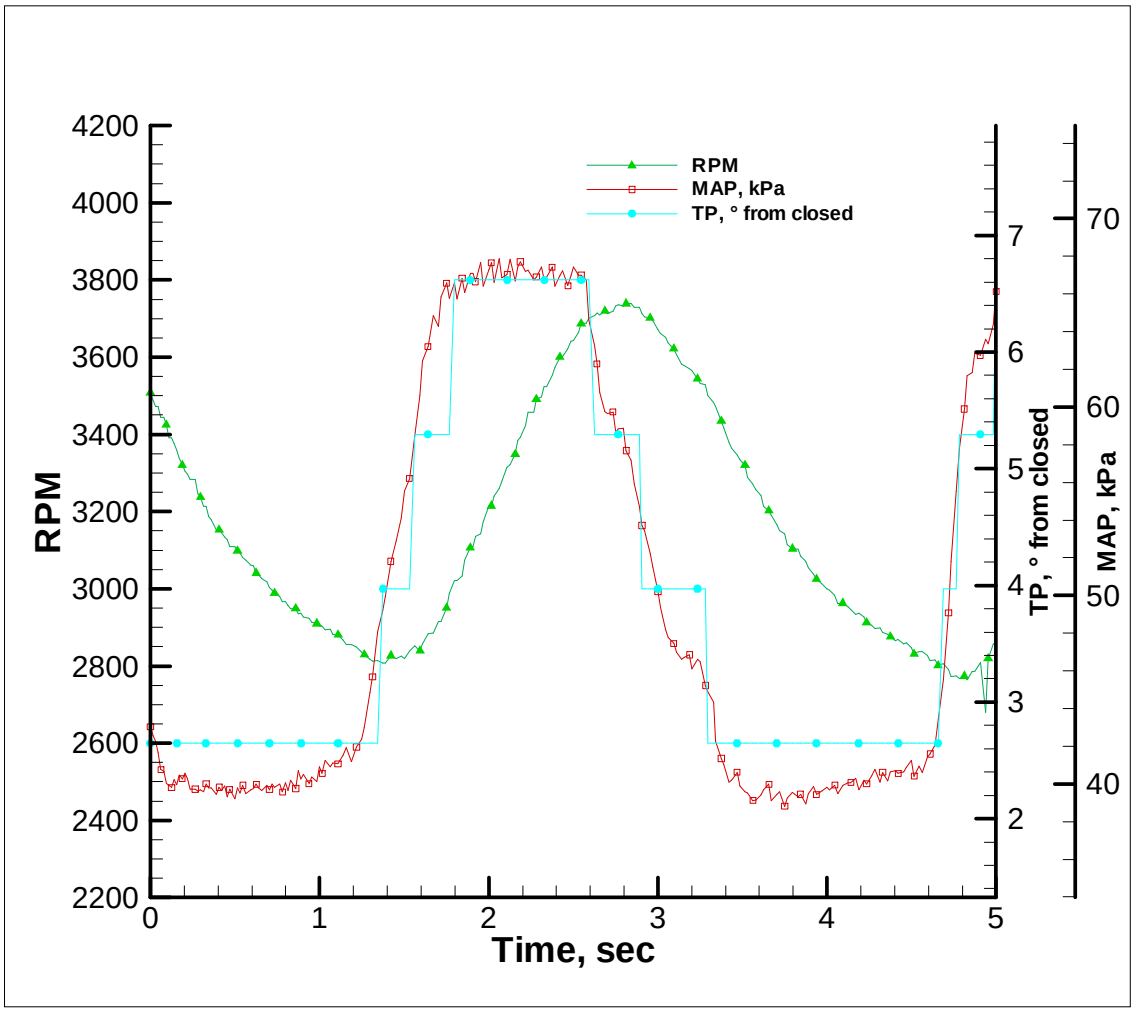


Figure 5.19: MAP, TP and RPM for high idle test with v5.9

The causes of this dynamic are numerous, and involve items that were not considered in this study. The rotational inertia of the engine and dyno were not used in the controller as application flexibility was desired. Modifying the controller to suit variations in rotational inertia was not desirable, and this was not used. Engine speed is very sensitive to throttle position when there is little load on the engine. Figure 5.20 shows the operational point of the engine during high idle over the throttle airflow curves shown earlier. Notice that during the entire operation, the engine follows the MAP curves with the highest sensitivity to airflow, further complicating the situation.

However, during a positive throttle ramp, such as during test 3, the sensitivity decreases as the load is applied, as shown in figure 5.21. Here, the decreased sensitivity to MAP and thus load with TP allows the controller to stabilize and hold a constant throttle position and speed.

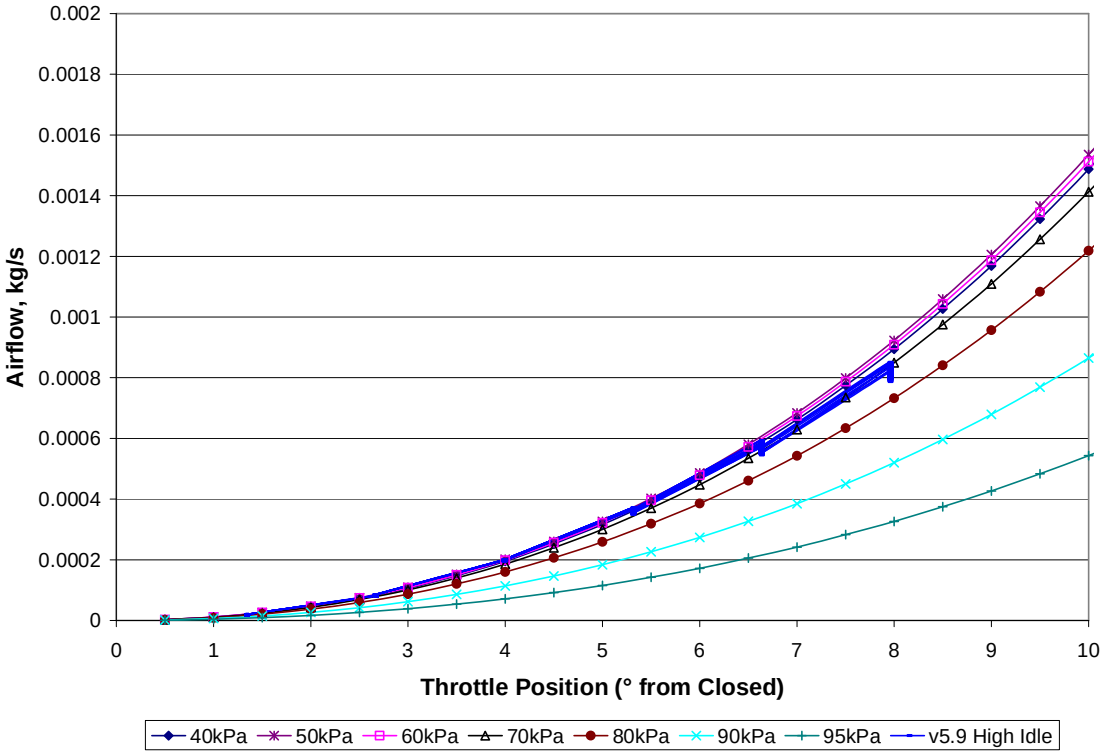


Figure 5.20: Airflow during high idle for v5.9 controller

For the positive load acceptance tests (tests 1-3), the initial speed at low loads would not settle (this same issue occurred at high speed idle since they would start at high idle). Once the load was applied, the speed settled within the operational targets. This follows the same trend seen in the steady state tests, where the speed stabilized at loads 15 ft-lbs and higher. From this point, the speed stabilized in around 5 seconds from the load application to the steady state target.

The negative load transients (tests 4-6) are shown in figures 5.22 and 5.23 below. Tests 4 thru 6 were ran on this setup, with similar results. While the rate at which the

load was removed had an impact on the rates of the A/F ratio declines, and the amount of speed overshoot present, the overall dynamics were similar.

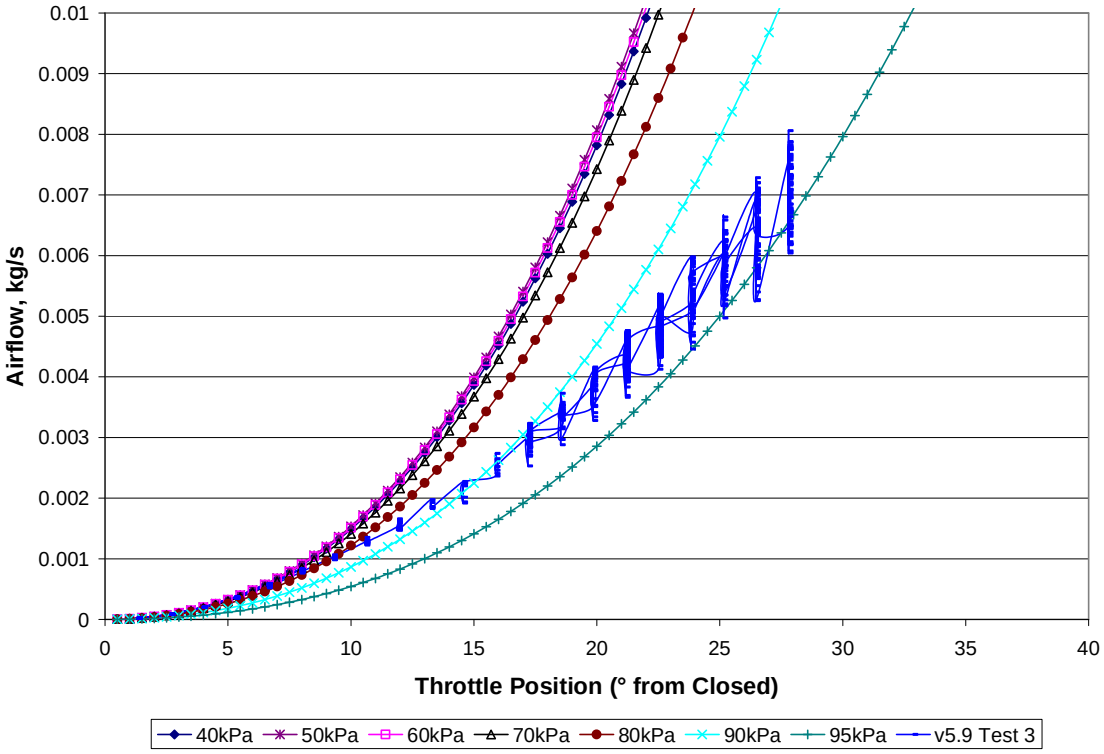


Figure 5.21: Airflow versus TP for the positive load transient test 3 with controller version 5.9

For all negative load transient tests, there is a considerable speed overshoot from the time the load is removed. Test 4 has a speed overshoot of 4600 RPM, test 5 was 4868, and test 6 was 5061 RPM. These are at least 1000 RPM higher than the maximum allowable speed of 3600 RPM, thus this is not a condition that can occur in the field.

By looking at figure 5.24 below, the RPM is plotted along with the throttle position. Even considering the throttle position measurement output has a precision of 1.3°, yet the throttle does not begin to move until 0.5 seconds after the load transient begins. At this point, the speed has already increased 200-800 RPM, depending on the rate at which the load is removed. To maintain high speed idle, the throttle needs to be opened 5°, so the actuator would need to close it 25° for this to happen. With the speed of the actuator slowed for the positive load transients, it cannot respond in time and the

speed has the overshoot. With the faster time constant of the unloaded engine, the speed undershoots as well, becoming part of the unloaded speed oscillations seen earlier in the high speed idle tests. As was seen on the steady state tests, the speed oscillated considerably once the load was removed.

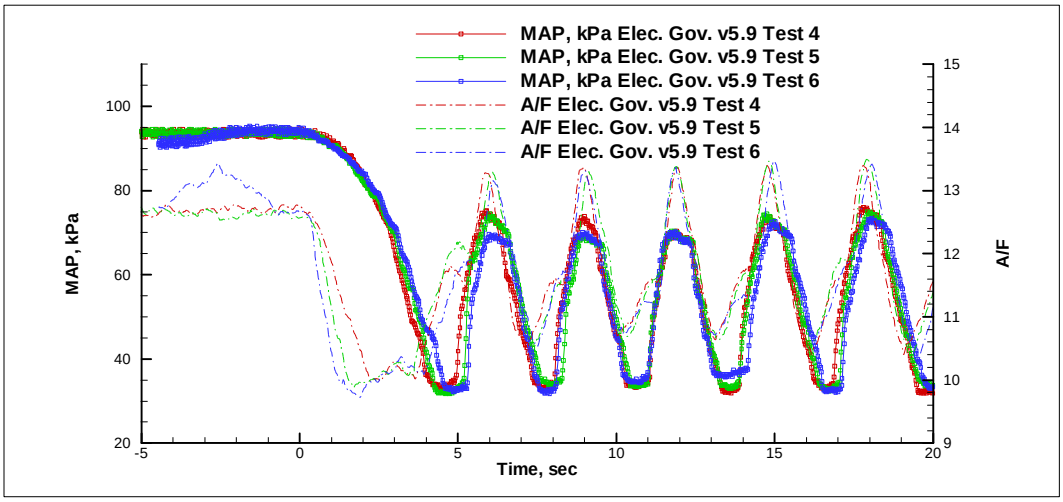


Figure 5.22: MAP and A/F ratio traces for transient tests 4-6 for electronic governor version 5.9

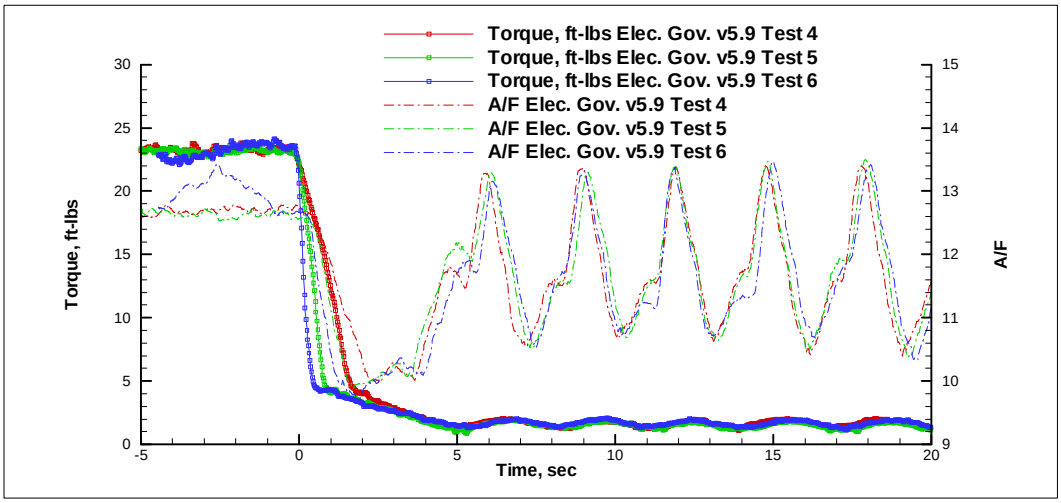


Figure 5.23: Load and A/F ratio traces for transient tests 4-6 for electronic governor version 5.9

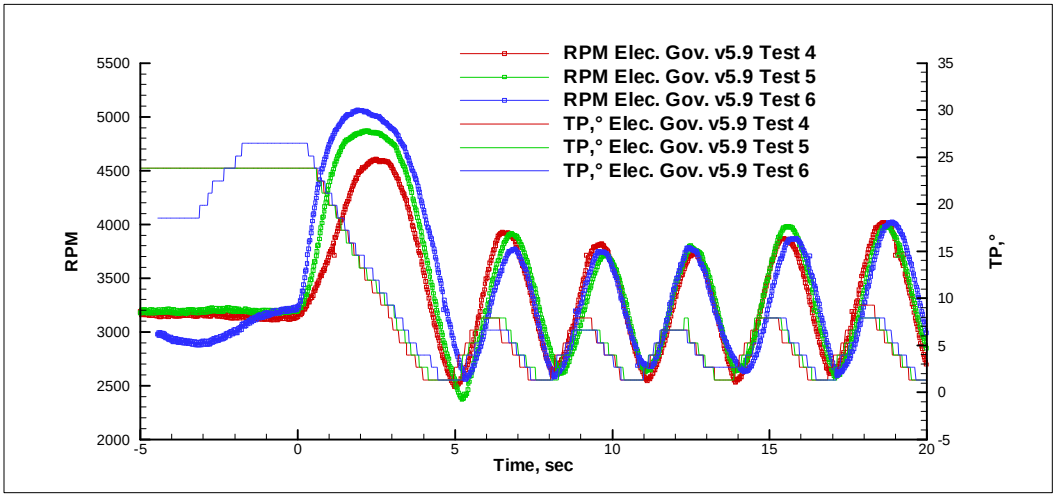


Figure 5.24: Speed and Throttle Position traces for transient tests 4-6 for electronic governor version 5.9

From this point, it is obvious the controller still operates too quickly for low idle, Also, during development, it is found that the controller has a limited precision, and once that is likely not adequate for the purposes of idle control given the sensitivities seen above. However, transient testing does make a counter point. During positive load transient testing, the speed still decreases more than the mechanical governor as seen in figure 5.25. The speed recovery is better than the previous version, indicating that the combination of position control and progressive calculation of position location do improve the response time. However, as seen in figure 5.26 below, the throttle position rate change does not vary significantly from version 4.4 to 5.9, and the rate the throttle changes is nearly constant for both the positive and negative transient tests. As a result, the speed response during a negative load transient, as seen in figure 5.24, still has the drastic overshoot due to slow throttle response.

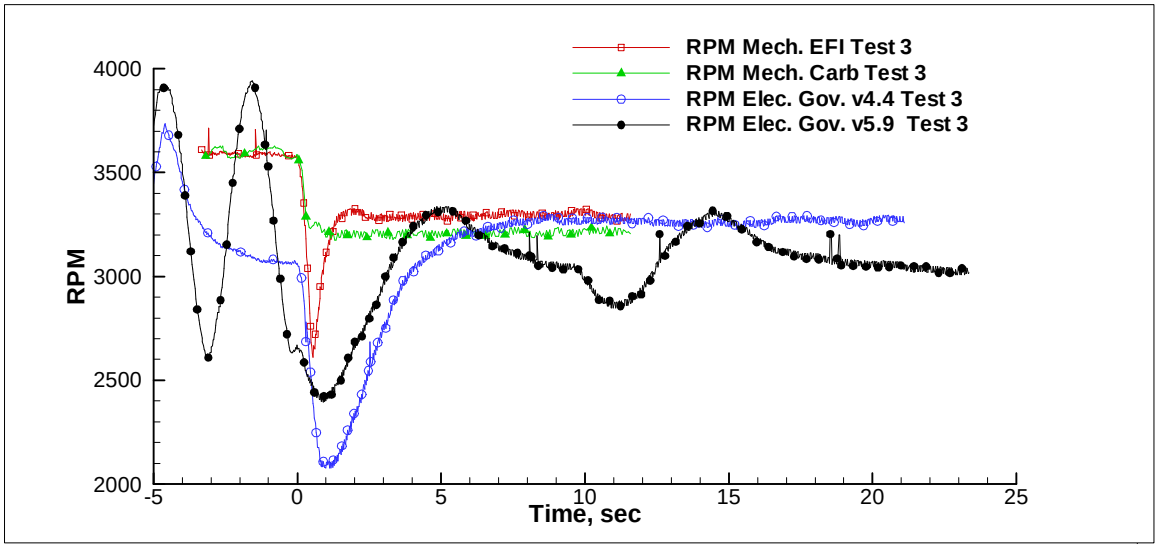


Figure 5.25: Speed traces for all governors for test 3

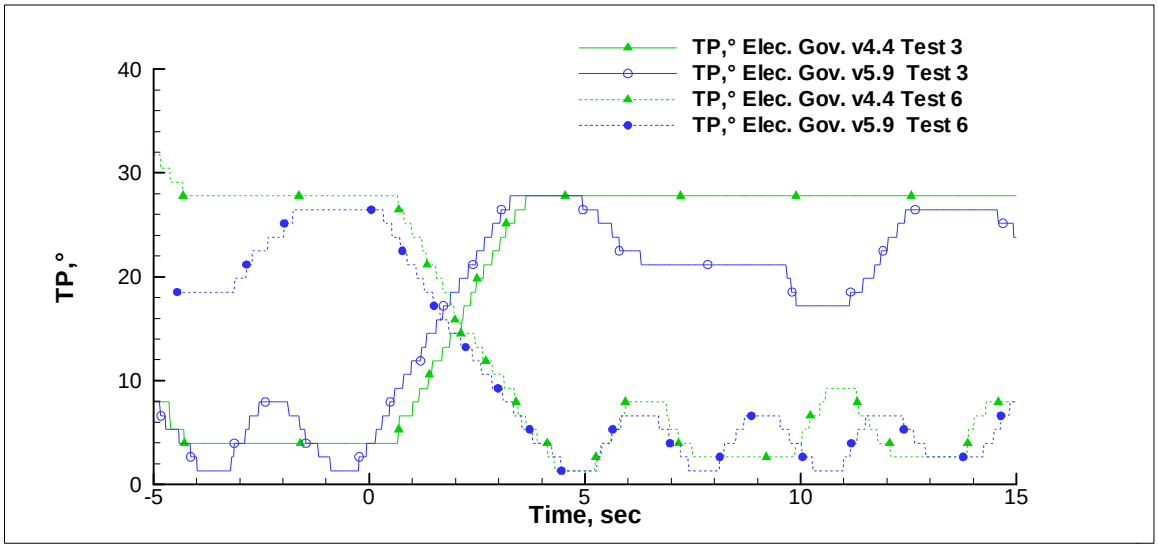


Figure 5.26: Throttle position traces for tests 3 and 6 for both electronic governor versions

Figure 5.26 indicates a limitation found in the servo motor's PWM response. The rate at which the motor's speed can vary is very limited, and the motor cannot move well below a 525 bit PWM duty cycle, which is a 50% duty cycle. The variability and

sensitivity to this on the small DC motor used indicates a motor with improved sensitivity should be used. Also, due to the static friction of the gear train and throttle linkage, the duty cycle needed to overcome this is nearly 100% (1000 bit), which indicates the motor is underpowered as well. This causes the throttle to respond slower in these circumstances, though once underway, it has been shown the mechanism responds too quickly. This can also attribute to some of the poor precision seen at low throttle openings as high duty cycles needed to overcome the static friction do not allow a slow and precise movement of the throttle.

For a positive load transient, the transient operating characteristics of the EFI system covered in section 3.4.2.1 dictate the primary system time response characteristics. From Figure 4.8 and knowing the impact of load application rate from the EFI transient tests 1-3, it was thought to open the throttle as slow as reasonably possible to minimize the A/F ratio spike, yet fast enough to keep the speed undershoot (due to a slow engine torque response) within the levels seen on the mechanical governor during testing presented earlier. The manifold filling dynamic shown in figures 3.19 and 3.20 is highly dependent on the rate at which the throttle is opened. Figure 5.27 shows the throttle airflow calculation for the transient tests 1 through 3 for the mechanical governor EFI engine. Notice the rate at which the airflow spikes, and the peak airflow is seen by the fastest opening throttle, test 3, and it decreases as the throttle is opened more slowly in tests 2 and 1.

The highly nonlinear nature of the manifold filling dynamic created a system response characteristic that is difficult to manipulate without changing the fuel delivery algorithm. For a positive load transient test, a slow throttle manipulation is ideal, however, on a negative load transient, the throttle needs to respond quickly as the system response is now driven by loading and inertial effects. This relationship the engine response has on load direction cannot be easily accommodated in the current controller software package, as the mathematical and programming limitations to provide differential and directional control were not feasible, especially to the development engineer without an extensive electronic and programming background.

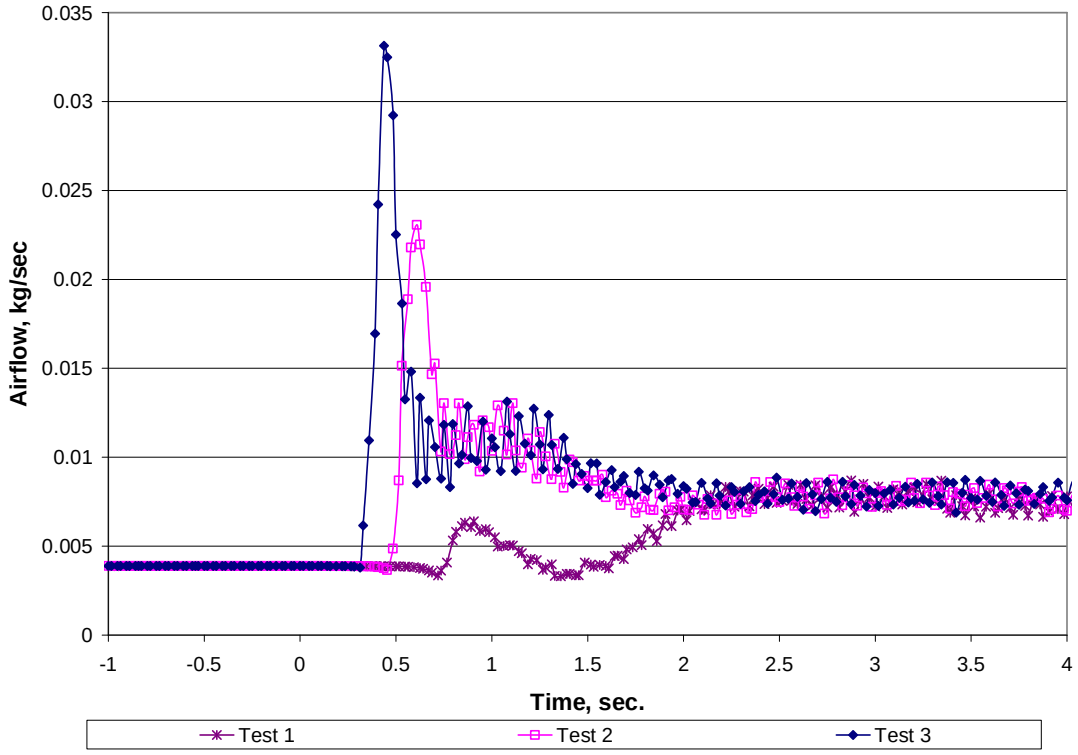


Figure 5.27: Throttle airflow for the transient tests 1 through 3 with the mechanical governor and EFI system

# 6. DISCUSSION AND CONCLUSIONS

The results seen from version 5.9 presented in section 5.3.8 show that the engine operating dynamics cannot be bypassed with a simple, inexpensive controller. The limitations and performance of the basic EFI system creates a system dynamic that was not seen on the current carbureted system. The manifold filling dynamic is studied, and its impact on performance shown. This dynamic creates a loss in torque during a positive throttle step, and subsequently a drop in speed as load increases. To provide consistent steady state fuel delivery, the manifold air pressure signal is filtered physically through a orifice. However, this increases the time response of the fuel delivery, exasperating the manifold filling dynamics. These dynamics were not previously understood, and they must be accommodated in the fuel delivery system if it is to be a robust platform. These issues can be compensated in a straight forward manner [16], given the processing and control needs are met. This level of control and processing is not currently available on the fuel system controller. The controller hardware needs to be updated, as does the program code capability.

The governor design chosen was a DC motor actuator as this provided the best balance between performance and cost targets. The DC motor utilizes a throttle position sensor and controller hardware that shares many components with the current fuel injection control unit. This will provide commonality, and provide the possibility of combining the systems at a later date. The throttle control system was approached as an independent unit from the EFI control unit, providing speed control to the engine system through engine speed feedback. The control unit was designed for programming flexibility within PIC BASIC framework, utilizing the PIC chip 16F876A. This chip provides quick processing and a PWM output, which was to provide variable speed control to the DC motor. A throttle position sensor was also used for position feedback and as an additional control input.

The programming code for this system went through numerous evolutions, each incorporating more of the engine dynamics learned. The initial attempts to drive the motor met with little success until version 4.0, where the PWM was fully implemented. Initial results indicated that the controller was capable of providing the targeted speed

droop characteristics on a constant speed governor curve, but high speed, low load operation showed instability. A portion of this instability was shown to be directly related to the manifold air pressure signal conditioning. The sensitivity of the throttle airflow to throttle position at these low loads combined with the EFI system dynamics were too complex to accommodate in the program code.

The transient response characteristics of the governor system were seen to be limited by the manifold filling dynamic, engine inertia, and loading. During a positive transient, the governor response needs to be slowed to account for the manifold filling dynamic. However, during a negative load transient, the system must respond quickly to ensure the speed does not overshoot past the maximum speed of the engine system. The delays incorporated in the final version of software do provide an improvement on positive transients, but they increase the response time during negative load transients, causing the engine to over speed, possibly compromising the integrity of the physical components. This duality was not anticipated in the setup of the electronic governor, and as a result both of these could not be accounted in practice.

From the papers presented in this study [11], [8], [7], [12], it is clear a PID controller has been the industry standard for this sort of control. In the interest of simplicity, the PID control was not utilized in this study, instead a more basic logic controller was attempted that used existing PIC chip technology implemented on the EFI controller and added only one extra sensor (the TPS sensor) to the system. This approach, while inexpensive and simple, does not provide the computational needs a PID or rate based controller would need. It is still not known if a PID controller is completely necessary to provide adequate speed regulation, though the cost associated with a PID controller is not known. The path with the PID is a proven one, and the implementation is not a difficult task once the EFI system has been improved.

In an effort to provide a simple and inexpensive solution, it is shown that the engine system is far more complex than originally understood. The underlying physics of the fuel control cannot be bypassed by a simple throttle control system. One must actively control both the airflow and fuel flow effectively for adequate speed and load control. In order to accomplish this additional work needs to be done on the current EFI system to provide transient compensation that accounts for the manifold filling dynamics,

similar to Hendricks [16], while properly utilizing the manifold air pressure signal for both transient and steady state operation. A more robust actuator motor, with more speed response bandwidth needs to be used to provide control flexibility. Additional throttle precision is needed for the nonlinear relationship of throttle airflow to throttle position.

Overall, this project proved that, even though the engine used is very basic, the physics and system dynamics remain complex. The tools available to the development engineer, particularly basic engine models and limited experimental facilities, are not enough to overcome the limitations induced by simple controllers and engine management systems. The sophistication of more expensive engine platforms is not from the need for performance, but by the need of the system at large. When considering an inexpensive utility engine, it is easy to overlook the complexity when cost limitations drive development direction and opportunity. However, in their simplicity, these systems become even more complex for the development engineer who has limited degrees of freedom for control and manipulation. This study can be a guide for the development engineer in that the models and results shown can provide a roadmap to create a system where the flexibility, though limited as it will be, will be adequate to meet the performance needs of the project.

# APPENDIX A.

# DYNOMOMETER AND INSTRUMENTATION INFORMATION

1. VERTICAL SHAFT DYNOMOMETER INFORMATION

Brake: Baldor 25hp 220V Vector Drive

Control: Baldor Vector Drive

Drive: Dayco cog belt with manual tensioning system

Torque Transducer: Lebow 2404-5K

**Lebow 2404-5K Reaction Torque Transducer**

| | | | | |
|---|---|---|---|---|
| Rated Capacity | 5000 | in-lbs | | |
| Nonlinearity | 0.02% | Full Scale | 1 | in-lbs |
| Hysteresis | 0.10% | Full Scale | 5 | in-lbs |
| Repeatability | 0.05% | Full Scale | 2.5 | in-lbs |
| Overload: | 50% | Full Scale | 2500 | in-lbs |

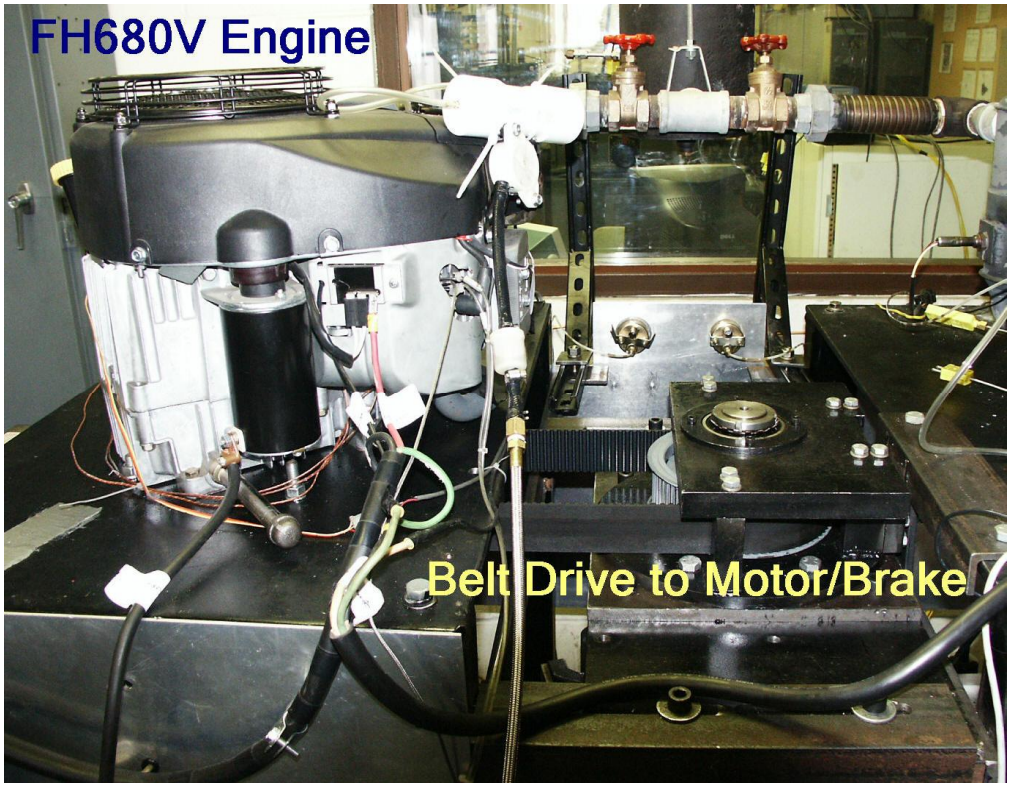


Figure A.1: Picture of vertical shaft dyno

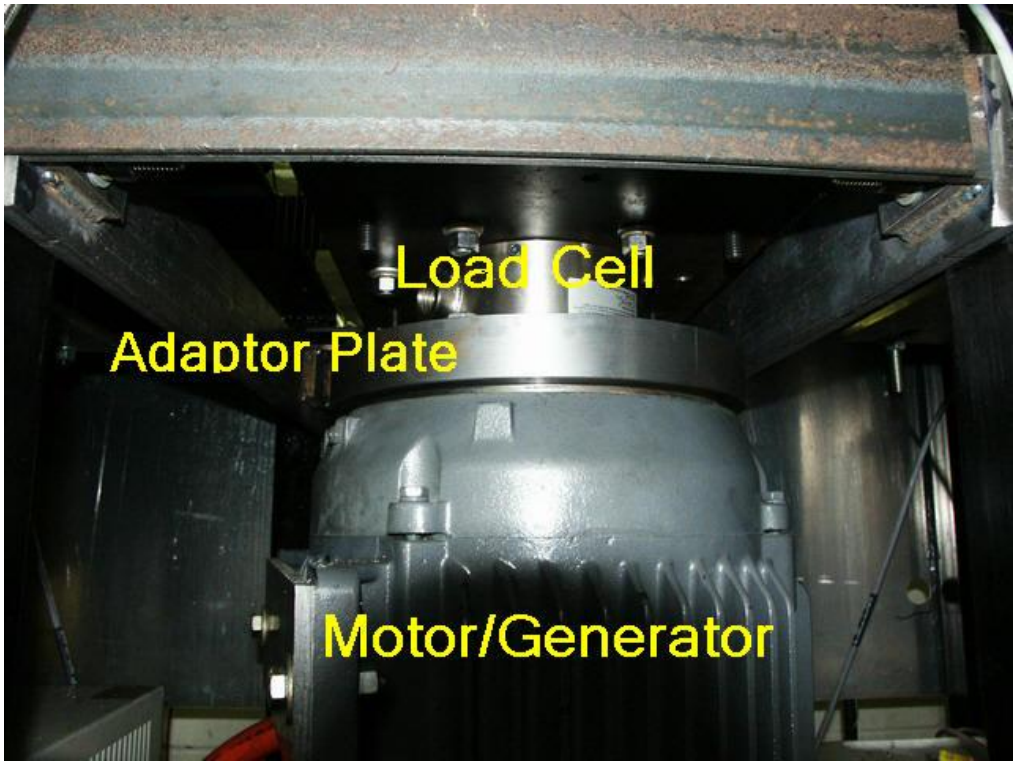


Figure A.2: Load cell and dyno brake on vertical dyno

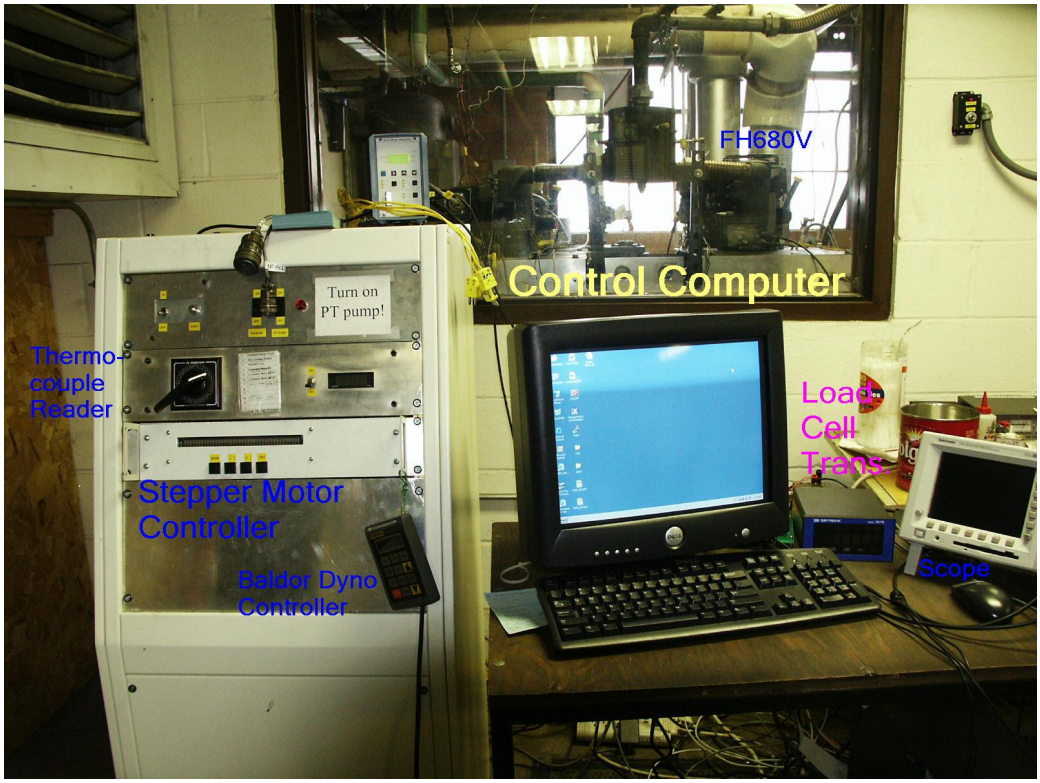


Figure A.3: Control room for vertical dyno.

2. WATER BRAKE DYNOMOMETER INFORMATION

Brake: Land – and –Sea Dyno-Mite water brake

Control: Manual valve

Drive: Direct Couple

Torque Transducer: Dyno-Mite

Torque Accuracy:  1.5% full scale of 200 ft-lbs

Speed Accuracy: ± 5 RPM

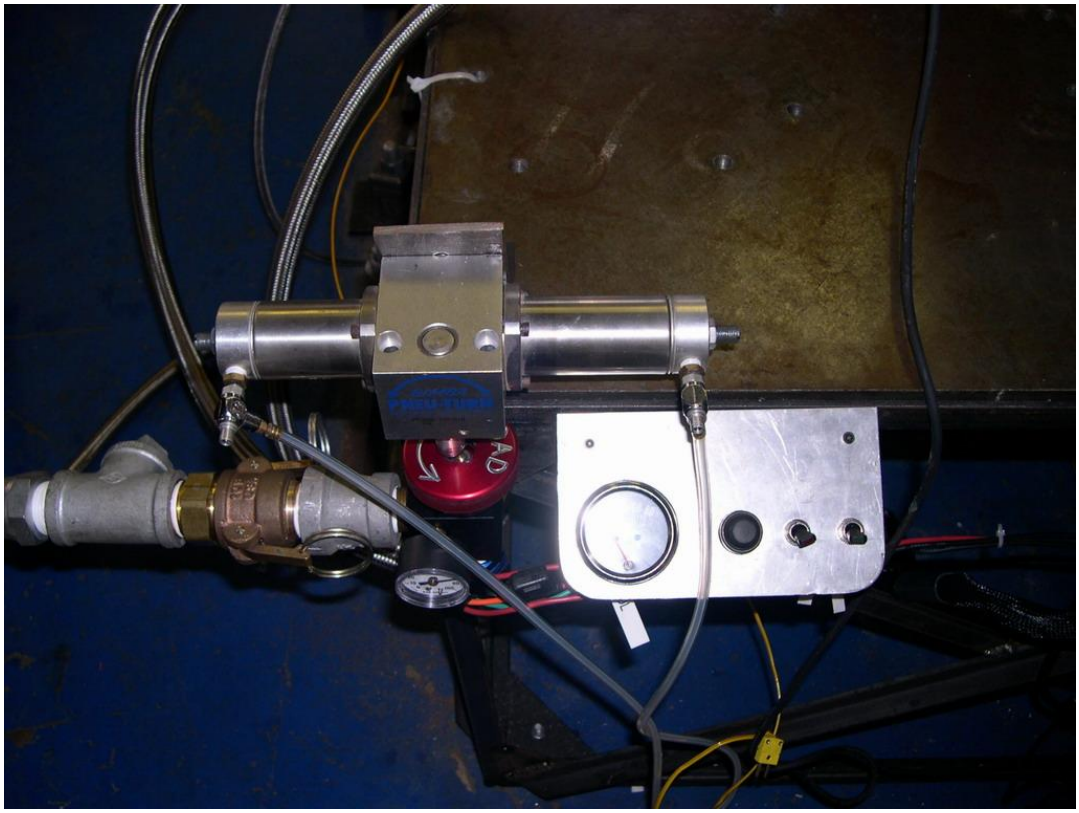

Figure A.4: Load Control Valve, Actuator, and control panel for horizontal shaft dyno.

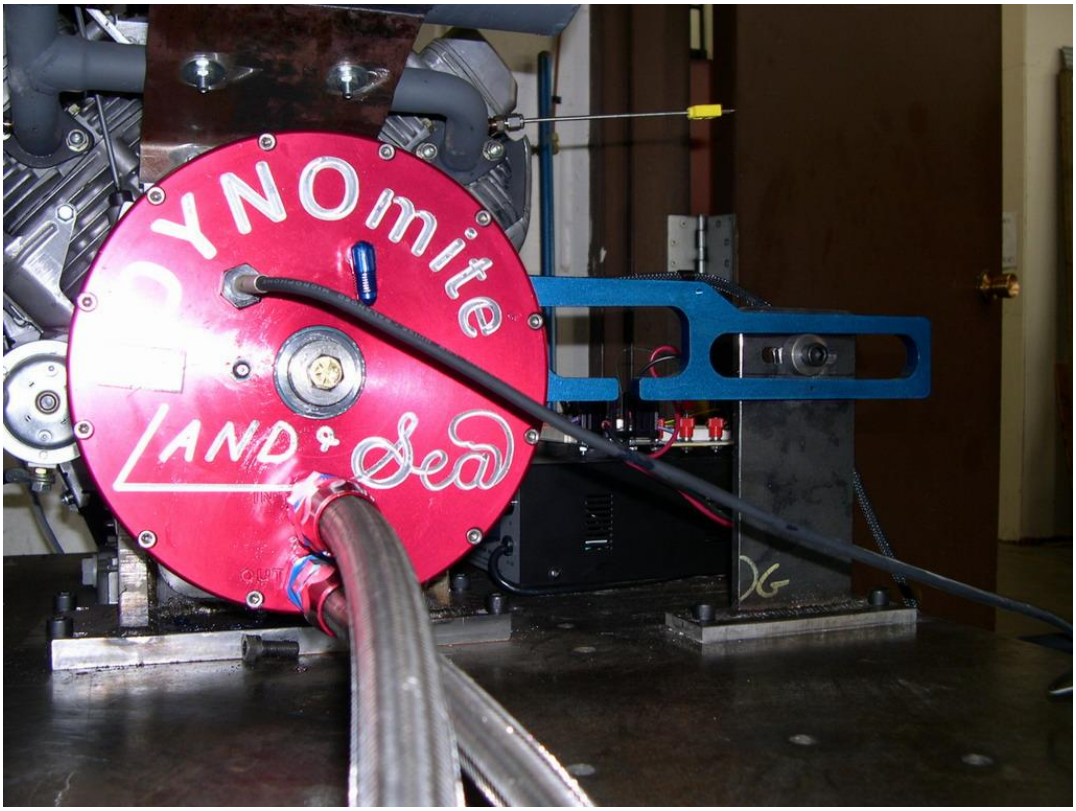


Figure A.5: Water Brake and Torque Arm for horizontal shaft dyno

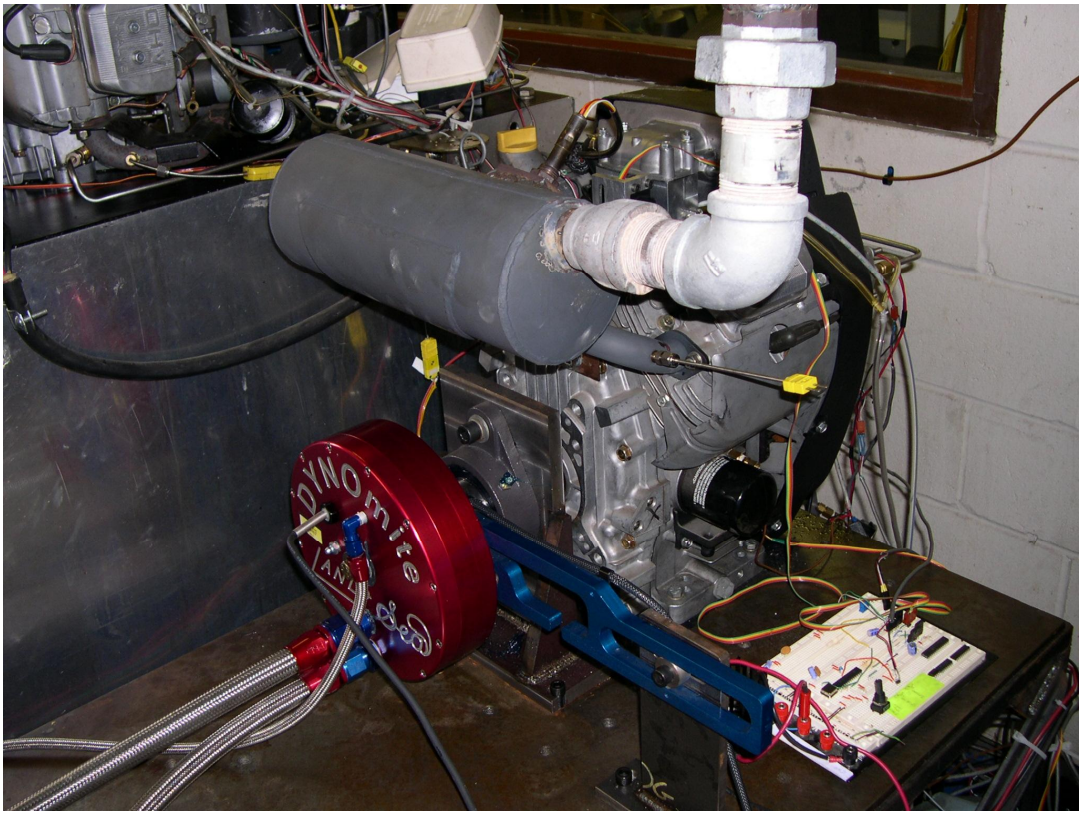


Figure A.6: Horizontal shaft dyno water brake and engine

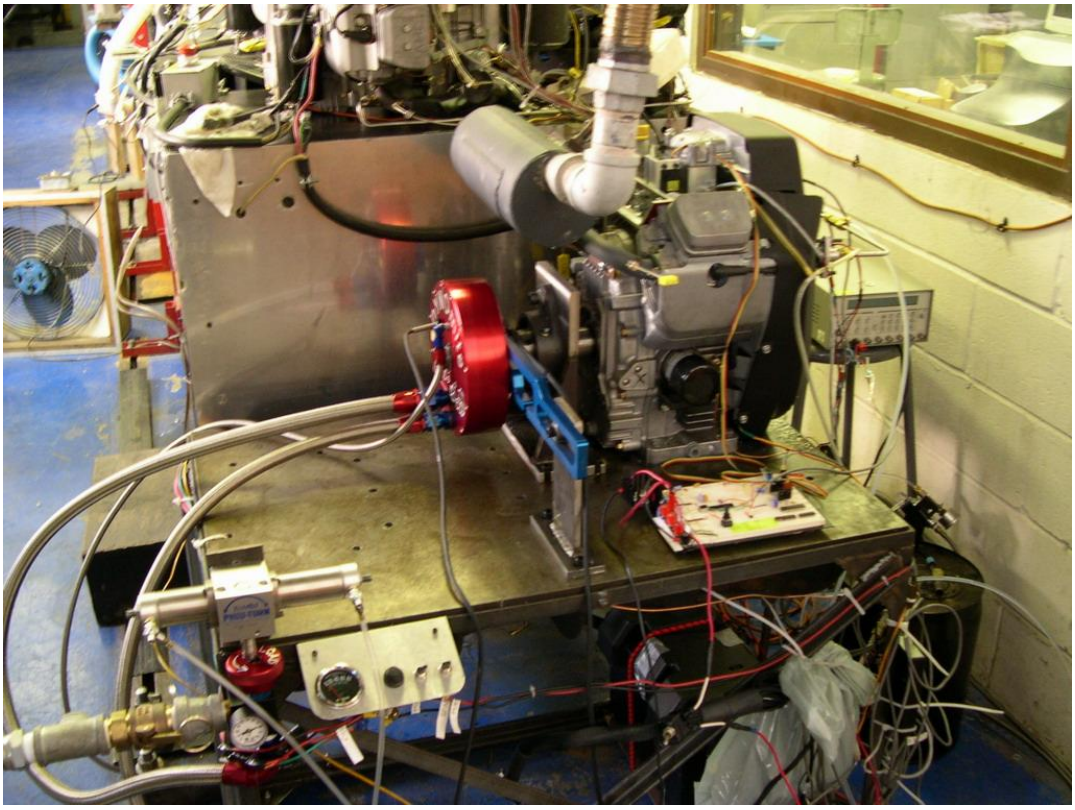

Figure A.7: Horizontal Shaft Dyno System

# APPENDIX B.

# TEST FUEL INFORMATION

1. FUEL CERTIFICATE OF ANALYSIS

Fuel: UTG 96 Lot Number 4EPU9601

Source: Chevron Phillips Chemical Company, LP

10001 Six Pines Drive

The Woodlands, TX 77380

| **Tests** | **Results** | **Specifications** | **Method** |
|---|---|---|---|
| Specific Gravity, 60/60 | 0.7412 | 0.734 - 0.744 | ASTM D-4052 |
| APR Gravity | 59.41 | 58.7 – 61.2 | ASTM D-1298 |
| Phosphorous, g/gl | <0.0011 | 0.005 Max | ASTM D-3231 |
| Sulfur, ppm | 27.0 | 15 – 40 | ASTM D-5453 |
| Corrosion, 50°C, 3 hrs | 1A | 1 Max | ASTM D-130 |
| Hydrogen, wt% | 13.457 | Report | ASTM D-5291 |
| Carbon, wt% | 86.543 | Report | ASTM D-5291 |
| Net Heat of Combustion (BTU/LB) | 18578 | Report | ASTM D-3338 |
| Oxidation Stability (minutes) | 1440+ | 1440 Min | ASTM D-525 |
| Existent Gums (mg/100ml)(washed) | 0.5 | 5 Max | ASTM D-381 |
| Reid Vapor Pressure | 9.2 | 8.7 – 9.2 | ASTM D-6378 |
| TEL (ml/gal) | <0.0008 | 0.005 Max | ASTM D-3237 |
| Benzene Content, lv% 0.02 | Report | | |
| **Distillation, °F** | | **ASTM D-86** | |
| IBP | 89.8 | 75 - 95 | |
| 5% | 115.0 | | |
| 10 | 124.7 | 120 - 135 | |
| 20 | 143.4 | | |
| 30 | 169.3 | | |
| 40 | 201.6 | | |
| 50 | 221.1 | 200 - 230 | |
| 60 | 234.3 | | |
| 70 | 245.7 | | |
| 80 | 266.0 | | |
| 90 | 311.2 | 300 - 325 | |
| 95 | 343.2 | | |
| EP | 394.2 | 415 Max | |
| Loss | 0.4 | | |
| Residue | 1.0 | | |

| **Hydrocarbon Type, Vol%** | | **ASTM D-1319** | |
|---|---|---|---|
| Aromatics | 33.4 | 35 Max | |
| Olefins | 1.6 | 10 Max | |
| Saturates | 65.0 | | |
| | | | |
| Research Octane Number | 96.1 | 96 Min | ASTM D-2699 |
| Motor Octane Number | 87.8 | Report | ASTM D-2700 |
| Antiknock Index | 92.0 | Report | |
| Sensitivity | 8.3 | 7.5 Min | |

# APPENDIX C.

# THROTTLE CONTROLLER CONTROL BOARD INFORMATION

# 1. CONTROLLER HARDWARE PICTRES AND DIAGRAMS

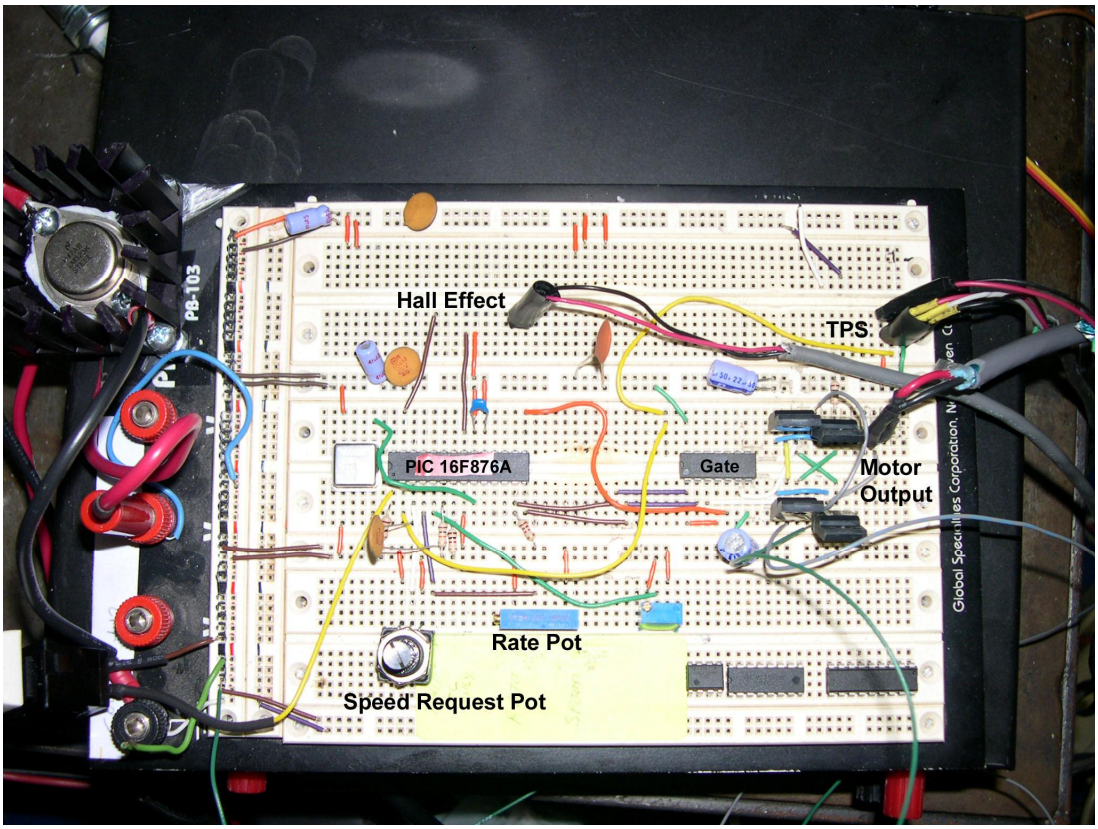


Figure C.1: Controller Prototype Board. Note the Hall Effect sensor input is not placed in the proper location when not operating.

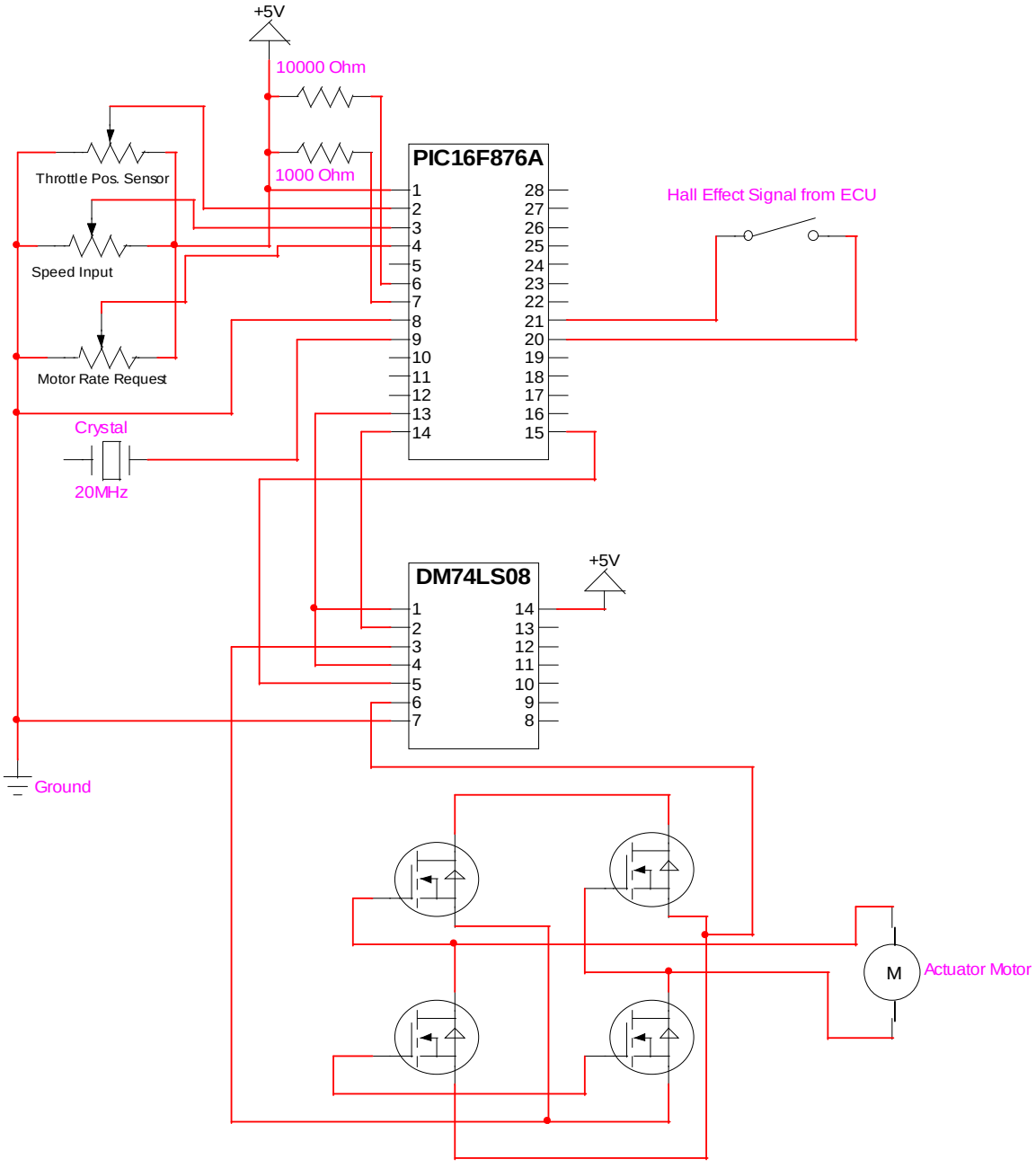


Figure C.2: Controller prototype version 5.9 circuit diagram

Table C.1: PIC16F876A Pin Out

| Pin Number | Input or Output | Use |
|---|---|---|
| 1 | Input | Source Voltage, +5V |
| 2 | Input | Throttle Position Sensor, 0-5V |
| 3 | Input | Speed Request Input, 0-5V |
| 4 | Input | Motor Request Input, 0-5V |
| 5 | N/A | Not Used |
| 6 | N/A | Unused, Kept +5V |
| 7 | N/A | Unused, Kept +5V |
| 8 | N/A | Ground |
| 9 | Input | Clock Input, 20MHz, Digital |
| 10 | N/A | Not Used |
| 11 | N/A | Not Used |
| 12 | N/A | Not Used |
| 13 | Output | PWM Output, 5V |
| 14 | Output | Motor Direction Output, Close Throttle, 5V |
| 15 | Output | Motor Direction Output, Open Throttle, 5V |
| 16 | N/A | Not Used |
| 17 | N/A | Not Used |
| 18 | N/A | Not Used |
| 19 | N/A | Not Used |
| 20 | Input | Hall Effect, Low Signal |
| 21 | Input | Hall Effect, High Signal |
| 22 | N/A | Not Used |
| 23 | N/A | Not Used |
| 24 | N/A | Not Used |
| 25 | N/A | Not Used |
| 26 | N/A | Not Used |
| 27 | N/A | Not Used |
| 28 | N/A | Not Used |

Table C.2: Controller Parts List

| Part Description | Quantity | Reference Number |
|---|---|---|
| Programmable PIC Chip | 1 | PIC16F876A |
| Throttle Position Sensor | 1 | Vishay Model 357 |
| Engine Speed Input Potentiometer | 1 | Vishay Model 248 |
| Actuator Speed Input Potentiometer | 1 | Vishay Model 248 |
| AND Gate | 1 | DM74LS08 |
| H Bridge Rectifier | 4 | IRIL |
| Crystal | 1 | 20 MHz |
| Motor and Gear Train | 1 | |
| Throttle Body | 1 | |
| Actuator Bracket | 1 | |
| Throttle Linkage | 1 | |
| Linkage Spring | 1 | |
| 1kOhm Resistor | 1 | |
| 10kOhm Resistor | 1 | |
| +5V Voltage Regulator | 1 | LM323K |
| Regulator Heat Sink | 1 | |
| Reset Switch | 1 | |

# APPENDIX D

## PICBASIC CODES, PLOTS, AND PHOTOGRAPHS ON CD-ROM

# 1. INTRODUCTION

Included in this thesis is a CD-Rom which includes the PIC BASIC code for all 6 throttle controller programs. These are written in basic ASCII text format, and can be viewed via numerous text programs. An outline of the contents of the CD-ROM is as follows.

# 2. CONTENTS

Info.TXT

PICBASIC Programs:

TCS_v1.0.bas

TCS_v2.0.bas

TCS_v3.0.bas

TCS_v4.4.bas

TCS_v4.5.bas

TCS_v5.9.bas

## BIBLIOGRAPHY


1. Environmental Protection Agency,"Regulatory Announcement: Proposed Emission Standards for New Nonroad Spark-Ignition Engines, Equipment, and Vessels," EPA 420-F-01-032, 2007

2. Koederitz, K.,"Investigation of Hydrocarbon Sources and Reduction in Small Four-Stroke Spark Ignition Engines," UMR PhD Dissertation, 2003

3. Kauchak, J. T.,"Basic Governing," SAE 840912, 1984

4. Howes, P., Law D., Dissanayake, D.,"The Electronic Governing of Diesel Engines for the Agricultural Industry," SAE 860146, 1986

5. Howes, P., Ives, A. P.,"The Development of an Electronic Engine Speed Governor for the Agricultural Industry," SAE 881302, 1988

6. Yama, H., Fujiwara, M., Fujii, Y., Nakahira, T.,"Development of High Reliability and Low Cost Electronic Governor System for Small Diesel Engine for Agricultural and Industrial Use," SAE 2001-01-1866, 2001

7. Sans, M.,"A Second Order Idle Speed Controller," SAE 880184, 1988

8. Iwai, T., Ohtoshi, K., Fukumori, E., Ohsawa, M.,"The Development of an Electronic Governor for the Power Generator System," SAE 901603, 1990

9. Takahashi, T., Ueno, T., Yamamoto, A., Sanbulchi, H.,"A Simple Model for Idle Speed Control," SAE 850291, 1985

10. Nakamura, T., Ohtoshi, K., Hirate, H., Sugimoto, T., Ohsawa, M., Nishizawa, H.,"Development of the Electronic Governor System for the Toyota X300 Forklift Truck," SAE 921655, 1992

11. Bustamante, J., Wicker, R., Diong, B.,"Design and Implementation of a V-Twin Engine Throttle Control System for Hybrid Power Generation," SAE 1999-01-3321, 1999

12. Yang, C.,"Model-Based Analysis and Tuning of Electronic Throttle Controllers," SAE 2004-01-0524, 2004

13. Emtage, A. L., Lawson, P. A., Passmore, M. A., Lucas, G. G., Adcock, P. L.,"The Development of an Automotive Drive-by-wire Throttle System as a Research Tool," SAE 910081, 1991

.

14. Heywood, J. B., *Internal Combustion Engine Fundamentals*, McGraw-Hill, ISBN 0-07-028637-X, 1988

15. Blair, G. C., *Design and Simulation of Four Stroke Engines*, SAE Publications ISBN: 0-7680-0440-3, 1999

16. Hendricks, E., Chevalier, A., Jensen, M., Sorenson, S. C., Trumpy, D., Asik, J.,"Modeling of the Intake Manifold Filling Dynamics," SAE 960037, 1996

17. Carlsson, P.,"Flow through a Throttle Body," Linköping University , 2007

18. Hendricks, E., Vesterholm, T.,"The Analysis of Mean Value Engine Models," SAE 920682, 1992

19. Aquino, C. F.,"Transient A/F Control Characteristics of the 5 Liter Central Fuel Injection Engine," SAE 810494, 1981

20. Hires, S. D., Overington, M. T.,"Transient Mixture Strength Excursions - An Investigation of Their Causes and the Development of a Mixture Strength Fueling Strategy," SAE 810495, 1981

21. Fozo, S. R., Aquino, C.F.,"Transient A/F Ratio Characteristics for Cold Operation of a 1.6 Liter Engine with Sequential Fuel Injection," SAE 880691, 1988

22. Bossert, J. C., Shin, Y., Cheng, W. K.,"Fuel Effects on Throttle Transients in PFI Ignition Engines," SAE 971613, 1997

23. Shayler, P. J., Tep, Y. C., Scarisbrick, A.,"Fuel Transport Characteristics of Spark Ignition Engines for Transient Fuel Compensation," SAE 950067, 1995

24. Hendricks, E., Sorenson, S. C.,"Mean Value Modeling of Spark Ignition Engines," SAE 900616, 1990

25. Hendricks, E., Vesterholm, T., Kaidantzis, P., Rasmussen, P., Jensen, M.,"Transient A/F Ratio Errors in Conventional SI Engine Controllers," SAE 930856, 1993

26. Hendricks, E., Vesterholm, T., Sorenson, S. C.,"Nonlinear, Closed Loop, SI Engine Control Observers," SAE 920237, 1992

27. Hendricks, E., Vesterholm, T., Kaidantzis, P., Rasmussen, P., Jensen, M.,"Nonlinear Transient Fuel Film Compensation," SAE 930767, 1993

28. Almkvist, G., Eriksson, S.,"An Analysis of Air to Fuel Ratio Response in a Multi Port Fuel Injected Engine Under Transient Conditions," SAE 932753, 1993

29. Tseng, T.C. and Cheng, W. K.,"An Adaptive Air/Fuel Ratio Controller for SI Engine Throttle Transients," SAE 1999-01-0552, 1999

30. Simons, M. R., Locatelli, M., Onder, C. H., Geering, H. P.,"A Nonlinear Wall-Wetting Model for the Complete Operating Region of a Sequential Fuel Injected SI Engine," SAE 2000-01-1260, 2000

31. Ladommatos, N. and Rose,D. W.,"On the Causes of In-Cylinder Air-Fuel Ratio Excursions During Load and Fuelling Transients in Port Injected Spark Ignition Engines," SAE 960466, 1996

32. Boam, D. J., Finlay, I. C., Matrins, J. J. G.,"A Model for Prediction Engine Torque Response during Rapid Throttle Transients in Port-injected Spark-ignition Engines," SAE 890565, 1989

33. Onder, C. H. and Geering, H. P.,"Measurement of the Wall Wetting Dynamics of a Sequential Injection Spark Ignition Engine," SAE 940447, 1994

34. Ye, Z.," A Simple Linear Approach for Transient Fuel Control," SAE 2003-01-0360, 2003

# VITA

Donald (Trae) Ray Hibler, III was born on September 6, 1979. He completed his Bachelor's of Science in Mechanical Engineering from the University of Missouri – Rolla in May 2003, and will be earning a Master's Degree in Mechanical Engineering from the same university in May 2009. He is currently employed by John Deere Power Systems in Waterloo, IA as a diesel engine development engineer.